



THE UNIVERSITY *of* EDINBURGH

## Edinburgh Research Explorer

# Structural determinants of peptide-dependent TAP1-TAP2 transit passage targeted by viral proteins and altered by cancer-associated mutations

### Citation for published version:

Padariya, M, Kote, S, Mayordomo, M, Dapic, I, Alfaro, J, Hupp, T, Fahraeus, R & Kalathiya, U 2021, 'Structural determinants of peptide-dependent TAP1-TAP2 transit passage targeted by viral proteins and altered by cancer-associated mutations', *Computational and Structural Biotechnology Journal*.  
<https://doi.org/10.1016/j.csbj.2021.09.006>

### Digital Object Identifier (DOI):

[10.1016/j.csbj.2021.09.006](https://doi.org/10.1016/j.csbj.2021.09.006)

### Link:

[Link to publication record in Edinburgh Research Explorer](#)

### Document Version:

Publisher's PDF, also known as Version of record

### Published In:

Computational and Structural Biotechnology Journal

### General rights

Copyright for the publications made accessible via the Edinburgh Research Explorer is retained by the author(s) and / or other copyright owners and it is a condition of accessing these publications that users recognise and abide by the legal requirements associated with these rights.

### Take down policy

The University of Edinburgh has made every reasonable effort to ensure that Edinburgh Research Explorer content complies with UK legislation. If you believe that the public display of this file breaches copyright please contact [openaccess@ed.ac.uk](mailto:openaccess@ed.ac.uk) providing details, and we will remove access to the work immediately and investigate your claim.



## Journal Pre-proofs

Structural determinants of peptide-dependent TAP1-TAP2 transit passage targeted by viral proteins and altered by cancer-associated mutations

Monikaben Padariya, Sachin Kote, Marcos Mayordomo, Irena Dapic, Javier Alfaro, Ted Hupp, Robin Fahraeus, Umesh Kalathiya

PII: S2001-0370(21)00391-3  
DOI: <https://doi.org/10.1016/j.csbj.2021.09.006>  
Reference: CSBJ 1207

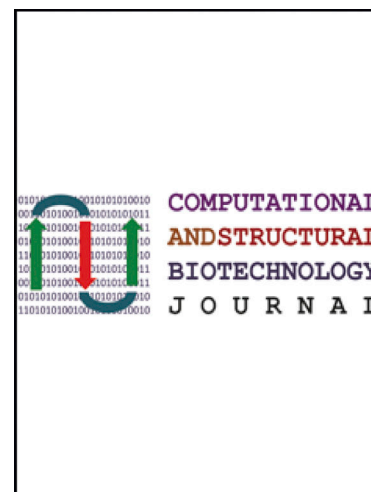
To appear in: *Computational and Structural Biotechnology Journal*

Received Date: 31 March 2021  
Revised Date: 6 September 2021  
Accepted Date: 6 September 2021

Please cite this article as: M. Padariya, S. Kote, M. Mayordomo, I. Dapic, J. Alfaro, T. Hupp, R. Fahraeus, U. Kalathiya, Structural determinants of peptide-dependent TAP1-TAP2 transit passage targeted by viral proteins and altered by cancer-associated mutations, *Computational and Structural Biotechnology Journal* (2021), doi: <https://doi.org/10.1016/j.csbj.2021.09.006>

This is a PDF file of an article that has undergone enhancements after acceptance, such as the addition of a cover page and metadata, and formatting for readability, but it is not yet the definitive version of record. This version will undergo additional copyediting, typesetting and review before it is published in its final form, but we are providing this version to give early visibility of the article. Please note that, during the production process, errors may be discovered which could affect the content, and all legal disclaimers that apply to the journal pertain.

© 2021 Published by Elsevier B.V. on behalf of Research Network of Computational and Structural Biotechnology.



# Structural determinants of peptide-dependent TAP1-TAP2 transit passage targeted by viral proteins and altered by cancer-associated mutations

Monikaben Padariya<sup>1,†,\*</sup>, Sachin Kote<sup>1</sup>, Marcos Mayordomo<sup>1</sup>, Irena Dapic<sup>1</sup>, Javier Alfaro<sup>1,2</sup>, Ted Hupp<sup>1,2</sup>, Robin Fahraeus<sup>1,3,4,5,\*</sup>, Umesh Kalathiya<sup>1,†,\*</sup>

<sup>1</sup> International Centre for Cancer Vaccine Science, University of Gdansk, ul. Kładki 24, 80-822 Gdansk, Poland

<sup>2</sup> Institute of Genetics and Cancer, University of Edinburgh, Edinburgh, Scotland EH4 2XR, United Kingdom

<sup>3</sup> Inserm UMRS1131, Institut de Génétique Moléculaire, Université Paris 7, Hôpital St. Louis, F-75010 Paris, France

<sup>4</sup> Department of Medical Biosciences, Building 6M, Umeå University, 901 85 Umeå, Sweden

<sup>5</sup> RECAMO, Masaryk Memorial Cancer Institute, Zlutykopec 7, 65653 Brno, Czech Republic.

<sup>†</sup>These authors contributed equally to this work.

\*Correspondence: monikaben.padariya@ug.edu.pl (M.P.), robin.fahraeus@inserm.fr (R.F.), umesh.kalathiya@ug.edu.pl (U.K.)

## Abstract

The TAP1-TAP2 complex transports antigenic peptide substrates into the endoplasmic reticulum (ER). In the ER, the peptides are further processed and loaded on the major histocompatibility class (MHC) I molecules by the peptide loading complex (PLC). The TAP transporters are linked with the PLC; a target for cancers and viral immune evasion. But the mechanisms whereby the cancer-derived mutations in TAP1-TAP2 or viral factors targeting the PLC, interfere peptide transport are only emerging. This study describes that transit of peptides through TAP can take place via two different channels (4 or 8 helices) depending on peptide length and sequence. Molecular dynamics and binding affinity predictions of peptide-transporters demonstrated that smaller peptides (8-10 mers; e.g. AAGIGILTV, SIINFEKL) can transport quickly through the transport tunnel compared to longer peptides (15-mer; e.g. ENPVVHFFKNIIVTPR). In line with a regulated and selective peptide transport by TAPs, the immunopeptidome upon IFN- $\gamma$  treatment in melanoma cells induced the shorter length (9-mer) peptide presentation over MHC-I that exhibit a relatively weak binding affinity with TAP. A conserved distance between N and C terminus residues of the studied peptides in the transport tunnel were reported. Furthermore, by adversely interacting with the TAP transport passage, or affecting TAP<sub>NBD</sub> domains tilt movement, viral proteins and cancer-derived mutations in TAP1-TAP2, may induce allosteric effects in TAP that block conformation of the tunnel (closed towards ER lumen). Interestingly, some cancer-associated mutations (e.g. TAP1<sub>R372Q</sub> and TAP2<sub>R373H</sub>) can specifically interfere with selective transport channels (i.e. for longer-peptides). These results provide a model for how viruses and cancer-associated mutations targeting TAP interfaces can affect MHC class I antigen presentation and how the IFN- $\gamma$  pathway alters MHC-I antigen presentation via the kinetics of peptide transport.

**Keywords:** *peptide; transporters; MHC-I; cancer mutations; viral factors; molecular dynamics; kinetics; TAP1; TAP2; in silico peptide screening; immunopeptidome; IFN- $\gamma$*

## 1. Introduction

Cytotoxic T lymphocyte response to infected or transformed cells depends on the presentation of peptide antigens on major histocompatibility complex class I (MHC-I) molecules. The majority of MHC-I presented peptides are generated in the cytosol by the proteasome and transported into the endoplasmic reticulum (ER) lumen for further processing by the ERAP aminopeptidases, before loaded onto MHC-I molecules by the dynamic multi-component assembly peptide-loading complex (PLC) (Figure 1) [1-3]. PLC (Figure 1) includes; TAP1 and TAP2 (transporter 1 and 2) heterodimer complex, MHC-I,  $\beta$ 2microglobulin ( $\beta$ 2m), the chaperones tapasin, calreticulin, and ERp57 (ER protein 57) [1-3]. The TAP transporters constitute functionally key components of the antigen presentation pathway since they link the cytosolic pool of peptides with the PLC and the ER-resident MHC-I molecules (Figure 1) [1].

The TAP transporters belong to the superfamily of ATP-binding cassette (ABC) transporters. Some of these transporters are associated with severe human diseases like cystic fibrosis [4, 5], and they play major roles in multidrug resistance of pathogenic bacteria, reduced efficacy of antitumor drugs, cholesterol metabolism, cell homeostasis, and immune response [6]. Therefore, understanding the functional mechanisms of ABC transporters is important for therapeutic development. The TAP1 (ABCB2) and TAP2 (ABCB3) transporters, each have an N-terminal transmembrane domain (TMD) and a C-terminal nucleotide-binding domain (NBD) [7]. In the core part of the TMDs, the outer TM helices bind the other PLC component tapasin, the inner helices are responsible for peptide binding and form the channel, which mediates the peptide translocation [8, 9]. Peptide binding to TAP is ATP-independent [10, 11], whereas peptide transport from the cytosol to the ER requires ATP binding and hydrolysis [12]. The TAP<sub>NBDs</sub> carry out the ATP hydrolysis to energize the conformational changes of the TMDs required for peptide translocation [1, 12].

Substantial effort has been made to understand the peptides that are translocated by the TAP1-TAP2 transporters. Several biochemical studies have identified the nucleotide binding structural motifs, roughly mapped the peptide binding region, and provided the secondary structures responsible for the crosstalk between ATP hydrolysis in the TAP<sub>NBDs</sub> and conformational changes of the TM helices [1, 13]. However, the picture is still incomplete, as it has not been conclusively integrated into a robust trajectory of how the TAP dynamics and the substrates move to carry out a transport cycle. The precise conformational changes that occur as a result of substrate or nucleotide binding to TAP1/TAP2 are also not characterized [1]. The TAP transporters show a common fold with all structurally characterized ABC transporters [6, 14]. Recent expansion of several new high-resolution transporter structures in different conformations produced many structural models of the TAP transporters [1, 6, 13, 15-18]. Thus, the structural understanding of the TAP1-TAP2 complex is largely based on such extrapolations. However, it has also been suggested that the transporters most likely do not undergo the same structural cycles and no common mechanism has been proposed [1, 14]. For this reason, the novel insights of TAP structures will be of importance.

Impaired TAP function results in reduced surface expression of MHC-I, as the empty MHC-I molecules are unable to present antigens to the immune system and is a common target for viral as well as cancer immune evasion [15, 19-23]. Approximately, 15-20% of all human cancers worldwide are linked to viruses and this percentage could grow in the future [24]. MHC-I surface expression abnormalities have been identified in virus-associated cancers and non-cancerous cells, and thus, delineate a significant mechanism of virus infected cells to evade proper immune response. In most cases, this downregulation has been related to impaired TAP expression, which could be a result of structural alterations or dysregulation [25-28]. Several viruses have evolved factors that block the function of TAP [29], including herpesviruses such as Epstein-Barr virus, human cytomegalovirus, and herpes simplex virus type 1 that establish lifelong persistence in the host [30]. Association of these viruses with certain types of cancer or human malignancies has been demonstrated and knowledge about their targets, as well as functioning mechanisms can be useful in the development of future antiviral treatment strategies [31]. In concert with this, we investigated the TAP1 and TAP2 transporters at the atomic level with a particular focus on how viruses inhibit TAP-mediated peptide translocation at a molecular level. The dynamics of the following TAP attacking viral immune evasion proteins were studied: BNLF2a from Epstein-Barr virus [32], CPXV012 from cowpox virus [33], ICP47 from herpes simplex virus type 1 [34, 35], US6 from human cytomegalovirus [36], and UL49.5 encoded by varicellovirus [37].

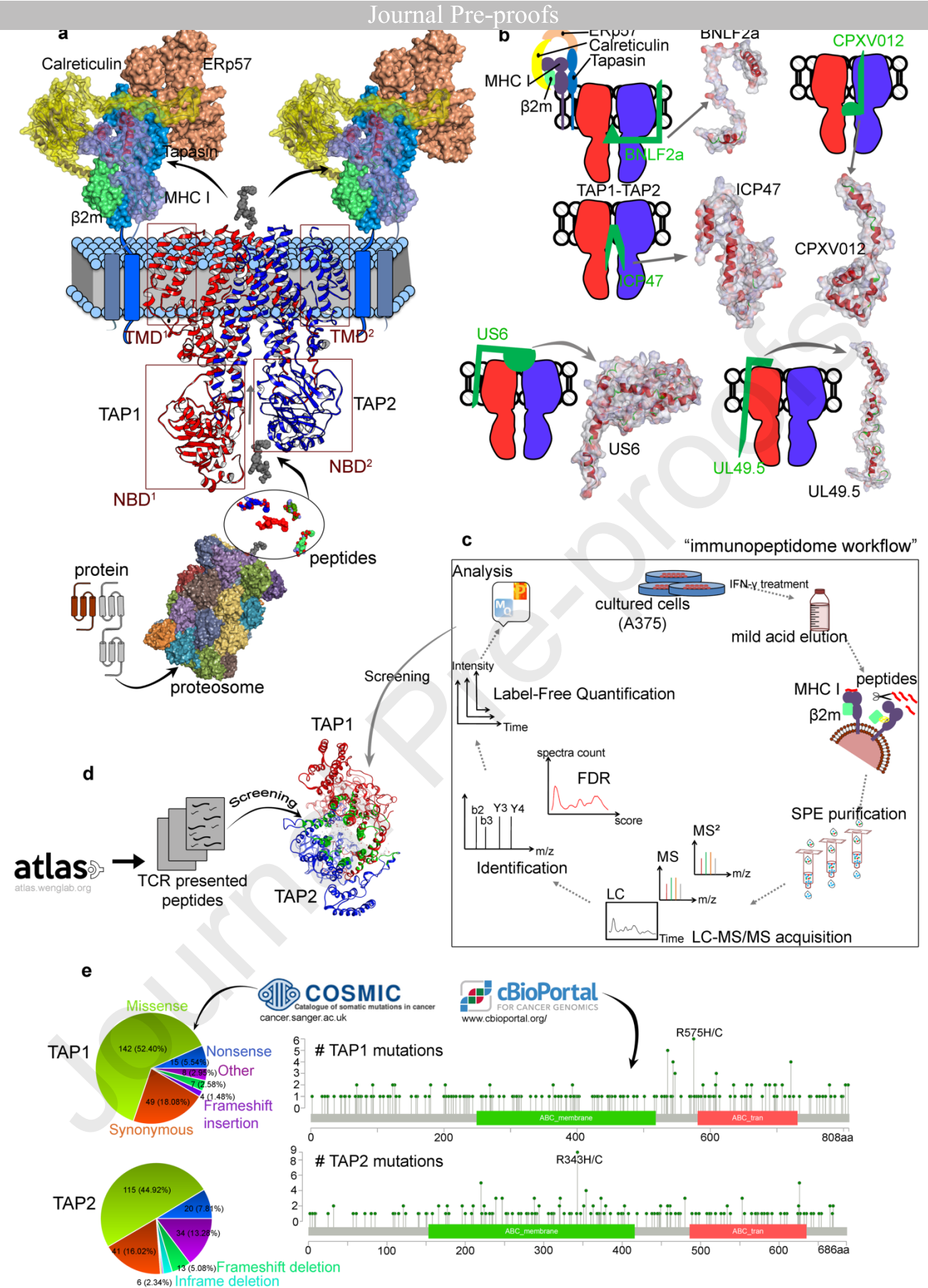


**Figure 1.** The TAP1 and TAP2 transporters molecular and structural aspects in the peptide-loading complex. **(a)** The modeled tertiary structures of TAP1-TAP2 heterodimeric transporters, including the N-terminal transmembrane domains (TMD) that were found missing in the cryo-EM structure

(pdb id.: 5u1d) [18, 23]. Antigenic peptide presentation by MHC-I begins with the degradation of cytosolic proteins into peptides by the proteasome, which are then transported across the ER membrane by the TAP transporters. Following, the peptides can be loaded over the surface of the MHC-I molecules residing in the peptide-loading complex (PLC), accommodated with several other components;  $\beta$ 2m, ERp57, tapasin, and calreticulin [1-3]. **(b)** Viral immune evasion proteins interacting with the TAP transporters. ICP47 binds to TAP from the cytosol and inhibits the peptide binding, US6 blocks ATP binding to TAP by interfering from the ER lumen, UL49.5 blocks TAP dependent peptide transport and also catalyses the degradation of the PLC. BNLF2a binds to the core TAP structure and arrest it in a transport-incompetent conformation, CPXV012 inhibits TAP dependent peptide translocation, and thus, interfere with the MHC-I-peptide assembly in the ER [38]. Cryo-EM structure of human TAP with ICP47 (pdb id.: 5u1d) [18, 23] was used as a template to model other TAP binding viral proteins BNLF2a, CPXV012, UL49.5, and US6. Three dimensional (3D) structures of viral protein are shown in ribbon representation with molecular surfaces. **(c)** The outline of the immunopeptidome workflow, representing the sample preparation to peptide identification protocol. **(d)** Datasets of TAP transported peptides retrieved from the ATLAS (Altered TCR Ligand Affinities and Structures) database (<http://atlas.wenglab.org/>). The peptides present in the crystal structure of TCR(T cells receptor)-peptide-MHC complexes were collected. In the 3D-structure of TAP, the defined active site for peptide screening is highlighted as green ribbons, red spheres represent hydrophilic and white sphere hydrophobic likeliness of the active site. **(e)** Cancer-associated mutations retrieved from the COSMIC (Catalogue of Somatic Mutations in Cancer; [cancer.sanger.ac.uk](http://cancer.sanger.ac.uk)) and cBioPortal (<https://www.cbioportal.org/>) databases for the TAP transporters. The pie chart from COSMIC represents different types of mutation with a number of samples labeled, as well as the percentage (%) of mutation covered. The scattered plot from cBioPortal, represents cancer mutations for TAP1 and TAP2 proteins along with its frequency.

To form a catalog of peptides likely to be transported by the TAP1-TAP2 complex, a systematic immunopeptidome workflow was applied as shown in Figure 1c. Peptide loaded on the MHC molecules in melanoma cells were identified by acid elution followed by mass spectrometry (MS) analysis. The virus infected cells form one key model with which to analyze the response of the immune system, however, some viruses escape immune surveillance by altering and inhibiting the MHC-I presentation pipeline. An alternative way to mimic the parts of the cellular immune response that occurs during viral infection can be to treat cells with interferons (IFNs) [39, 40]. Interferons are important cytokines, produced in response to viral infection, alert the immune system, and enhance cellular response to the infection (increase the presentation of MHC molecules) [41]. Thus, analyzing the effect of IFNs on the MHC-I immunopeptidome in cultured human cells can provide a model for examining the effects of viral infection on the MHC peptidome [40]. The type I (IFN- $\alpha$  and IFN- $\beta$ ) and type II (IFN- $\gamma$ ) IFNs are key cytokines in the antiviral response. IFN- $\beta$  is secreted from most cells in response to viral infection involving dendritic cells and many other cell types in the body [40, 42]. At later stages of immune response, IFN- $\gamma$  is secreted from T-cells and other immune cells [40]. The interferons strongly affect cellular metabolism and gene expression, including MHC-I as well as MHC-II molecules and also upregulate antigen processing and presentation components such as; ER aminopeptidase 1/2 and the TAP transporters [8, 40, 42, 43, 44-46]. Moreover, when cells are treated with IFN- $\gamma$ , the regular proteasomes are replaced by the immunoproteasomes [46]. This replacement has been associated with an enhanced immune response and the peptides produced by immunoproteasomes mainly contain hydrophobic or basic C termini, which are preferred substrates for the TAP transporters and also appear to be more efficient at binding to MHC-I [8, 40, 43]. Consequently, immunoproteasomes are believed to enhance the MHC-I antigenic peptide generation and presentation [47]. Additionally, the enhancement of MHC presentation by IFN treatment may add neoepitopes to the presented peptidome that can induce even stronger immune responses [40].

We were also interested to know if the transport of peptides through the TAP is affected by IFN-  $\gamma$  treatment. IFN-  $\gamma$  is known to induce the immunoproteasome with a different protease

composition and to alter the length and cleavage sites of peptides and we wanted to see if this could affect peptide interaction with the TAP and presentation on MHC molecules. The A375 cells were treated with IFN- $\gamma$  and peptides were identified using mass spectrometry. Detected peptides were further *in silico* screened with the TAP1-TAP2 model, to investigate the peptide transport process from the cytosol to the ER via the TAP transporters. Additionally, to extend our analysis, a set of peptides from the ATLAS (Altered TCR Ligand Affinities and Structures) database (<http://atlas.wenglab.org>) were compiled, which are known to be presented on TCR as well as the structures of TCR-peptide-MHC complexes are known [48]. Interactions of these peptides with the TAP1-TAP2 complex were analyzed, along with tracing protein-peptide binding affinities.

The cancer-associated mutations and viral proteins may share a common trend towards TAP transporters, which is attenuation of their activity. Defective TAP transporters in few tumor tissues have been identified by down-regulation of TAP mRNA or mutations. It has been proposed that by inducing a TAP attenuation mechanism the tumor cells escape immune response [15], and similarly, by down-regulating TAP1 levels, along with reducing MHC-I cell surface expression, the HPV (human papillomavirus) virus evades immune recognition [49, 50]. Several studies have linked TAP transporter polymorphisms and the risk for the high-grade cervical intraepithelial neoplasia (CIN), cervical cancer, and pulmonary tuberculosis [150]. Einstein et al. suggest that the TAP1 I333V and TAP1 D637G mutations reduce a high-grade CIN [49, 50]. The review by Rupert et al. highlighted defects in the TAP1 or TAP2 transporters can be the cause of bare lymphocyte syndrome (BLS) I, and during the viral infection the patients with BLS lacked increased susceptibility [51]. Ozbas-Gerceker et al. applying the PCR-RFLP (restriction fragment length polymorphism) method determined that polymorphism in TAP1<sub>-333</sub> and TAP2<sub>-565</sub> can be associated with multiple myeloma-MM and chronic lymphoid leukemia-CLL, respectively [52]. Moreover, the TAP2<sub>-665</sub> GG genotype could be a risk factor for different hematological malignancies [52]. The study of immunohistochemical expression of TAP1 and TAP2 in breast cancer patients suggested that their overexpression could be the cause of an aggressive breast tumor [53].

Therefore, to analyse the effects of somatic mutations on the TAP1 and TAP2 transporters, a large number of mutational hotspots for TAP1 and TAP2 genes were retrieved from the Catalogue of Somatic Mutations in Cancer (COSMIC, <https://cancer.sanger.ac.uk/cosmic>) [54], and cBio Cancer Genomics Portal (cBioPortal, <http://cbioportal.org>) databases [55]. Effects of point mutations on TAP1-TAP2 plasticity were determined by stability and binding affinity changes with respect to each other. In addition, the TAP1 and TAP2 genes were further investigated considering the single nucleotide polymorphism (SNPs) as well as the number of mutations that have been distributed within the human population. The regions in the TAP1-TAP2 transporters exposed bind to different viral proteins and were analysed in terms of the frequency of mutations or SNPs in those regions. Recently, a proteasome-dependent, but TAP-independent pathway has been described, showing that the well-known SIINFEKL peptide (the classical peptide epitope from ovalbumin presented by the MHC-I) can be imported into purified phagosomes in an ATP-dependent but TAP-independent manner [9, 56-58]. Considering this fact, SIINFEKL peptide was also included with the TAP transporters as model for 8-mer peptides, as well as to make a comparative analysis with other studied peptides. To analyse the molecular consequences of cancer driving mutation and peptide binding with TAP1-TAP2 complex, the functionally important mutations and a set of peptides were further assessed by molecular dynamics simulations (MDS) [59].

## 2. Materials and Methods

### 2.1. Experimental design and the sample preparation

#### 2.1.1. Cell culture with the treatment of IFN- $\gamma$ , as well as peptide isolation by mild acid elution

The melanoma A375 cells were previously described [60], and these A375 p53-wild-type status cells were grown in DMEM (Dulbecco's Modified Eagle's Medium) medium (invitrogen) supplemented with 10% heat-inactivated fetal bovine serum, 1% penicillin/streptomycin

(invitrogen), and incubated at 37°C with 5% CO<sub>2</sub>. The parental A375 cells were grown over 10 cm diameter plates, and for the treatment cells were exposed to 100 IU/ml IFN- $\gamma$  for 24h. Following the protocol described in [61], mild acid elution (MAE) was performed with citrate phosphate pH 3.3 buffer. Biological replicates of  $50 \times 10^6$  cells from both conditions (with and without IFN- $\gamma$  treatment) were used. MHC associated peptides were released by MAE, using 1.5 mL of citrate phosphate buffer at pH 3.3 for the  $50 \times 10^6$  cell samples. Cell suspensions were then pelleted and the resultant supernatants were considered as MHC-I peptides samples for further purifications. Followingly, the peptide sample extracts were desalted using Oasis HLB cartridges (30 mgs; water). Finally, the bound material was eluted with 1 mL H<sub>2</sub>O/80% methanol (MeOH)/0.2% formic acid (FA) v/v, and diluted to H<sub>2</sub>O/40% MeOH/0.2% FA v/v. Peptides were loaded on ultrafiltration devices (Microcon-10kDa centrifugal filters, Millipore) to isolate peptides < 10,000 Da, and remove higher molecular weight proteins. The resulting flow through content peptides was dried using vacuum centrifugation, which were then stored at -80°C until MS analysis.

### 2.1.2. Mass spectrometry and the peptide sequencing

Vacuum dried MHC presented peptides were reconstituted in 30  $\mu$ L of loading buffer composed of 0.08% trifluoroacetic acid (TFA)/2.5% acetonitrile (ACN) (v/v). Further, these peptides were analyzed by LC-MS/MS (Liquid chromatography–mass spectrometry cells) using an Ultimate 3000 nanoLC system coupled online to an Orbitrap Exploris 480 mass spectrometer (both from Thermo Fisher Scientific). The peptide samples (6  $\mu$ L) initially were loaded onto  $\mu$ -precursor column (C18 PepMap 100, 5  $\mu$ m, 100 Å) 300  $\mu$ m i.d. x 5 mm length cartridge trap column (P/N 160454, Thermo Fisher Scientific) for 10 min at a 5  $\mu$ L/min flow rate. Peptides were separated on a C18 reversed-phase analytical column (C18 PepMap 100 RSLCnano column) 75  $\mu$ m, i.d. x 150 mm length, 2  $\mu$ m, 100 Å (P/N 164534, Thermo Fisher Scientific). LC solvents were composed of 0.1% FA in water (v/v) (solvent A) and 0.1% FA in water with 80% ACN (v/v/v) (solvent B). Peptides were eluted over a nonlinear gradient of 2.5-35% and 35-60% of B for 80 min and 15 min, respectively, at a flow rate of 300 nL/min controlled by the Ultimate 3000 nanoLC system. Finally the column was washed with 95% B for 10 min. Samples were analyzed in data-dependent acquisition (DDA) mode with the following settings; survey scan (MS1) range was set to 300 to 1650 m/z with a resolving power of 120000 (at 200m/z) and an AGC target value of 300% with a maximum injection time of 100 ms. Data was acquired with the data-dependent "top20" method, isolating the 20 most intense ions and fragment them by higher-energy collisional dissociation (HCD) with applied normalized collision energy 30%. MS/MS resolution was 60000 (at 200 m/z), AGC target value of 100% with a maximum injection time of 100 ms. For the MHC-I presented peptides, in case of unassigned precursor ion charge states, or charge states of four and above, no fragmentation can be performed. Dynamic exclusion of fragmented m/z values from the further selection set for the 20s, and inject 6  $\mu$ L of the first sample again (for technical duplicate). Followingly, the system was washed with two standard wash runs, before loading any next biological sample.

### 2.1.3. Peptide identification and label-free quantification

The database quests were implemented adopting the MaxQuant package (version 1.6.12.0) [62, 63], to search the peak list against the human UniProt ([www.uniprot.org](http://www.uniprot.org)) database (downloaded on 12.08.2020 consisting of 75,093 entries) using the built-in Andromeda search engine [64]. Mass tolerances for precursor and product ions were set to 20 ppm and 0.02 Da, respectively. Searches were performed without enzyme specificity and variable modifications for deamidation (N, Q) and oxidation (M). Possible sequence matches were restricted to 7-25 amino acids (aa), the mass of a maximum peptide of 4600 Da. The initial allowed mass deviation of the precursor ion to 10 ppm, and the maximum fragment mass deviation was set to 10 ppm. Further, the statistical analysis was performed with Perseus software (version 1.6.10.45). The FDR (false discovery rate) level was 5%, and protein abundance calculated using normalized spectral protein intensity (LFQ intensity; label-free quantification) on MaxQuant software, as previously described



[65]. LFQ intensity values were set as Log<sub>2</sub> transformed, and peptide groups quantified in all runs were considered for further analysis.

## 2.2. Peptide structure optimization and their binding affinities with the TAP1-TAP2 transporters

### 2.2.1. TAP transporters, peptides, and the viral factors model generation

Adopting the “Hidden Markov method” implemented in the Phyre2 server (<http://www.sbg.bio.ic.ac.uk/phyre2>) sequence alignments with the known protein structures were generated and based on the principles of homology modeling [66, 67], the derived alignments were used to generate full protein tertiary structures. The intensive mode of Phyre2 successfully inserted the lacking segments in the TAP1, TAP2, and ICP47 structures (pdb id.: 5u1d) [18, 23], as well as generated the complete modeled tertiary structures of BNLF2a, CPXV012, UL49.5, and US6 viral factors. Based on the percentage identity and alignment coverage the following templates were selected to model the proteins structures: TAP1 (pdb id.: 5u1d-chain A and 5yke-chain B), TAP2 (pdb id.: 5u1d-chain B and 5ykf-chain-H), ICP47 (pdb id.: 5u1d), BNLF2a (pdb id.: 5zaz), CPXV012 (pdb id.: 2lq0), UL49.5 (pdb ids.: 6qan and 6qbj), and US6 (pdb id.: 1otc). The resulting modeled structures were subjected to energy minimization in Molecular Operating Environment (MOE; Chemical Computing Group Inc., Montreal, QC, Canada) [68] applying the CHARMM27 forcefield [69]. Furthermore, the tertiary structures for the 3957 peptides from immunopeptidome analysis (with and without IFN- $\gamma$  treatment), peptides from ATLAS (Altered TCR Ligand Affinities and Structures) database [48], and SIINFELK peptide [56] were constructed and energy minimized using the homology modeling algorithms incorporated in the MOE (Chemical Computing Group Inc., Montreal, QC, Canada) package. Relaxed modeled structures of the peptides, TAP transporters, and viral proteins were subsequently used in the protein-protein or protein-peptide docking pipelines.

### 2.2.2. Protein-protein docking, in silico point mutation, and virtual screening of peptides with the TAP transporters

The rigid body docking protocol from the MOE (Chemical Computing Group Inc., Montreal, QC, Canada) [68] was used to achieve the complexes of TAP1-TAP2 with each viral protein inhibitor (ICP47, BNLF2a, CPXV012, UL49.5, and US6). The CHARMM27 forcefield [69] was used for energy minimization, 500 conformations per protein-protein docking were generated and ranked or scored using the Generalized Born/Volume Integral (GB/VI, kcal/mol) [70] binding energies. Followingly, the refinement step based on molecular mechanics was carried out to analyse the best 100 poses of individual viral protein with the TAP1-TAP2 complex.

Peptides identified in the immunopeptidome analysis from the melanoma A375 cells (with and without IFN- $\gamma$  treatment), and other 57 antigenic peptides (56 from ATLAS database [48] and SIINFELK [56]) were screened against the TAP1-TAP2 complex using the MOE package (Chemical Computing Group Inc., Montreal, QC, Canada). The binding site in the TAP transporters for each peptide was identified through the “MOE site-finder” module, which computes the putative binding sites in a protein structure using a geometric approach with additional physico-chemical information such as; polarity or charge [68, 71-72]. The “Alpha Shapes” construction [68, 72] geometric method was used to compute the possible residues that can be considered for peptide docking to the pocket formed by the TAP1-TAP2 transporters. Following the determination of potential peptide binding sites in the TAP1-TAP2 complex, the protein-peptide docking was performed using the MOE (Chemical Computing Group Inc., Montreal, QC, Canada) package applying the CHARMM27 forcefield [69]. The MOE (Chemical Computing Group Inc., Montreal, QC, Canada) docking architecture formulates four different components involving; the generation of ligand-conformation, optional pharmacophore filtering, ligand placement with its scoring in the pocket, and flexible/rigid receptor and ligand refinement with re-scoring. For placement of peptide in the TAP1-TAP2 complex, the “Triangle Matcher” protocol was applied (the optimized TAP structures were defined as rigid, whereas the peptides were set as flexible allowing their structures a high degree of freedom) [68, 72]. Peptides are placed by superposing triplets of peptide atoms and

triplets or receptor site points; the poses that clash with the protein were subsequently removed. To treat peptide flexibility in the protein-peptide molecular docking, 1000 conformations of each peptide were produced from their placement in the TAP binding site and the resulting complexes were evaluated using the GBVI/WSA dG (kcal/mol) binding affinity scoring [70, 73], a forcefield based scoring function that calculates the free energy of binding of the peptide from a given position. Particularly, for the dataset containing 3957 immunopeptidome peptides, the best 5 optimized poses as ranked by binding affinity (GBVI/WSA dG) with the TAP were stored, and for the 57 peptides retrieved from the available crystal structures, the top 10 poses were saved. Furthermore, these best peptides influencing the binding energies and interactions with TAP proteins were considered for further evaluations.

Cancer derived mutations in the TAP1 and TAP2 proteins were subjected to the “Sequence Design” protocol of the protein design module in the MOE (Chemical Computing Group Inc., Montreal, QC, Canada) package. This pipeline computes the frequency with probability of amino acids at the residual mutation sites (mutation expression) [72]. The goal was to obtain the stability or binding affinity trade-offs, when peptide binds to wild-type and the mutated TAP transporters. In addition to applying this approach, all cancer hotspot residues were mutated using 20 other amino acids [A, R, N, D, C, Q, E, G, H, I, L, K, M, F, P, S, T, W, Y, and V]. The structural model for each single mutation was generated, the energy window was set to 10 kcal/mol, RMSD limit was 0.25 Å, and residues farther than 4.5 Å were kept fixed. The “LowMode MD” was used with default parameters to produce a thorough conformational ensemble [74]. The resultant TAP mutations significantly affecting the stability and peptide binding affinity, were further selected for the MD simulations [59].

### 2.2.3. Single nucleotide polymorphisms in the TAP1 and TAP2 genes

The Genome Aggregation Database (gnomAD) [75], an online resource containing genome and exome sequencing variants from diverse projects and investigators, was used in order to detect the distribution of the SNPs (single nucleotide polymorphisms) across the TAP1 and TAP2 genes. Variants of these genes were downloaded in CSV format and processed in R environment (version 3.6.3), using the g3viz package to plot the protein modifications occurring downstream of the genome mutations.

### 2.2.4. The molecular dynamic simulations and system setup

Initial orientation of the wild-type or mutant TAP1-TAP2 transporters embedded in the membrane, and in complex with peptide or the viral protein was defined using the PPM server ([https://opm.phar.umich.edu/ppm\\_server](https://opm.phar.umich.edu/ppm_server)) [76]. Optimizing the free energy of transfer from water to the membrane environment, the PPM server thoroughly cross-verify dozens of transmembrane and peripheral proteins and peptides [76]. Resulting positioned complexes were used as an input for the CHARMM-GUI membrane builder (<http://www.charmm-gui.org/?doc=input/membrane.bilayer>) [77], to prepare the membrane-embedded complexes. The CHARMM-GUI platform provides a series of CHARMM inputs necessary to generate membrane embedded complexes for MD simulations [77]. The supramolecular PLC is expressed in the endoplasmic reticulum, and the TAP1-TAP2 resides in the ER membrane to transport the peptide across the membrane [78]. Thus, to better understand the protein dynamics in the membrane environment, TAP complexes were embedded in a membrane containing 660 palmitoylcholine (POPC) lipids and 66 cholesterol molecules [79], accommodating the larger separation of TAP<sub>NBDs</sub>. The membrane composition was evenly distributed throughout both leaflets of the bilayer. Other parameters applied were; rectangle box type, tetragonal crystal type, and a water thickness of 22.5 Å on the top as well as on bottom of the system. A heterogeneous lipid bilayer was generated using the replacement method [77, 80], and the distance-based algorithm was used as an ion-placing method. The following 24 TAP-membrane complexes were further investigated using the MD simulation technique: apo-form (TAP1-TAP2 and pep18-alone), with viral protein (TAP1-ICP47-TAP2, TAP1-BNLF2a-TAP2, TAP1-CPXV012-TAP2, TAP1-UL49.5-TAP2, and TAP1-US6-TAP2), with

peptides (TAP1-SIINFEKL-TAP2, TAP1-pep18-TAP2, TAP1-pep20-TAP2), with mutations (TAP1<sub>E446K/W</sub>-TAP2, TAP1<sub>V437F/I</sub>-TAP2, TAP1<sub>R372Q</sub>-TAP2, TAP1-TAP2<sub>D370N/W</sub>, TAP1-TAP2<sub>G208F/S</sub>, and TAP1-TAP2<sub>R373H</sub>), and mutation+peptide (TAP1<sub>R372Q</sub>-pep18-TAP2, TAP1<sub>R372Q</sub>-SIINFEKL-TAP2, TAP1-pep18-TAP2<sub>R373H</sub>, and TAP1-SIINFEKL-TAP2<sub>R373H</sub>).

The MD simulations were performed using the NAMD package [81] with CHARMM36 forcefield [82-84], and the TIP3P [85] water model. The particle-mesh Ewald method [86] was used to treat long-range electrostatics with a grid spacing of 1 Å, and a cut-off of 12 Å was used for van der Waals interactions. The force based switching was used with a switching distance of 10 Å. Periodic boundary conditions (PBC) were applied with constant pressure and temperature (NPT) ensemble to avoid finite size effects. Langevin dynamics [87] was used to maintain constant temperature with a damping coefficient of 1 ps<sup>-1</sup>. The Nose-Hoover Langevin piston method [88] was applied to control the constant pressure with a decay period of 50 fs with a damping timescale of 25 fs. SHAKE algorithm [89] with a time step of 2 fs was used to constrain all the non-polar bonds involving hydrogen atoms. Equilibration of the system was performed for 10 ns at 303.15 K and the equilibrated systems were subsequently used to perform MD production runs for 100 ns at 303.15 K. The visual molecular dynamics (VMD) [90], MOE (Chemical Computing Group Inc., Montreal, QC, Canada), and BIOVIA Discovery Studio visualizer (Dassault Systèmes, BIOVIA Corp., San Diego, CA, USA) packages were used to analyse the molecular dynamics trajectories.

### 3. Results and discussions

A systematic immunopeptidome workflow was implemented, and a set of peptides presented over the MHC-I molecules in the melanoma A375 cells were isolated (Figure 1c). Based on the sequences of the MHC-I bound peptides, their tertiary structures were generated using the homology modeling techniques; in order to analyse the pattern of binding as well as peptide translocation through TAP transporters. Furthermore, the binding and dynamics of viruses with TAP complex as well as the cancer mutations targeting the TAP transporter process were analyzed.

#### 3.1. Human melanoma cells immunopeptidome, and screening of peptides against the TAP transporters

The melanoma A375 cells were grown *in vitro* under typical cell culture conditions, and the cells characterized with and without iIFN- $\gamma$  treatment in order to define the IFN- $\gamma$  induced changes on the MHC antigen processing and presentation pathway (Figure 1c). The distribution and length of the identified peptides from the both conditions (Figure 2a and Table S1-S3), suggest that there were more peptides identified in the IFN- $\gamma$  treated cells (3081 peptides, Table S1) compared to that of the non-treated (termed as wild-type in this study) cells (1968 peptides, Table S2). About 1104 peptides were common in IFN- $\gamma$  treated and non treated samples, whereas 1974 peptides were found on IFN- $\gamma$  treated cells and 863 peptides only in the wild-type (non-treated) (Figure 2b-2f). Exclusively, in the IFN- $\gamma$  treated samples, a few self-peptides from the TAP1 (AALPAAALW, LLYESPERY, RSLQENIAY, RTALPRIF, SAMPTVRSF, and TEVDEAGSQL) and TAP2 (YLHSQVVSV) were identified (Figure 2g).

Interestingly, the immunopeptidome data highlights that the majority of MHC-I associated peptides have a length distribution of 9 or 10 mers, and a few peptides around 15-mer in length (Figure 2d). Particularly, the MHC-I antigen processing involves proteasome-mediated protein degradation as well as TAP-mediated peptide transport, and these processes can generate and handle peptides longer than the canonical 8-10 aa (amino acids) long [91, 92]. Stryhn et al. [92] examined the size dependence of peptide binding to MHC-I as well as stimulating T-cells, in proteolytically controlled assay systems by systematically extended the N- and/or C-terminals of optimally sized peptides. Their findings support the consensus view that MHC-I binding and T-cell recognition tends to focus on short well-defined peptides. However in some cases, longer peptides can also bind to MHC-I and such extensions may be accommodated by protrusion out of the MHC-I and can potentially be recognized by T-cells [92]. In some cases the T-cell can detect the identity of

the extension (that it could be part of the specificity of the T-cell immune response) and such extensions may play a physiological role [92]. The crystal structures of peptide bound MHC-I molecules argue in the favor of peptide-size restrictions and suggest that when the anchors are appropriately positioned, slight variations in size can be accommodated through zigzagging or bulging in the middle [92, 93]. However, structures involving a protruding C+1 extension has been determined in which, the C-terminal residue was found to extend up and out of the F-pocket and the corresponding side chains of MHC-I was found to be re-oriented to accommodate the peptide extension [92]. This explains the flexibility of the otherwise apparently closed binding cleft of the MHC-I allowing for binding of different peptide sizes as long as the binding energy is sufficient [92]. Moreover, it has been shown that naturally bound peptides eluted off the MHC-I spans a size range from 6-33 residues, although the majority (~ 80%) were of the canonical 8-11 aa [92, 94, 95]. The proteasome generates peptides varying in size from 4-24 aa, and it has been estimated that ~30% of the peptides are 8 aa or longer. The TAP transporter can translocate peptides up to 40 residues long, though 8-13 residues long peptides are transported most efficiently [92, 96].

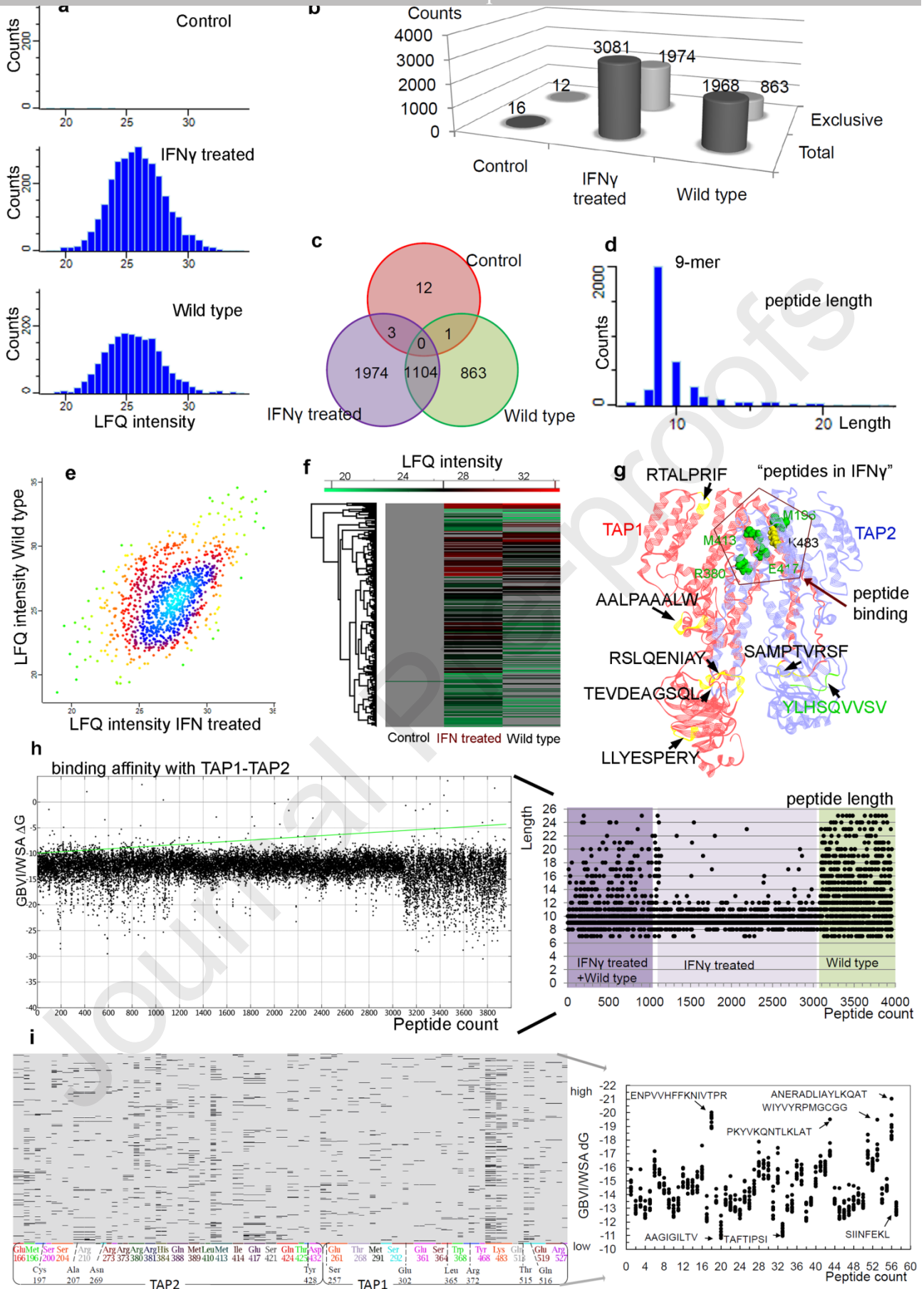


**Figure 2.** Comparative immunopeptidome analysis. **(a)** Logarithmized log<sub>2</sub>(x) data, after reverse filtering the rows using categorical columns, for the MHC-I peptide presentation from the control,

IFN- $\gamma$  treated, and non-treated (termed as wild-type in this study) samples. **(b)** Peptide counts per sample, as well as the exclusive MHC-I peptides for a particular sample. **(c)** Venn diagram representing the common and unique peptides in all three/two respective samples. **(d)** Length distribution of the MHC-I peptide that were identified in all three samples (control, IFN- $\gamma$  treated, and untreated/wild-type). **(e)** and **(f)** Scatter plot and heat map describing the LFQ intensities between wild-type vs IFN- $\gamma$  treated samples. **(g)** TAP1 and TAP2 peptides identified (presented over MHC-I molecule) only in the IFN- $\gamma$  treated samples, labeled in black (marked yellow) are from TAP1 and in green are from TAP2. **(h)** Identical 3957 peptides from three samples (control, IFN- $\gamma$  treated, and non-treated) were screened against the TAP1 and TAP2 transporters. Right panel represents the peptide length (differentiated according to the samples), and the left panel represents particular peptide binding affinity with TAPs (five different conformations per peptide). In panel **g**; residues K483 (TAP1) and M196, R380, M413, and E417 (TAP2) were found commonly interacting with the 3957 peptides (from control, IFN- $\gamma$  treated, and non-treated), docked with TAP1 and TAP2 are highlighted (yellow from TAP1 and green from TAP2). **(i)** Barcodes represent (left panel) fingerprint analysis of peptides (from the ATLAS database [48]) forming interactions with TAP1 and TAP2 proteins (Table S4), and the selected peptide fingerprints as a matrix (one row per entry, one column per fingerprint bit) in which a set bit is drawn as a black rectangle. X-axis shows the residue numbers that correspond to each group of fingerprint bits, and is coded with an arbitrary sequence of colors. The scattered plot (right panel) represents the binding affinity of each peptide against TAP transporters. Peptides with the highest and lowest binding affinity are highlighted, and few were selected for MD simulations in order to examine their kinetics. The plot (right panel) presents a binding affinity of 10 conformations for each peptide against the TAP1-TAP2 transporters.

*In silico* virtual screening of peptide datasets was performed against the TAP1-TAP2 transporters and the resultant TAP-peptide complexes were ranked by the docking score (GBVI/WSA dG, kcal/mol; Figure 2h and 2i). The MHC-I peptide having the length of 8, 9, or 10 mers shows a binding affinity between -10 to -15 kcal/mol (GBVI/WSA dG; Figure 2h) with the TAP1-TAP2 transporter. Peptides having a length of 14-26 amino acids formed binding affinities with the TAP transporters in the range of -20 to -25 kcal/mol (GBVI/WSA dG; Figure 2h). Overall, the peptides identified from the IFN- $\gamma$  treated samples exhibited less affinity with the TAP proteins, compared to the peptide from the untreated cells. In addition, the binding affinity difference of peptides from IFN- $\gamma$  treated and untreated samples exhibited a correlation with the length of peptide, i.e. and peptides from IFN- $\gamma$  treated have short length (peptides 1100-3100 in Figure 2h and Table S5), whereas peptides from untreated are comparatively longer (peptides 3100-3957 in Figure 2h and Table S5). Based on the peptide binding affinities with TAP transporters and the higher number of 9-10 mers identified in the immunopeptidome (Figure 2d and 2h), it could be proposed that peptides having weak binding affinity with the TAP1-TAP2 transporters could exhibit faster transport from the cytosol to the ER. Moreover, it has previously been reported that TAP transporters can translocate 8-13 residue peptides most efficiently [92, 96, 97]. The IFN- $\gamma$  treated cells had a higher number of peptides identified compared to the untreated, suggesting that upon inducing immunity, a majority of shorter length peptides have a lower TAP1-TAP2 binding affinity (Figure 2d and 2h). In addition, more residues (M196, R380, M413, and E417) from TAP2 were involved in interacting with the peptide, and fewer peptides were detected from TAP2 itself, whereas the reversed was observed for the TAP1 (only residue K483 binds to the peptide; Figure 2g). These peptide interacting TAP residues were previously reported [15].

To further investigate and validate the findings, peptide datasets from the ATLAS database [48] were retrieved alongside the immunopeptidome dataset from the melanoma cells. For these peptides the structures of each TCR-peptide-MHC complex is known, and were screened against the TAP1-TAP2 transporter model (Figure 2i, S1, S2, and Table S4). Analysis of the immunopeptidome data and peptides from ATLAS database [48] (Figure 2h and 2i) correlated with each other, in terms of binding affinity versus peptide length data (Figure S3a and S3b). Most

peptides with 8 or 9 mers exhibited lower binding affinity compared to the longer peptides (Figure S3c and S3d). TAP1 and TAP2 residues forming the interactions with the studied set of peptides were identified, which highlights an overlap between immunopeptidome peptides and peptides from ATLAS database (Figure S3a and S3b). Additionally, the binding conformations of a few peptides showing highest and least affinity to TAP were: pep56 (ANERADLIAYLKQAT) -21.03 kcal/mol, pep18 (ENPVVHFFKNIVTPR) -20.02 kcal/mol, pep53 (WIYVYRPMGCGG) -19.49 kcal/mol, pep43 (PKYVKQNTLKLAT) -19.52 kcal/mol, pep57 (SIINFEKL) -13.44 kcal/mol, pep20 (AAGIGILTV) -12.46 kcal/mol, and pep33 (TAFTIPSI) -11.87 kcal/mol. Among which the molecular dynamics of the pep18, pep20, and SIINFEKL (8-mer model) peptides with the TAP1-TAP2 transporters were further analysed (Figure 2i and S2).

### 3.2. Scaling effects of viral proteins and somatic mutations on the TAP transporters

The modeled viral protein structures were screened against the predicted active sites, and the data suggests that all selected viral protein inhibitors targeted the peptide transport pockets of TAP proteins through different possible interactions. The binding free energy reports (GBVI/WSA dG; kcal/mol) and binding mode of viral proteins to TAP structure are shown in Figure 3a. Among different viral proteins screened against the TAP1-TAP2 complex, the ICP47 protein formed the highest affinity (-108.18 kcal/mol), and in the second position is the BNLF2a protein with binding affinity of -90.08 kcal/mol, whereas the proteins CPXV012, US6, and UL49.5 obtained almost similar affinity (-81.71 kcal/mol, -85.27 kcal/mol, and -85.28 kcal/mol, respectively). The binding mode of viral protein inhibitors to TAP correlates with the proposed models [38]; four out of five viral proteins targeted the helical regions (Figure 3a) of TAP1 and showed a similar pattern of blocking the peptide translocation cavity of the TAP transporter. The US6 protein binds to both TAP transporters at the loop regions toward the ER lumen, with almost similar affinity (Figure 3a).

Single nucleotide polymorphisms are one of the most common forms of genetic variation, and a large number of human genes associated with viral infections comprise SNPs [98]. For both TAP1 and TAP2 transporters, the SNPs were identified and to assess the polymorphisms, the residues from TAP transporters involved in binding with the viral proteins (within 8 Å; BNLF2a, CPXV012, ICP47, US6, and UL49.5) were traced (Figure 3b and Table S6-S7). Overall, both TAP1 and TAP2 transporters behave differently when correlating SNPs to that of the TAP interacting residues with viral proteins. Exclusively for TAP1, the frequency of SNPs was found lower in the regions binding to viral proteins (Figure 3b). These data suggest that the viruses may aim for the most conservative TAP1 regions (Figure 3b and Table S6-S7). On the contrary, for TAP2 the frequency of SNPs was found higher in the regions binding with viral proteins (Figure 3b). Like the SNPs in the TAP transporters (Figure 3b), a similar trend was observed in the analysis of cancer-associated mutations in both TAP transporters, i.e. for TAP1 protein regions with less cancer variants were targeted by viruses, whereas in TAP2 highly mutated regions were involved in binding with viral protein (Figure 1e and 3b).

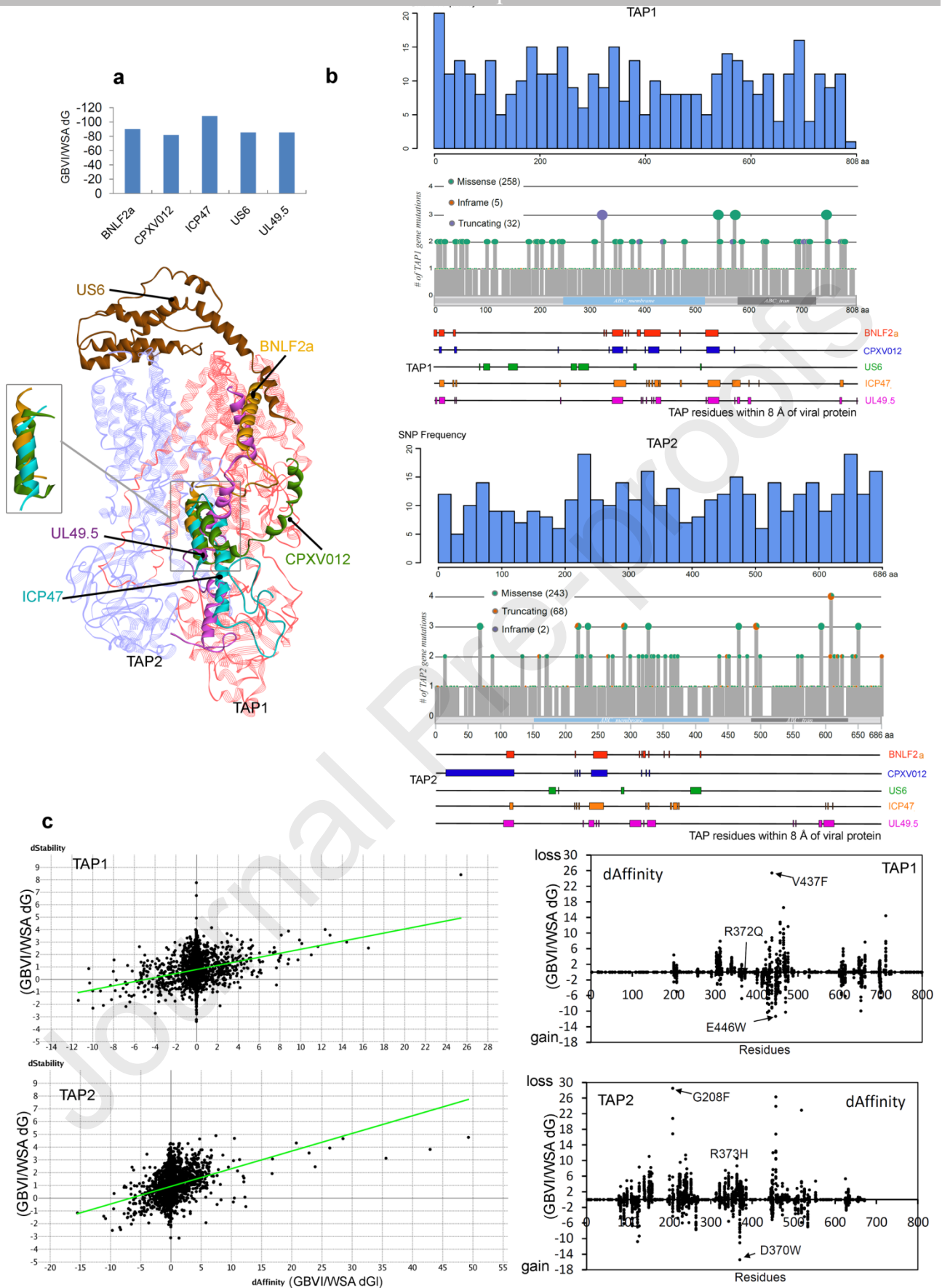


**Figure 3.** *In silico* screening of viral proteins, peptides, and cancer-associated mutations on the TAP1-TAP2 transporters. **(a)** Viral proteins (BNL2a, CPXV012, ICP47, US6, and UL49.5) docked with the TAP transporters, and the binding conformations for each studied viral components



resembles almost a complementary state (Figure 1b), as well as proposed in different studies [18, 23, 38]. In addition, 4 out of 5 viral proteins assembled a similar conformational pattern to block the peptide transportation cavity in TAP proteins. **(b)** Lollipop plots for the TAP1 and TAP2 gene mutations, colours in the figure represent different types of polymorphism. In the top panel of each lollipop plot, a bar plot represents the cumulative frequency of mutations for each 20 amino acids. On the bottom panel, the regions of interaction from the TAP1 and TAP2 proteins with the viral proteins are represented in different colours (identified in virtual screening; Figure 3a). **(c)** Mutational landscape of TAP1 and TAP2 proteins, datasets of cancer variants from COSMIC (cancer.sanger.ac.uk) and cBioPortal (www.cbioportal.org) were screened with the TAP transporters tracing their change in stability (GBVI/WSA dG, kcal/mol) and affinity (GBVI/WSA dG, kcal/mol) upon mutation (applying residue scan methodology in MOE [68]). In addition to the cancer-associated mutations from COSMIC (cancer.sanger.ac.uk) and cBioPortal (www.cbioportal.org), each amino acid was mutated with other 20 amino acids [A, R, N, D, C, Q, E, G, H, I, L, K, M, F, P, S, T, W, Y, and V] to search for mutations that change the binding affinity (GBVI/WSA dG, kcal/mol). The left panel describes a comparison of change in structural stability with change in binding (TAP1-TAP2) affinity upon introducing each amino acid variant. The right panel scatter plot describes the effects of mutant residues (from TAP1 or TAP2) on the protein-protein binding affinity (GBVI/WSA dG, kcal/mol).

Mutations in a protein may affect its structural stability, disrupt protein interactions, render proteins non-functional, and potentially promote tumor progression [72]. Therefore, along with the cancer-associated variants from the TAP transporter retrieved from the COSMIC (cancer.sanger.ac.uk) and cBioPortal (www.cbioportal.org), and screened for change in structural stability and binding (TAP1-TAP2) affinity, these hotspots regions or amino acids were also screened by mutated with the other 20 amino acids (Figure 3c). The findings suggest that point mutations in either TAP1 or TAP2 are sufficient to alter the protein-protein interactions, which can significantly affect the peptide binding or the peptide transport process (Figure 3c). Screening (fingerprint) analysis indicate that TAP1 or TAP2 peptide interacting interface (Figure 2i), are also found mutated in different cancer types. Such residue variants are; R372Q, S364R, S364I, Q516K, E519K, and R527K from TAP1 protein, and E166G, E166K, M196V, R210L, R373H, and S200F from TAP2 (Figure 3c). Considering the peptide binding region [15] and protein-protein interface, cancer mutations and their binding affinity, TAP1<sub>R372Q</sub> and TAP2<sub>R373H</sub> were further studied by MD simulations. In addition, the cancer derived mutants inducing highest (best) and lowest binding affinity were selected for MD simulation analysis: TAP1<sub>V437I</sub> (-7.92 kcal/mol), TAP1<sub>V437F</sub> (25.43 kcal/mol), TAP1<sub>E446K</sub> (-5.99 kcal/mol), TAP1<sub>E446W</sub> (-11.35 kcal/mol), TAP2<sub>D370N</sub> (-1.23 kcal/mol), TAP2<sub>D370W</sub> (-15.43 kcal/mol), TAP2<sub>G208S</sub> (1.62 kcal/mol), and TAP2<sub>G208F</sub> (28.53 kcal/mol; Figure 3c).

### 3.3. Viral components with similar modulatory actions towards the TAP transporters

Viral proteins (for example; BNLF2a, CPXV012, ICP47, US6, and UL49.5) can significantly manipulate the peptide transport process by binding directly with the TAP1 or TAP2 transporters. Therefore, to understand the molecular recognition of the TAP1-Virus-TAP2, and particular the different viral proteins (BNLF2a, CPXV012, ICP47, US6, and UL49.5) we simulated their interactions with the TAP transporters (Figure 4a, represents TAP1-ICP47-TAP2 complex). Evaluating the stability for simulated systems solving the RMSD (root-mean-square deviation of all non-hydrogen atoms) equation, suggests that the majority of the viral protein predominantly destabilizes TAP1 (Figure 4b), compared to that of TAP2 alone. Particularly, for TAP1 such a visible difference was detected for UL49.5 and BNLF2a, whereas for TAP2 the UL49.5 induced the highest fluctuation and BNLF2a the least (Figure 4b). The apo-form of TAP1 showed a persistent RMSD plot (~8 Å) during the 100 ns of MD simulations, whereas the TAP2 showed a slightly increasing flexibility over time that stabilized between ~70-100 ns (Figure 4b). The RMSD findings

suggest that the UL49.5 exhibited the highest fluctuations and BNLF2a was the most stable of the viral proteins (Figure 4b).

Moreover, solving the RMSF (root mean square fluctuation) equation over C $\alpha$  atoms of each amino acid revealed a similar nature for both TAP transporters, i.e., a majority of residues in the apo-system were more stable as compared to the viral-bound systems, except for some residues in TAP2 (for example 390-410 aa; Figure 4c). Such behavior of TAP2 residues from RMSF correlated with the RMSD data which showed a slightly increasing flexibility of TAP2 over time (Figure 4b). The dynamics of the TAP1/2-viral protein complex dynamics suggest that upon binding of the viral proteins, an allosteric effect inducing increased amino acid fluctuations in several regions of both transporters were indicated (Figure 4c). Interestingly, the TAP1 peptides (97RTALPRIF104, 206AALPAAALW214, 432SAMPTVRSF440, 653RSLQENIAY661, 694TEVDEAGSQL703, and 744LLYSPERY752) and TAP2 peptide (541YLHSQVVSV549) presented on MHC-I IFN- $\gamma$  treated melanoma cells (Figure 2a), originates from the highly fluctuating regions directly interacting with viral factors or allosterically affected by viral binding (Figure 4c).

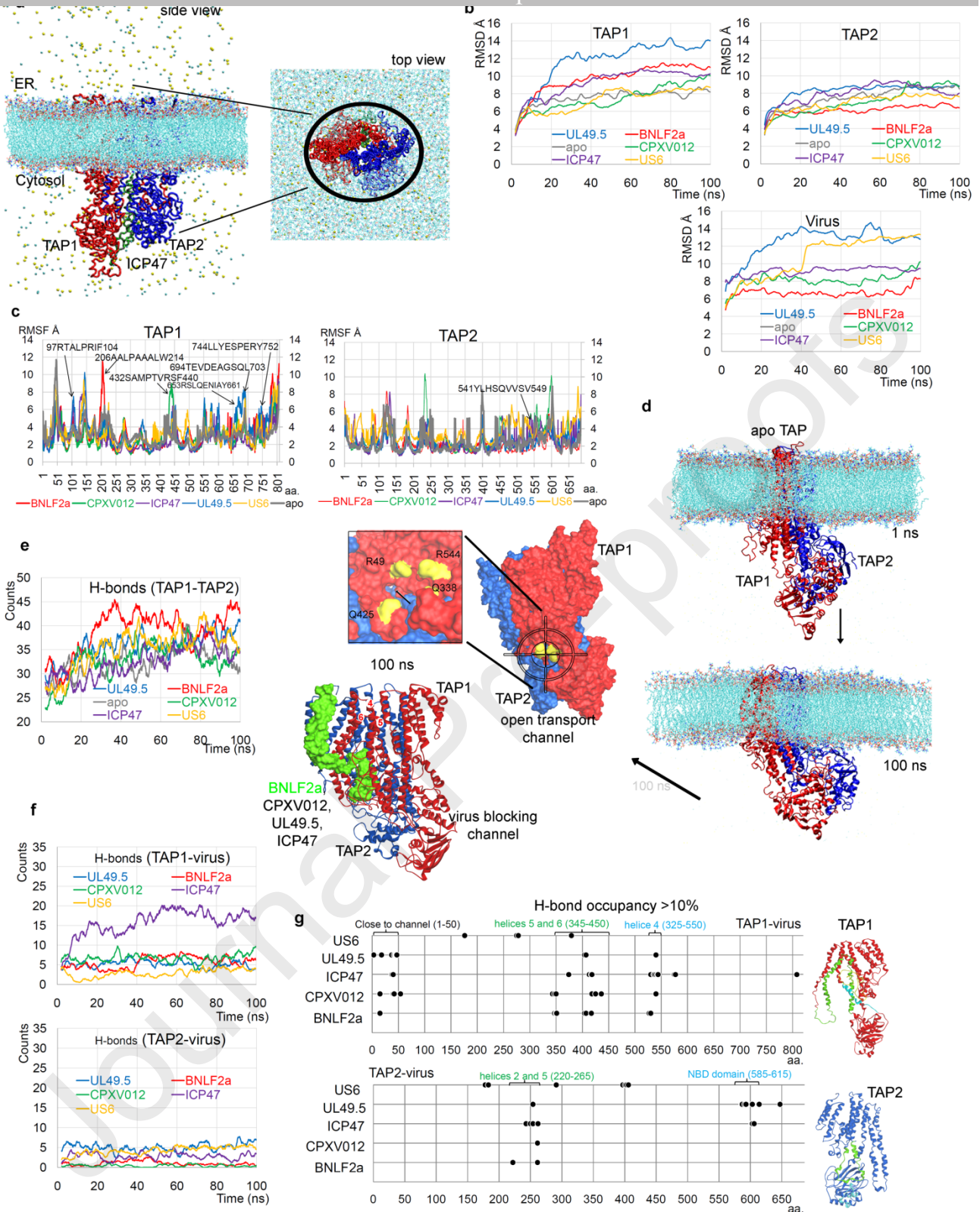


**Figure 4.** The binding interfaces of different viral proteins (BNLF2a, CPXV012, ICP47, US6, and UL49.5) with the TAP1 and TAP2 transporters. **(a)** One molecular dynamic cell in periodic boundary conditions (for example, the TAP1-ICP47-TAP2 complex), which includes proteins, water, and ions. **(b)** RMSDs of the TAP transporters from the MD simulations, and the bottom panel describes the RMSDs of viral factors. **(c)** RMSFs of individual amino acids from both TAP transporters. **(d)** Structural dynamics of the TAP1-TAP2 transporters representing the tilt movement of the TAP1/2<sub>NBD</sub> domains forming an entry gate or transport channel open toward the cytosol. In addition, the majority of the studied viral proteins in this work were found interacting with the

passage or open transport channel which could block the peptide from invading the transport channel. TAP1 helices (helix\_4; 501-544 aa, helix\_5; 338-376 aa, helix\_6; 384-425 aa) forming an open cytosolic passage and binding with the viral proteins are labeled. **(e)** The intermolecular hydrogen bond interactions formed between the TAP1 and TAP2 proteins during the MD simulation time course and with occupancy  $\geq 10\%$ , in the presence and absence of different viral proteins. **(f)** Hydrogen bond interactions between the viral protein and the TAP transporters. **(g)** Residues from TAP1 or TAP2 involved in binding viral proteins with occupancy  $\geq 10\%$ , and the right panel represents the position of these regions over the protein structure.

The structural dynamics of the TAP1-TAP2 complex in the presence and absence of a viral proteins revealed that, in all simulated systems the TAP<sub>NBD</sub> domains formed a tilt movement toward the cytosol membrane (Figure 4d and Videos S1, S2). Such displacement of the TAP<sub>NBD</sub> domains creates a passage in the transport channel formed by TAP1 (helix\_4; 501-544, helix\_5; 338-376, helix\_6; 384-425) and TAP2 (helix\_5; 249-289, helix\_6; 294-344); opened towards cytosol (Figure 4d). From these data it may be proposed that the opening or closing of the cytosolic passage by the TAP transporters (TAP<sub>NBD</sub> domains) can be associated with ATP hydrolysis, and thus, resulting in the peptides being directly presented to the PLC complex. This cytosolic “open-state” transport channel of the TAP proteins, may intake peptides from cytosol-towards-ER and was targeted by 4 (BNLF2a, CPXV012, ICP47, and UL49.5) out of 5 studied viral proteins blocking the transport channel (Figure 4d and S4).

Viral proteins have increased the protein-protein intermolecular interactions between TAP transporters compared to that of the apo-system (Figure 4e and Table S8). A slight difference is observed concerning the viral proteins when interacting with TAP1 or TAP2, i.e., BNLF2a, CPXV012, and ICP47 formed a higher number of interactions with TAP1, whereas UL49.5 and US6 shared relatively equal interactions with both transporters (Figure 4f). These intermolecular transporter-viral interactions (Figure 4f) together with the SNPs data and cancer mutations (Figure 1 and 3), suggest that in the case of TAP1 protein regions with lower SNPs frequency as well as a few cancer variants was found making higher interactions with viral factors. On the contrary viral factors binds highly mutated TAP2 regions. Long lasting interactions  $\geq 10$  ns between TAP-viral proteins were identified and are presented in Table S9. Particularly, a higher number of residues from TAP1 were involved in the interactions with viral components, compared to the TAP2 gene (Table S9). TAP1 amino acids from helices 4, 5, and 6 (residues range 345-450 aa and 325-550 aa), as well as from residue range 1-50 aa located close to the transport channel were found to interact with viral factors (Figure 4g and Table S9). Additionally, the TAP2 residues in range 220-265 aa (from helices 2 and 5) and 585-615 aa (TAP<sub>NBD</sub> domain) were involved in binding viral proteins (Figure 4g and Table S9). Several amino acids from TAP1 or TAP2 were found in common when interacting with BNLF2a/CPXV012/ICP47/UL49.5 viral factors. Exceptionally, the US6 protein have a unique interacting residues from the transporters that were not identified in other studied TAP-virus complexes (Figure S4b). For the TAP1 protein, residue E540 was found interacting with three different viral proteins (UL49.5, ICP47, and CPXV012), and residues D15/R347/E350 and R40/E418/E536 were found common binding with BNLF2a/CPXV012 and ICP47/CPXV012, respectively. From the TAP2 transporter, residues S254 and K603 were involved in binding with the ICP47 and UL49.5 viral factors (Figure S4b).

### 3.4. Distinctive behavior by TAP transporters to drive short vs long peptide antigens towards the ER lumen

To understand the kinetics or movements of the peptides through TAP transport tunnel, the MD simulations were performed for three different peptides that vary in lengths; pep18 (15 aa), pep20 (9 aa), and SIINFEKL (8 aa). The deviation and fluctuation plots (Figure S5) explain that all systems have reached their stability, and in particular, TAP1 showed more flexibility in complex with longer peptide; pep18 (Figure S5a). Individual amino acid fluctuations for the TAP proteins suggest that the presence of shorter peptides (pep20 and SIINFEKL) induced stability in the

transporter, compared to pep18 peptide (15-mer; Figure S5b). Moreover, the self-peptides of TAP1 and TAP2 identified in the immunopeptidome data (Figure 2) were highly flexible region in viral bound systems (Figure 4b), the majority of these regions lacked such fluctuation differences in the peptide-bound systems (Figure S5a).

The structural movements of the TAP transporters towards the ER lumen, suggests that the TAP transporters can have two separate cytosol-to-ER peptide passages (Figure 5a and 5b). Figure 5b, represents four helices from each TAP protein that can be involved in the placing of the peptides toward the ER lumen, and to measure the opening or closing of the transportation cavity the area based on the C $\alpha$  (C-alpha) atoms from the respective helices were identified; area 1 (TAP1; S496 and S501, TAP2p; D185) and area 2 (TAP1; ASP278, TAP2; S393 and S408) (Figure 5b, 6, and 7). Particularly, for the SIINFEKL (8-mer) that is smaller in length compared to the pep18 (15-mer), only the passage formed by two helices from each TAP1 and TAP2 was found open. Passage 1 or area 1 is in the closed conformation, whereas area 2 is in the open state that could allow the SIINFEKL peptide to be transported. In the presence of pep20 (9-mer), a moderate opening as well as closing state of the transport passage was observed, i.e., during the first 25 ns only area 2 formed an open-state conformation, whereas at the end of MD simulation (~85-100 ns), only area 1 formed an open-state (Figure 5a and 5b). However, the pep20 system comparatively had less differences between both areas as that of the SIINFEKL system. This could be a consequence of a different sequence composition of peptides that can have different interactions with TAP transporters. For the system with pep18, both passages formed by 8 helices (4 from each TAP1 and TAP2) are in the open state. These differences in conformations by TAP correlates well with the areas computed as shown in Figure 5a, i.e., area 1 for systems with SIINFEKL peptide reaches upto 250 Å<sup>2</sup> and area 2 is mainly limited to 90 Å<sup>2</sup>. On the contrary, with pep18, both area 1 and area 2 are found in the open state, which ranges from ~110-300 Å<sup>2</sup> (Figure 5a). Overall, based on the areas computed on TAP transporter towards ER-opening, a difference in the transport of longer vs shorter peptides was identified. However, the sequence composition of the peptide can also affect the rate of such conformation by the transporters (Figure 5a and 5b).

Additionally, there are efforts made to understand the mode of substrate translocation and transports by different ABC exporters, and the most common proposed/suggested is the IF-to-OF (inward- to outward-facing) conformational transition/switch [99-102]. Particularly, the IF-to-OF switch has been confirmed by the cryo-electron microscopy (cryo-EM) [100] for the heterodimeric TmrAB (Thermus thermophilus multidrug resistance proteins A and B); a TAP structural homolog which also can restore antigen processing in human TAP-deficient cells [100, 102]. In the TmrAB transporters during the inward-facing (IF state; TmrAB allows binding of nucleotides and peptide, which has a closed state at the top) conformations of the NBD domain can obtain a wide distance and in the outward-facing (OF state; abolished peptide binding and nucleotide exchange, which opens in the top) the conformation the NBD domains is represented in a close contact. Hence, to analyze such conformational switch movements by the NBD domains (TAP1<sub>NBD</sub> 550-808 aa and TAP2<sub>NBD</sub> 450-686 aa) from the TAP1 and TAP2 heterodimer, we measured the distance centre of mass between NBD domains from both TAP transporters in the presence or absence of the peptide. The dynamic behavior of the apo-systems; wild-type (Figure 4d) and mutated (Figure 4c), have shown a closed conformation towards the ER lumen (IF conformation; NBD has wide distance), whereas in the presence of peptide the transport channel is found in the open state towards the ER lumen (OF conformation, NBD has close contact; Figure S6). The distance between NBD domains in the wild-type apo-system remained higher (~42.31 Å) throughout the MD simulations (Figure S6), whereas in the presence of peptide the distance dropped to 34.03 Å from 42.31 Å. These findings correlate with the area computed for the transport channel (Figure 5a), that when the channel opens towards the ER lumen, the NBD domain forms a closed conformation (Figure S6), as observed in the IF-to-OF conformational switch for other ABC transporters [99-102].

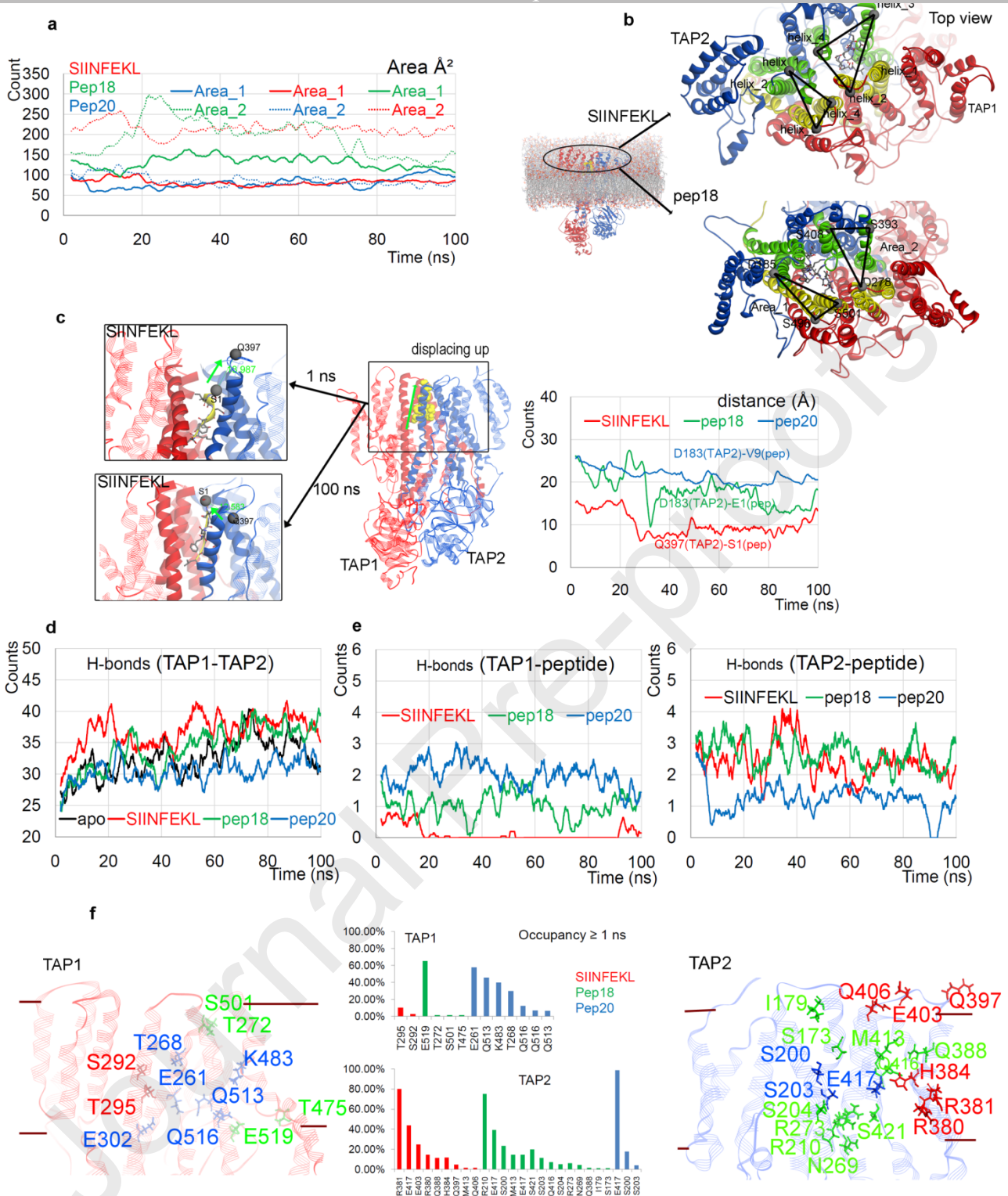


**Figure 5.** The binding interface with dynamics of the pep18, pep20, and SIINFEKL peptides with TAP transporters. **(a)** and **(b)** Area computed considering the four helices each from TAP1 or TAP2 involved in forming the passage for the transportation of the peptide, as represented in **b**. C-alpha (CA or C $\alpha$ ) atoms coordinates of each residue were traced over time evaluation of the molecular dynamics; area 1 = TAP1 (SER496 and SER501) and TAP2 (ASP185) and area 2 = TAP1 (ASP278) and TAP2 (SER393 and SER408). Helices residues range; TAP1 = 256-275 aa (helix\_1), 281-329 aa (helix\_2), 451-495 aa (helix\_3), 501-544 aa (helix\_4), and TAP2 = 145-181 aa (helix\_1), 189-226 aa (helix\_2), 356-395 aa (helix\_3), and 405-440 aa (helix\_4). **(c)** The displacement of the peptides from the centre of the transportation cavity towards the ER lumen. In addition, to measure the movements of peptides in the transport tunnel, distance between the TAP2

(from top, toward ER lumen) and peptide C $\alpha$  atoms were computed for the selected amino acids; Q397(TAP2)-S1(SIINF EKL), D183(TAP2)-E1(pep18), and D183(TAP2)-V9(pep20). **(d)** and **(e)** Intermolecular hydrogen bond interactions between the TAP1 and TAP2 (protein-protein), and TAP1/TAP2-peptide, respectively. **(f)** TAP residues involved in forming hydrogen bond interactions with pep18, pep20, and SIINF EKL peptides with an occupancy of  $\geq 1\%$ .

To understand the kinetics of the peptide inside the TAP cavity, the distance between the TAP residue from the top or surface open towards the ER lumen and the residue from the peptide heading upwards in the cavity was traced (Figure 5c). The distance between Q397(TAP2)-S1(SIINF EKL) dropped from 15 Å to 5 Å (Video S3), suggesting a peptide upward displacement mechanism. A similar trend in the drop of distance between TAP amino acids from top and from the peptide residue was observed for pep18 and pep20 (Figure 5c and Video S4). Comparing the drop down of distances with each peptide, it was observed that a shorter peptide (SIINF EKL) has initiated movements relatively earlier compared to the longer peptide (pep18; Figure 5c). Considering the conformational dynamics and visualizing such distance movement by the peptide in the channel, it is suggested that the actual movement is coming from the peptides (figure 5c).

Hydrogen bonds between TAP1-TAP2 in the presence of the peptide (Figure 5d), suggest that a higher number of interactions occur when there is an increase in the movement (opening of the cavity as shown in Figure 5a and 5b). Particularly, the system with the SIINF EKL and pep18 peptides obtained more protein-protein interactions compared to that of the apo-form and pep20 system (Figure 5d). In addition, higher numbers of arginine-glutamic acid residue pairs were observed forming the TAP1-TAP2 interaction interface (Table S10). Furthermore, the interactions between the peptides and TAP1/2, suggests that SIINF EKL and pep18 obtained few interactions with TAP1 but more interactions with TAP2, whereas the opposite behavior was observed for pep20 (Figure 5e). These findings demonstrate that when the TAP1-TAP2 cavity is in its open conformation towards the ER lumen and the SIINF EKL peptide reaches the top of the TAP transport channel (as shown in Figure 5c), peptide mostly interact with TAP2 (Figure 5e). It can also be proposed that TAP1 can be responsible for pulling the peptide from the cytosol and positioning it in the TAP cavity. For each peptide systems (pep18/pep20/SIINF EKL) different amino acids from TAP1 were involved in binding with peptides, and a similar behavior was observed for TAP2 but with some exceptions (Figure 5f and Table S11). The S203, Q388, and M413 amino acids from the TAP2 proteins were found to be involved in common in at least two peptide systems (Figure 5f and Table S11). The review by Elisa et al. [8] described a 3D homology model of the human TAP complex based on TmrAB along with essential residues necessary for the antigen processing by TAP [8, 103]. Comparing such residues with our peptides screened against the TAP transporters and molecular dynamics data (occupancy > 1 ns), suggest several common residues traced by Elisa et al. [8, 103]. Particularly, the TAP1 E519 and TAP2 R380 residues form high occupancy interactions 65.03 % and 14.59 % (Table S11) with the peptides, respectively. Additionally, TAP1 residues T475, K483, S501, Q513, Q516, and E519 (Table S11) form high occupancy interactions with the studied peptides residing into the peptide binding regions P435-M480 and Q513-R547 determined by mutation studies [8, 103]. Similarly, the TAP2 residues R380, R381, H384, Q388, M413, Q416, E417, and S421 (Table S11) show stable high occupancy interactions with the studied peptides, and belongs to the peptide binding region R354-M389 and I414-M433 determined by mutagenesis [8, 43, 103]. Moreover, here we would like to highlight that during our screening of peptides to the TAP complex, the peptide binding cleft was selected for screening (Figure 2g and S2), and therefore, higher number of residues that were identified from MD simulation data associate to the peptide binding regions [8, 43, 103]. The electron paramagnetic resonance (EPR) studies have shown a conserved distance of  $\sim 2.5$  nm or  $\sim 25$  Å between the N and C terminus of the peptides bound with TAP proteins [8, 43]. Hence, to trace such behavior of peptides varying in length studied by MD simulations, we measured the distance based on the C $\alpha$  atoms (Figure S7a) of N and C terminus residues of the peptides; pep57 (SIINF EKL), pep18 (ENPVVHFFKNIVTPR), and pep20 (AAGIGILTV). All three studied peptides have a similar N

and C terminus distance at a particular time step, similar to EPR studies [8, 45]. Particularly, the 15-mer (pep18) peptide has a maximum distance of 37.38 Å, the 9-mer peptide (pep20) has the highest distance of 21.57 Å, and the 8-mer peptide (SIINFEKL) has 21.92 Å distance (Figure S7a). Furthermore, during the 100 ns MD simulation the average distance for the SIINFEKL peptide termini was 19 Å, pep18 was 32 Å, and pep20 was 14 Å. Comparing these N and C terminus distances with the movements of the peptide towards the ER lumen in the TAP binding cavity during simulations (Figure 5c), it was observed that pep20 has comparatively slower movements as that of other two peptides (SIINFEKL and pep18), and higher number of interactions with TAP1 compared to TAP2 (Figure 5c). These observations may suggest that the conformation of the peptides can influence the distance and the movement / kinetics of the peptides within the transporter cavity, and from the structural aspects these conformations may vary based on the peptide sequences. The crystal structure of the SIINFEKL peptide with MHC-I is available (pdb id.: 3p9l [104]), as well as for the peptides pep18 (pdb id.: 3pl6 [105]) and pep20 (pdb id.: 3qdj [106]) complexed with the MHC-I and TCR receptors (Figure S7b). Therefore, we computed the distance between N and C terminus of peptides when presented to MHC-I molecules, which correlates with the highest distance observed for each peptide during MD simulations (Figure S7a).

### 3.5. Cancer-associated variants affecting protein-protein interface, as well as peptide transportation

Single cancer-associated point mutations can significantly affect the heterodimer formation of the TAP transporters as well as the peptide transport process, and thus, to elucidate such mechanism, MD simulations were performed for the selected mutations in TAP showing high versus low binding affinity (Figure 3c). The cancer-associated variants at positions 446/437 and 208/370 (located at the protein-protein interface; Figure 6a right panel) in the TAP1 and TAP2 proteins, respectively, produce a distinctive binding affinity between TAP1-TAP2 complexes (TAP1<sub>E446K</sub>, -5.99 kcal/mol; TAP1<sub>E446W</sub>, -11.35 kcal/mol; TAP1<sub>V437F</sub>, 25.43 kcal/mol; TAP1<sub>V437I</sub>, -7.92 kcal/mol; TAP2<sub>D370N</sub>, -1.23 kcal/mol; TAP2<sub>D370W</sub>, -15.43 kcal/mol; TAP2<sub>G208F</sub>, 28.53 kcal/mol, and TAP2<sub>G208S</sub>, 1.62 kcal/mol; Figure 3c). In addition, the mutant TAP1<sub>R372Q</sub> and TAP2<sub>R373H</sub> were also considered for MD simulations, because of its placement at the region where the peptide binds (Figure 6a right panel). These mutations were studied in the presence or absence of two different peptides (pep18 and SIINFEKL). Particularly, cancer-associated variants TAP1<sub>R372Q</sub> (found in cervical squamous cell carcinoma, colon adenocarcinoma, glioblastoma multiforme, and cervical squamous cell carcinoma), TAP2<sub>R373H</sub> (prostate adenocarcinoma and glioblastoma multiforme), and TAP2<sub>D370N</sub> (found in skin cancer, non-melanoma) are positioned in the peptide binding region (Figure S8). Additionally, in this position the cancer variant TAP1<sub>I333V</sub> (found in B-Lymphoblastic Leukemia/Lymphoma and Acute myelomonocytic leukemia (cBioPortal, <http://cbioportal.org>)), is well studied in terms of its involvement in cancer [49, 50]. Since these cancer-associated mutations (Figure 6a and S9a) maybe involved in the TAP suppression mechanism and reducing MHC-I cell surface, a set of 14 mutated TAP1-TAP2 systems were constructed for MD simulations in the presence or absence of peptides (Figure 6 and 7).

Except the TAP1<sub>V437I</sub> all other variants (TAP1<sub>E446K</sub>, TAP1<sub>E446W</sub>, TAP1<sub>V437F</sub>, and TAP1<sub>R372Q</sub>) have induced flexibility in the TAP1 transporter (Figure 6a, S9, and S10). Upon mutation in TAP1, the complexed TAP2 protein showed a stable behaviour in all mutated constructs (Figure 6a and S9a). On the contrary, the majority of cancer-associated mutations in TAP2 (TAP2<sub>D370N</sub>, TAP2<sub>D370W</sub>, TAP2<sub>G208S</sub>, and TAP2<sub>R373H</sub>) have induced stability in the TAP2 protein; excluding the TAP2<sub>G208F</sub> (Figure 6a, S9a, and S10b). In addition, the TAP1 protein only showed higher flexibility when complexed TAP2<sub>G208F</sub> (Figure 6a and S9a). These findings suggest that cancer-associated variants affect both TAP transporters with significantly different effects (Figure 6a). Furthermore, RMSDs of individual mutated residues at the protein-protein interface suggest that similar as found in initial screen (Figure 3c) both variants TAP1<sub>E446K/W</sub> and TAP1<sub>V437F/I</sub> have contrary behavior, and complementarity was observed for TAP2<sub>D370N/W</sub> and TAP2<sub>G208F/S</sub> (Figure S9b). Interestingly, the variants located at the peptide binding pocket of the TAP1-TAP2 complex have diverse



conformations; the TAP1<sub>R372Q</sub> variant was found highly stable, whereas the TAP2<sub>R373H</sub> showed a paradoxical data (Figure S9b).

Increasing flexibility in TAP1 in the mutated form (in the absence of peptide), induced a higher number of intermolecular protein-protein (hydrogen bonds; H-bonds) interactions compared to that of the wild-type system, except for the TAP1<sub>V437F</sub> variant (Figure 6b and Table S12). Though, adversely for the TAP2 protein, cancer-associated mutation which induces stability (Figure 6a), there were higher protein-protein interactions found for mutant apo-systems (Figure 6b and Table S12). These findings suggest that the cancer-associated mutations either induce stability or flexibility in the TAP1 or TAP2 proteins (in the absence of peptide) can unfavorably affect the TAP1-TAP2 complex, by forming a higher number of protein-protein interactions. The conformation dynamics of the TAP transporters in the TAP1<sub>E446K/W</sub> (446 aa is also positioned at the region presented to MHC I; Figure 2g) systems suggest that, upon mutation, TAP<sub>NBD</sub> domains lack the tilt movement, which results distortion in the opening of pore towards the cytosol, and the closed ER lumen conformation (Figure 6c; left panel). TAP1<sub>V437F</sub> and TAP1<sub>V437I</sub> formed a closed ER lumen pore, whereas only TAP1<sub>V437F</sub> showed tilt movement of the TAP<sub>NBD</sub> domain lacking the complete opening of the cytosolic pore.

The TAP2 mutations at position 370 belongs to the region where it can hinder movement of the helices (Figure 5b) and also affect the pore opening towards the cytosol; TAP2<sub>D370W</sub> showed a distorted but open cytosolic pore with moderate tilt movement of the TAP<sub>NBD</sub>, whereas the TAP2<sub>D370N</sub> lacked such conformation. Analysis of the structural behavior as well as the RMSDs suggest that TAP2<sub>D370W</sub> induces rigidity resulting in the opened cytosolic pore with moderate tilt TAP<sub>NBD</sub> movement (Figure 6c; right panel). For both TAP2<sub>G208F</sub> and TAP2<sub>G208S</sub> systems the tilt TAP<sub>NBD</sub> movement is observed as well as the open cytosolic pore, however, it is closed toward the ER lumen (Figure 6c). The mutations at the peptide binding region (TAP1<sub>R372Q</sub> and TAP2<sub>R373H</sub>) have the tilt movement with the open cytosolic passage, but TAP2<sub>R373H</sub> lacks the ER lumen opening. Overall, mutations in TAP1 completely block both ER and cytosolic pores of the TAP transporter that may hinder the intake and evacuation of the peptides from cytosol-to-ER, whereas mutation in the TAP2 protein mainly blocks the ER lumen pore (Figure 6c).

Protein-protein interactions with an occupancy  $\geq 50\%$  (from 100 ns) were identified in the studied mutated systems (Figure S11). Comparing TAP1-TAP2 intermolecular binding residues from mutated systems with the wild-type, suggests that TAP1 residues E302, D357, and R639 are frequently involved in TAP2 binding for the mutated systems, but not in wild-type (Figure S11). Except for the TAP1<sub>E446K</sub> system, TAP1 residues D306, E334, E443, and E446 were interacting with TAP2 in wild-type as well as in the mutated systems. Particularly, in the wild-type situation, the TAP1 E446 residue was involved in the binding with TAP2, which when E446K mutation hindered such an interaction. The mutated TAP1<sub>E446K</sub> and wild-type system lack common protein-protein interactions (Figure S11). The R373 residue from TAP2 was traced in the majority of the mutated systems (Figure 6 and S11) as well as wild-type binding with TAP1, excluding the TAP2<sub>R373H</sub> mutated system. Additionally, the TAP2 residues R235, E348, E349, Y366, Y366, and R381 binding with TAP1 were frequently traced in mutated systems (Figure S11).

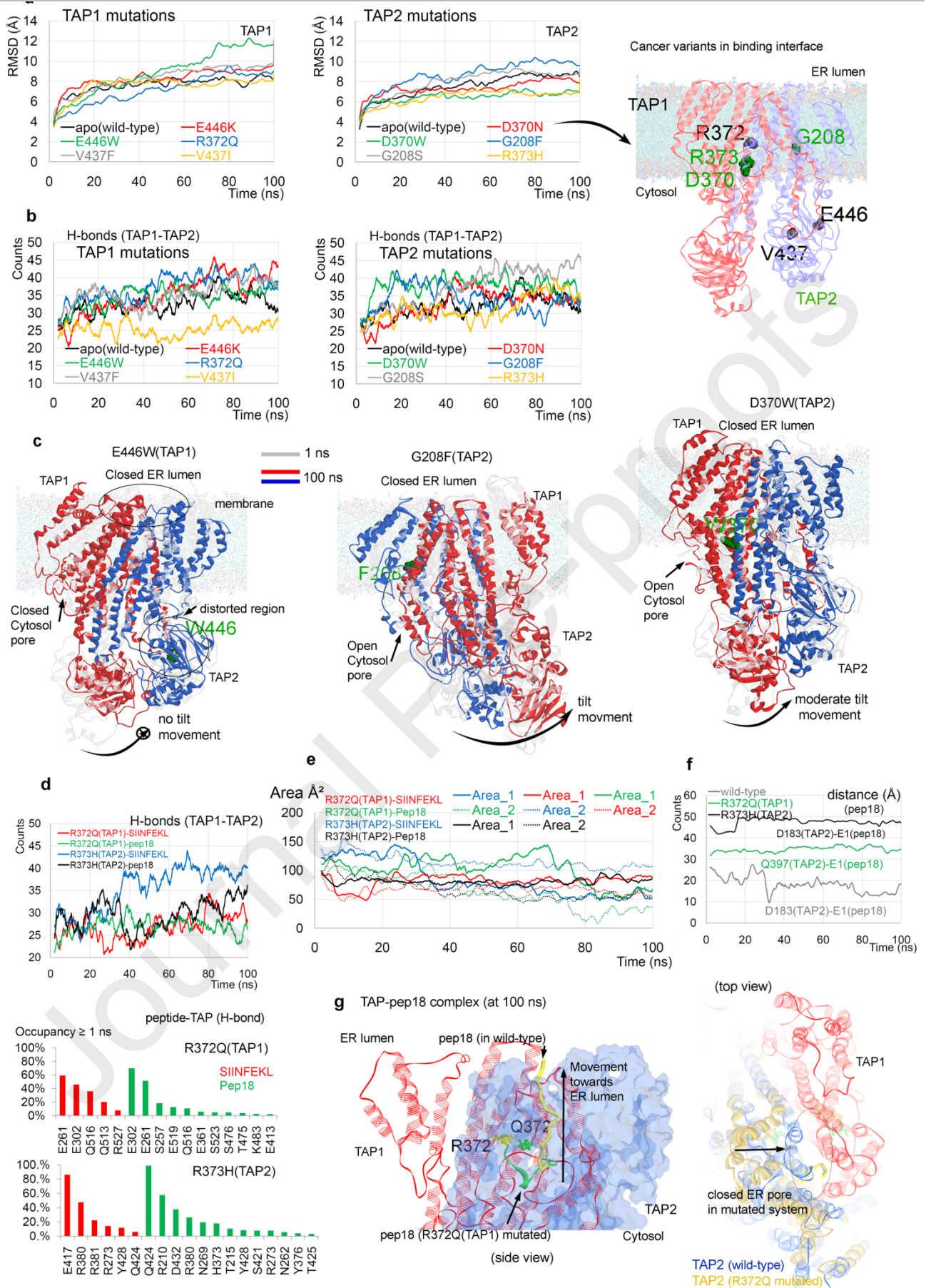


**Figure 6.** Mutations affecting the protein-protein interfaces of the TAP transporters, as well as the transport of the peptides. **(a)** RMSDs of the TAP transporters in the presence of the cancer-

associated mutations, and the right panel of the protein structure represents positions of cancer-associated mutations on the protein-protein interface. **(b)** Intermolecular protein-protein hydrogen bonds between TAP transporters in presence of the cancer-associated variants. **(c)** Conformation dynamics of the TAP proteins from different mutated systems, representing distinct conformational states upon point mutation. The protein structures were retrieved from the beginning and end of the MD simulations. **(d)** Intermolecular hydrogen bond interactions between TAP transporters, and the bottom panel represents binding residues of TAP with SIINFEKL or pep18 peptides in the presence of mutations. **(e)** Area computed for four helices forming the passage for the transportation of the peptide, as represented in Figure 5b. **(f)** Distance between the peptide residue and the TAP2 (from top) residue facing from the ER lumen. **(g)** Conformation dynamics with comparison of the mutated and wild-type system, showing the mutated variants induce rigidity and hinder the transportation of the peptide from cytosol to the ER lumen. Protein coordinates were extracted from the end of the MD simulations.

The direct consequences of cancer-associated variants over the peptide transport process by TAP heterodimer were evaluated by performing MD simulation of peptide in the presence of mutated TAP1-TAP2 complex. Both TAP1<sub>R372Q</sub> and TAP2<sub>R373H</sub> cancer-associated mutations are located in the peptide binding region and were involved in the interactions with peptides, hence were selected for MD simulations with two different peptides; pep18 and SIINFEKL (Figure 2i). During the initial screen (Figure 2i), pep18 peptide produced a strong binding affinity (-20.02 kcal/mol) with the TAP1-TAP2 complex but the SIINFEKL peptide (-13.44 kcal/mol) had comparatively weak affinity. The mutated TAP1 was found highly flexible compared to the mutated TAP2, and pep18 as well the variant residue TAP1<sub>R372Q</sub> itself were found destabilized (Figure S12). Among mutated systems with peptide, the TAP1-SIINFEKL-TAP2<sub>R373H</sub> complex had a higher number of protein-protein interactions, and the TAP1<sub>R372Q</sub>-pep18-TAP2 complex is the lowest to form such binding (Figure 6d and Table S13). Comparing these protein-protein interactions from peptide bound mutated systems (TAP1<sub>R372Q</sub> and TAP2<sub>R373H</sub>; Figure 6d) with mutated apo-systems (Figure 6b), the data suggest that peptide bound system has comparatively less TAP1-TAP2 intermolecular interactions.

Peptide-protein interactions suggest that both pep18 and SIINFEKL peptides formed a higher number of hydrogen bond interactions with the TAP2 protein, compared to that of the TAP1 (Figure S12c and Table S14). Particularly, pep18 peptide formed more interactions with TAP1 protein in the TAP1<sub>R372Q</sub>-pep18-TAP2 system (Figure S12c). For the TAP1<sub>R372Q</sub> system, the SIINFEKL peptide formed H-bond with more number of residues having an occupancy  $\geq 1$  ns. The pep18 peptide and TAP1(E519) residue formed high occupancy interactions in the wild-type system (Figure 5f), whereas lower occupancy binding with TAP1 is observed in the TAP1<sub>R372Q</sub> system (Figure 6d). In addition, for the TAP2<sub>R373H</sub> system the SIINFEKL peptide had residues E417, R380, and R381 in common with the wild type and mutated systems (Figure 5f and 6d), similarly the pep18 peptide formed interactions with R210, S421, R273, and N269 residues.

The area from the top of the TAP transport tunnel (towards the ER lumen; residues as described in Figure 5b) for all four mutated systems with peptides (Figure 6e), suggest a closed ER lumen conformation in the mutated complexes. For both peptides pep18 and SIINFEKL, the mutation in the TAP1<sub>R372Q</sub> and TAP2<sub>R373H</sub> blocks the movement of the peptide to upwards from cytosol-to-ER (Figure 6f, 6g, S13, and Videos S4, S5), particularly the TAP2<sub>R373H</sub> residue was found interacting with pep18 peptide (Table S14). Distances between the peptide and the TAP residues from the top (ER lumen; Figure 6f) demonstrated that, in the mutated TAP1<sub>R372Q</sub> and TAP2<sub>R373H</sub> systems, pep18 peptide has a higher distance value. Analysing the structural conformations of peptides in the presence of the mutation and wild type systems, the cancer-associated mutation induces rigidity in the TAP1-TAP2 complex, and hence, lacks an 'open' conformation towards the ER lumen. For an example (Figure 6g, 7, S138, and Video S5), the movement of pep18 in the wild type as well as mutant system is shown, the peptide can shift upwards to the ER for the wild-type system, whereas for mutant the cavity pore is closed towards

the ER lumen. For the opening of the cavity pore towards the ER in the wild-type system, a higher degree of conformations were observed in the TAP2 protein (Figure 6g; left panel). Moreover, one shall also consider that mutations may have selection over each peptide, i.e., different cancers or the same cancer might have different mutations. Therefore, the mutational effect that blocks the movement of the peptide to upwards from cytosol-to-ER (Figure 6g and S13) maybe seen in TAP1<sub>R372Q</sub> (found in cervical squamous cell carcinoma, colon adenocarcinoma, glioblastoma multiforme, and cervical squamous cell carcinoma) and TAP2<sub>R373H</sub> (found in prostate adenocarcinoma and glioblastoma multiforme).

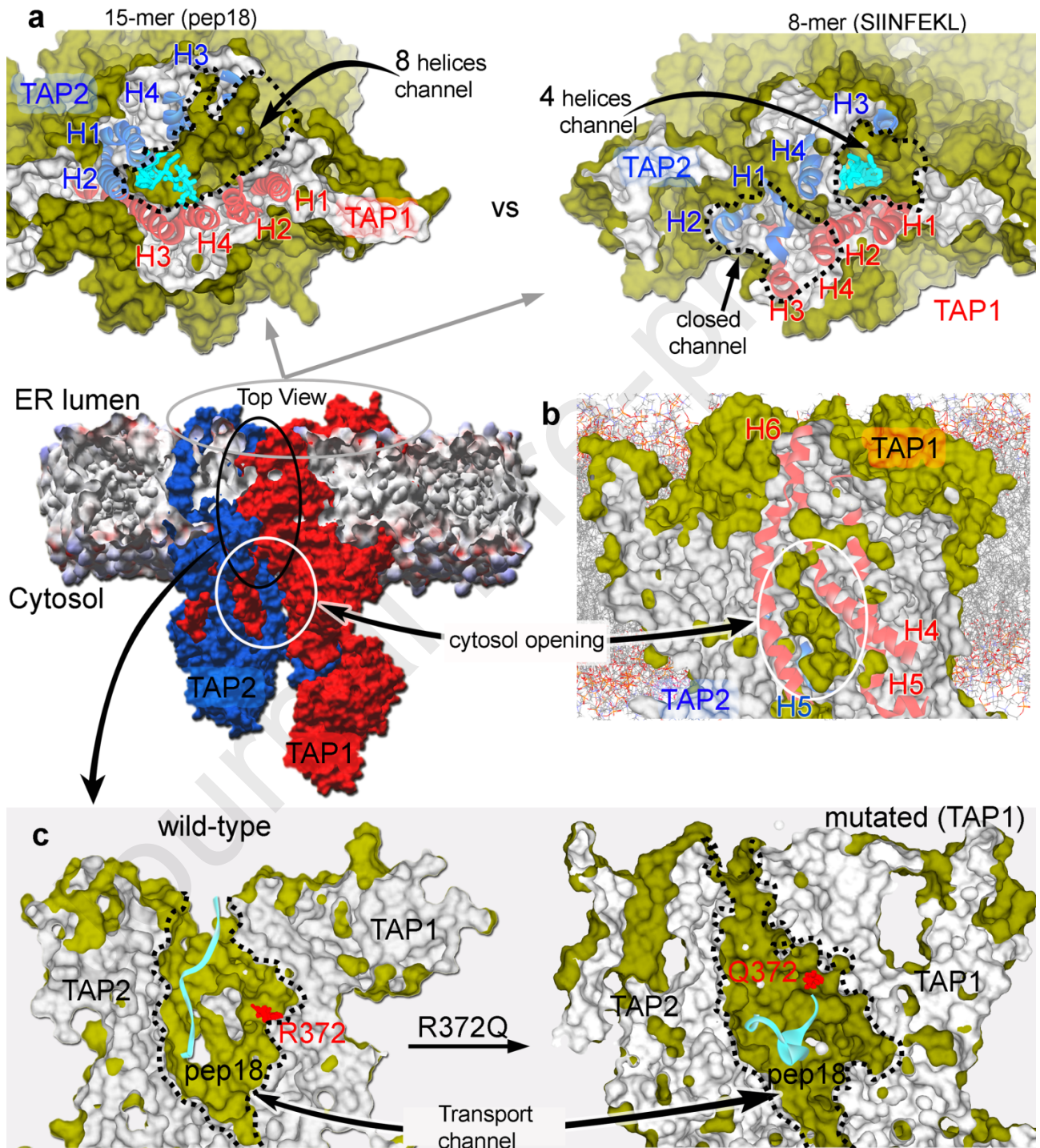


**Figure 7.** Structural rearrangements of TAP1-TAP2 transporters examined in the presence of peptide or cancer-associated variants. The protein structures retrieved from the end of MD simulations are represented as surface and slab view, and therefore, the internal regions are in silver color and the surface regions are in dark green. **(a)** TAP transporters adopted different

conformations to transport peptides from cytosol-to-ER, based on the peptide length (for example; 15-mer, ENPVVHFFKNIVTPR, pep18; and 8-mer, SIINFEKL). For a 15-mer peptide, TAP has a 8-helices (four helices from each TAP) transport channel, whereas for an 8-mer peptide, it has a 4-helices (two helices from each TAP) transport channel. Helices are numbered according to Figure 5b. **(b)** Cytosolic facing passage in an ‘open state’ observed during MDS, formed by helix\_4 (501-544 aa), helix\_5 (332-376 aa), helix\_6 (384-425 aa) from TAP1 and helix\_5 (250-288 aa) from TAP2. Alone, helix\_4 from TAP1 is involved in ER opening as well as cytosolic opening. **(c)** Mutation in the TAP transport channel (shown in green) can block the peptide in the cavity, for example, TAP1<sub>R372Q</sub> hinders peptide movement towards ER. *Color Scheme*; TAP1 in red, TAP2 in blue, and peptide in cyan.

#### 4. Conclusions

Our work highlights the structural and functional insights into the molecular architecture of the peptide transit by the TAP1 and TAP2 transporters, and how cancer-derived mutations (from COSMIC and cBioPortal) as well as different viral factors (BNL2a, CPXV012, ICP47, US6, and UL49.5) targeting TAP proteins may suppress the MHC class I pathway. This results in immune escape by the cancer and/or virus-carrying cell. To investigate the kinetics of the peptide transport process, different immunopeptidome datasets (MHC-I bound peptides presented by melanoma A375 cells) were generated in the presence/absence of interferon- $\gamma$  (IFN- $\gamma$ ) treated samples to obtain peptide datasets for the TAP models, along with considering a set of peptides known to be presented on the TCR (from ATLAS database). Higher numbers of peptides were identified in the IFN- $\gamma$  treated melanoma cells (3081 peptides) compared to that of the untreated cells (1968 peptides), suggesting an induced anti-cancer immunity pathway is being activated. These IFN- $\gamma$  treated cells generated peptides with length of 8 to 10 mers that showed the binding affinity between -10 to -15 kcal/mol (GBVI/WSA dG) with the modeled TAP1-TAP2 transporters. The majority of shorter length peptides from IFN- $\gamma$  treated cells have less binding affinity with the TAP transporters. Exclusively in the IFN- $\gamma$  treated cells the following peptides were identified from the TAP transporters itself; TAP1 (AALPAAALW, LLYESPERY, RSLQENIAY, RTALPRIF, SAMPTVRSF, and TEVDEAGSQL) and TAP2 (YLHSQVVSV). In addition, more residues from TAP2 were involved in interacting with the peptides, and fewer peptides were detected from TAP2 itself, whereas the opposite was observed for the TAP1.

Viral proteins predominantly destabilize the TAP1 protein, compared to that of the TAP2, particularly, for the UL49.5 and BNL2a. Among the studied viral proteins, the UL49.5 protein exhibited the highest fluctuations and BNL2a was the most stable protein. Interestingly, the peptides identified in the immunopeptidome data upon IFN- $\gamma$  treated melanoma cells, originates from the highly fluctuating regions of the TAP transporters upon viral binding (or the allosteric effects). The structural dynamics of the TAP1-TAP2 complex in the presence and absence of a viral protein in the complex, revealed that in all simulated systems the TAP<sub>NBD</sub> domains formed a tilt movement toward the membrane cytosolic face, which generates a passage or the peptide transport channel open towards the cytosol. This cytosolic passage was targeted by 4 (BNL2a, CPXV012, ICP47, and UL49.5) out of 5 studied viral proteins. The BNL2a, CPXV012, and ICP47 viral proteins formed a higher number of interactions with TAP1, whereas UL49.5 and US6 shared relatively equal interactions with both TAP proteins. In addition, the TAP1 regions with lower SNPs frequency and cancer variants were found making higher interactions with viral factors (proposing an adaptive mechanism, overcoming the protein-protein interactions that might result from amino acid changes), whereas the viral protein binds to the TAP2 region which is highly mutated. Exceptionally, the US6 protein has unique interactions with the transporters, whereas other BNL2a/CPXV012/ICP47/UL49.5 viral factors have several amino acids in common when binding with TAP proteins.

Individual amino acid fluctuations for the TAP proteins suggest that presence of shorter peptides (pep20 and SIINFEKL) induced stability in the transporter, compared to longer peptide

(pep18). TAP self peptides or regions from the immunopeptidome showing higher flexibility in viral systems, lacked such behavior in the peptide-bound systems. The structural movements of the cavity formed by the TAP transporters open towards the ER lumen, which may be proposed to transport the peptides from cytosol-to-ER in two different ways via an opening of the tunnel (4 or 8 helices involvement). Particularly, for the SIINFEKL (8-mer), which is smaller in length compared to that of the pep18 (15-mer), only the one passage formed by two helices from each TAP1 and TAP2 was found open, whereas for pep18 both passages, or areas, formed by 8 helices (4 from each TAP1 and TAP2) were in the open state. However, such difference in the opening of the passage towards the ER lumen may also vary based on the peptide sequences. The distance measured for each peptide from the top of the TAP models towards the ER lumen suggests that a shorter peptide (SIINFEKL) has an initiated movement relatively earlier compared to the longer peptide (pep18). At a point when the TAP1-TAP2 cavity is in its open conformation towards the ER, and the peptide reaches the top of the transport tunnel it mainly interacts with the TAP2 protein. The S203, Q388, and M413 amino acids from the TAP2 proteins were found common in at least two peptide systems. Similar as that observed in the EPR studies, a conserved distance of about 25 Å between the N and C terminus of the peptides bound with TAP proteins was observed in our analysis; the 15-mer (pep18) has a distance of 37.38 Å, the 9-mer (pep20) has 21.57 Å distance, and 8-mer (SIINFEKL) has 21.92 Å distance.

The TAP1 or TAP2 amino acids binding with peptides in fingerprint analysis, were also found mutated in different cancer types, which suggest that point mutation either from TAP1 or TAP2 is sufficient to alter the protein-protein binding which may affect the peptide transport process. Interestingly, the variants located at the peptide binding pocket of the TAP1-TAP2 complex have diverse conformations; the TAP1<sub>R372Q</sub> variant was found highly stable compared to that of the TAP2<sub>R373H</sub>. The mutations in TAP1 may completely block both ER and cytosolic passage of the TAP transporter which may hinder the intake and evacuation of the peptides from cytosol-to-ER (blocks the IF-to-OF conformation), whereas mutation in the TAP2 protein mostly blocks the ER pore only. The mutated system TAP1-SIINFEKL-TAP2<sub>R373H</sub> had a higher number of protein-protein interactions, and the TAP1<sub>R372Q</sub>-pep18-TAP2 complex is one of the lowest to form such binding. Considering both pep18 and SIINFEKL peptides, the mutation in the TAP1<sub>R372Q</sub> and TAP2<sub>R373H</sub> blocks the movement of the peptide upwards in the transport channel. For the opening of the transport cavity pore towards the ER lumen in the wild-type system, a higher degree of conformations is observed in the TAP2 protein, whereas the structural conformations of peptides in the presence of the mutation systems suggest that the cancer mutation induces rigidity in the TAP1-TAP2 complex, and therefore, lacks the 'open' conformation towards the ER lumen.

Overall, considering the binding affinities of the peptide with transporters it could be proposed that smaller peptides (8, 9, or 10 mers) may transport comparatively quickly through the transport channel. Furthermore, by adversely interacting with the TAP transport passage, or affecting the TAP<sub>NBD</sub> tilt movement, viral proteins and cancer-derived mutations may induce allosteric effects or rigidity in the TAP complex blocking the IF-to-OF conformation of the tunnel. The areas from the TAP transporter towards ER-opening and the distance centre of mass between TAP<sub>NBD</sub> domains, highlights a difference in the transport of longer vs shorter peptides. However, the sequence composition of peptide can affect the rate of such conformations by the transporters. These findings would propose a model for how different viral factors and cancer-derived mutations alter the peptide transport process by directly targeting the TAP proteins, and how the IFN- $\gamma$  induced signaling pathway alters TAP-peptide loading and, ultimately, MHC-I antigen presentation.

## Fundings

The APC was funded by the International Centre for Cancer Vaccine Science, University of Gdansk (Fundacja na rzecz Nauki Polskiej: MAB/3/2017). U.K. is supported by the grant: 2020/36/C/NZ2/00108, from The National Science Centre (Narodowe Centrum Nauki, Krakow, Poland). Partly funded by European Regional Development Fund (ENOC,

## Acknowledgments

The International Centre for Cancer Vaccine Science project is carried out within the International Research Agendas programme of the Foundation for Polish Science co-financed by the European Union under the European Regional Development Fund. Authors would also like to thank the PL-Grid Infrastructure, Poland for providing their hardware and software resources.

## Conflicts of Interest

The authors declare no conflict of interest.

## References

- [1] Praest P, Liaci AM, Förster F, Wiertz EJHJ (2019) New insights into the structure of the MHC class I peptide-loading complex and mechanisms of TAP inhibition by viral immune evasion proteins. *Mol Immunol* 113: 103-114.
- [2] Sadasivan B, Lehner PJ, Ortmann B, Spies T, Cresswell P (1996) Roles for calreticulin and a novel glycoprotein, tapasin, in the interaction of MHC class I molecules with TAP. *Immunity* 5: 103-114.
- [3] Park B, Lee S, Kim E, Cho K, Riddell SR et al. (2006) Redox regulation facilitates optimal peptide selection by MHC class I during antigen processing. *Cell* 127: 369-382.
- [4] Stefková J, Poledne R, Hubáček JA (2004) ATP-binding cassette (ABC) transporters in human metabolism and diseases. *Physiol Res* 53: 235-243.
- [5] Perria CL, Rajamanickam V, Lapinski PE, Raghavan M (2006) Catalytic site modifications of TAP1 and TAP2 and their functional consequences. *J Biol Chem* 281: 39839-39851.
- [6] Parcej D, Tampé R (2010) ABC proteins in antigen translocation and viral inhibition. *Nat Chem Biol* 6: 572-580  
Erratum in: (2010) *Nat Chem Biol* 6: 782.
- [7] Dean M, Annilo T (2005) Evolution of the ATP-binding cassette (ABC) transporter superfamily in vertebrates. *Annu Rev Genomics Hum Genet* 6: 123-142.
- [8] Lehnert E, Tampé R (2017) Structure and dynamics of antigenic peptides in complex with TAP. *Front Immunol* 8: 10.
- [9] Marijt KA, van Hall T (2020) To TAP or not to TAP: alternative peptides for immunotherapy of cancer. *Curr Opin Immunol* 64: 15-19.
- [10] van Endert PM, Tampé R, Meyer TH, Tisch R, Bach JF et al. (1994) A sequential model for peptide binding and transport by the transporters associated with antigen processing. *Immunity* 1: 491-500.
- [11] Uebel S, Meyer TH, Kraas W, Kienle S, Jung G et al. (1995) Requirements for peptide binding to the human transporter associated with antigen processing revealed by peptide scans and complex peptide libraries. *J Biol Chem* 270: 18512-18516.
- [12] Neeffjes JJ, Momburg F, Hämmerling GJ (1993) Selective and ATP-dependent translocation of peptides by the MHC-encoded transporter. *Science* 261: 769-771  
Erratum in: (1994) *Science* 264: 16.
- [13] Seyffer F, Tampé R (2015) ABC transporters in adaptive immunity. *Biochim Biophys Acta* 1850: 449-460.
- [14] Locher KP (2016) Mechanistic diversity in ATP-binding cassette (ABC) transporters. *Nat Struct Mol Biol* 23: 487-493.
- [15] Eggensperger S, Tampé R (2015) The transporter associated with antigen processing: a key player in adaptive immunity. *Biol Chem* 396: 1059-1072.
- [16] Abele R, Tampé R (2011) The TAP translocation machinery in adaptive immunity and viral escape mechanisms. *Essays Biochem* 50: 249-264.
- [17] Mayerhofer PU, Tampé R (2015) Antigen translocation machineries in adaptive immunity and viral immune evasion. *J Mol Biol* 427: 1102-1118.
- [18] Oldham ML, Hite RK, Steffen AM, Damko E, Li Z et al. (2016) A mechanism of viral immune evasion revealed by cryo-EM analysis of the TAP transporter. *Nature* 529: 537-540.
- [19] Lankat-Buttgereit B, Tampé R (2002) The transporter associated with antigen processing: function and implications in human diseases. *Physiol Rev* 82: 187-204.
- [20] Ljunggren HG, Stam NJ, Ohlén C, Neeffjes JJ, Höglund P et al. (1990) Empty MHC class I molecules come out in the cold. *Nature* 346: 476-480.
- [21] Praest P, Luteijn RD, Brak-Boer IGJ, Lanfermeijer J, Hoelen H et al. (2018) The influence of TAP1 and TAP2 gene polymorphisms on TAP function and its inhibition by viral immune evasion proteins. *Mol Immunol* 101: 55-64.
- [22] Yewdell JW, Bennink JR (1999) Mechanisms of viral interference with MHC class I antigen processing and presentation. *Annu Rev Cell Dev Biol* 15: 579-606.
- [23] Oldham ML, Grigorieff N, Chen J (2016) Structure of the transporter associated with antigen processing trapped by herpes simplex virus. *Elife* 5: e21829.

- [24] McLaughlin-Dubin ML, Munger K (2008) Viruses associated with human cancer. *Biochim Biophys Acta* 1782: 127-150.
- [25] Ritz U, Seliger B (2001) The transporter associated with antigen processing (TAP): structural integrity, expression, function, and its clinical relevance. *Mol Med* 7: 149-158.
- [26] Hicklin DJ, Marincola FM, Ferrone S. (1999) HLA class I antigen downregulation in human cancers: T-cell immunotherapy revives an old story. *Mol Med Today* 5: 178-186.
- [27] Marincola FM, Jaffee EM, Hicklin DJ, Ferrone S (2000) Escape of human solid tumors from T-cell recognition: molecular mechanisms and functional significance. *Adv Immunol* 74: 181-273.
- [28] Seliger B, Maeurer MJ, Ferrone S (1997) TAP off-tumors on. *Immunol Today* 18: 292-299.
- [29] Verweij MC, Horst D, Griffin BD, Luteijn RD, Davison AJ et al. (2015) Viral inhibition of the transporter associated with antigen processing (TAP): a striking example of functional convergent evolution. *PLoS Pathog* 11: e1004743.
- [30] Vossen MT, Westerhout EM, Söderberg-Nauclér C, Wiertz EJ (2002) Viral immune evasion: a masterpiece of evolution. *Immunogenetics* 54: 527-542.
- [31] Tashiro H, Brenner MK (2017) Immunotherapy against cancer-related viruses. *Cell Res* 27: 59-73.
- [32] Hislop AD, Rensing ME, van Leeuwen D, Pudney VA, Horst D et al. (2007) A CD8+ T cell immune evasion protein specific to Epstein-Barr virus and its close relatives in Old World primates. *J Exp Med* 204: 1863-1873.
- [33] Alzhanova D, Edwards DM, Hammarlund E, Scholz IG, Horst D et al. (2009) Cowpox virus inhibits the transporter associated with antigen processing to evade T cell recognition. *Cell Host Microbe* 6: 433-445.
- [34] Hill A, Jugovic P, York I, Russ G, Bennink J et al. (1995) Herpes simplex virus turns off the TAP to evade host immunity. *Nature* 375: 411-415.
- [35] Früh K, Ahn K, Djaballah H, Sempé P, van Endert PM et al. (1995) A viral inhibitor of peptide transporters for antigen presentation. *Nature* 375: 415-418.
- [36] Hewitt EW, Gupta SS, Lehner PJ (2001) The human cytomegalovirus gene product US6 inhibits ATP binding by TAP. *EMBO J* 20: 387-396.
- [37] Koppers-Lalic D, Reits EA, Rensing ME, Lipinska AD, Abele R et al. (2005) Varicelloviruses avoid T cell recognition by UL49.5-mediated inactivation of the transporter associated with antigen processing. *Proc Natl Acad Sci U S A* 102: 5144-5149.
- [38] Loch S, Tampé R (2005) Viral evasion of the MHC class I antigen-processing machinery. *Pflugers Arch* 451: 409-417.
- [39] Schuren AB, Costa AI, Wiertz EJ (2016) Recent advances in viral evasion of the MHC class I processing pathway. *Curr Opin Immunol* 40: 43-50.
- [40] Komov L, Melamed Kadosh D, Barnea E, Admon A (2021) The effect of interferons on presentation of defective ribosomal products as HLA peptides. *Mol Cell Proteomics* 20: 100105.
- [41] García-Sastre A (2017) Ten strategies of interferon evasion by viruses. *Cell Host Microbe* 22: 176-184.
- [42] Padariya M, Sznarkowska A, Kote S, Gómez-Herranz M, Mikac S et al. (2021) Functional interfaces, biological pathways, and regulations of interferon-related DNA damage resistance signature (IRDS) genes. *Biomolecules* 11, 622.
- [43] Hergert M, Baldauf C, Schölz C, Parcej D, Wiesmüller KH et al. (2011) Conformation of peptides bound to the transporter associated with antigen processing (TAP). *Proc Natl Acad Sci U S A* 108: 1349-1354.
- [44] Saric T, Chang SC, Hattori A, York IA, Markant S et al. (2002) An IFN-gamma-induced aminopeptidase in the ER, ERAP1, trims precursors to MHC class I presented peptides. *Nat Immunol* 3: 1169-1176.
- [45] Zhou F (2009) Molecular mechanisms of IFN- $\gamma$  to up-regulate MHC class I antigen processing and presentation. *Int Rev Immunol* 28: 239-260.
- [46] Strehl B, Seifert U, Kruger E, Heink S, Kuckelkorn U et al. (2005) Interferongamma, the functional plasticity of the ubiquitin-proteasome system, and MHC class I antigen processing. *Immunol Rev* 207: 19-30.
- [47] Arellano-Garcia ME, Misuno K, Tran SD, Hu S (2014) Interferon- $\gamma$  induces immunoproteasomes and the presentation of MHC I-associated peptides on human salivary gland cells. *PLoS One* 9: e102878.
- [48] Borrmann T, Cimons J, Cosiano M, Purcaro M, Pierce BG et al. (2017) ATLAS: A database linking binding affinities with structures for wild-type and mutant TCR-pMHC complexes. *Proteins* 85: 908-916.
- [49] Natter C, Polterauer S, Rahhal-Schupp J, Cacsire Castillo-Tong D, Pils S et al. (2013) Association of TAP gene polymorphisms and risk of cervical intraepithelial neoplasia. *Dis markers* 35: 79-84.
- [50] Einstein MH, Leanza S, Chiu LG, Schlecht NF, Goldberg GL et al. (2009) Genetic variants in TAP are associated with high-grade cervical neoplasia. *Clin Cancer Res* 15: 1019-1023.
- [51] Abele R, Tampé, R (2004) The ABCs of immunology: structure and function of TAP, the transporter associated with antigen processing. *Physiology (Bethesda)* 19: 216-224.
- [52] Ozbas-Gerceker F, Bozman N, Gezici S, Pehlivan M, Yilmaz M et al. (2013) Association of TAP1 and TAP2 gene polymorphisms with hematological malignancies. *Asian Pac J Cancer Prev* 14: 5213-5217.
- [53] Henle AM, Nassar A, Puglisi-Knutson D, Youssef B, Knutson, KL (2017) Downregulation of TAP1 and TAP2 in early stage breast cancer. *PloS one* 12: e0187323.
- [54] Forbes SA, Beare D, Boutselakis H, Bamford S, Bindal N et al. (2017) COSMIC: somatic cancer genetics at high-resolution. *Nucleic Acids Res* 45: D777-D783.



- [55] Cerami E, Gao J, Dogrusoz U, Gross BE, Sumner SO et al. (2012) The cBio cancer genomics portal: an open platform for exploring multidimensional cancer genomics data. *Cancer Discov* 2: 401-404 Erratum in: (2012) *Cancer Discov* 2: 960.
- [56] Grotzke JE, Sengupta D, Lu Q, Cresswell P (2017) The ongoing saga of the mechanism(s) of MHC class I-restricted cross-presentation. *Curr Opin Immunol* 46: 89-96.
- [57] Merzougui N, Kratzer R, Saveanu L, van Endert P (2011) A proteasome-dependent, TAP-independent pathway for cross-presentation of phagocytosed antigen. *EMBO Rep* 12: 1257-1264.
- [58] Lawand M, Abramova A, Manceau V, Springer S, van Endert P (2016) TAP-dependent and -independent peptide import into dendritic cell phagosomes. *J Immunol* 197: 3454-3463.
- [59] Karplus M, McCammon JA (2002) Molecular dynamics simulations of biomolecules. *Nat Struct Biol* 9: 646-652 Erratum in: (2002) *Nat Struct Biol* 9: 788.
- [60] Faktor J, Grasso G, Zavadil Kokas F, Kurkowiak M, Mayordomo MY et al. (2020) The effects of p53 gene inactivation on mutant proteome expression in a human melanoma cell model. *Biochim Biophys Acta Gen Subj* 1864: 129722.
- [61] Lanoix J, Durette C, Courcelles M, Cossette É, Comtois-Marotte S et al. (2018) Comparison of the MHC I immunopeptidome repertoire of B-cell lymphoblasts using two isolation methods. *Proteomics* 18: e1700251.
- [62] Cox J, Matic I, Hilger M, Nagaraj N, Selbach M et al. (2009) A practical guide to the MaxQuant computational platform for SILAC-based quantitative proteomics. *Nat Protoc* 4: 698-705.
- [63] Cox J, Hein MY, Lubner CA, Paron I, Nagaraj N et al. (2014) Accurate proteome-wide label-free quantification by delayed normalization and maximal peptide ratio extraction, termed MaxLFQ. *Mol Cell Proteomics* 13: 2513-2526.
- [64] Tyanova S, Temu T, Cox J (2016) The MaxQuant computational platform for mass spectrometry-based shotgun proteomics. *Nat Protoc* 11: 2301-2319.
- [65] Cox J, Neuhauser N, Michalski A, Scheltema RA, Olsen JV et al. (2011) Andromeda: a peptide search engine integrated into the MaxQuant environment. *J Proteome Res* 10: 1794-1805.
- [66] Kelley LA, Sternberg MJ (2009) Protein structure prediction on the web: a case study using the Phyre server. *Nat Protoc* 4: 363-371.
- [67] Kelley LA, Mezulis S, Yates CM, Wass MN, Sternberg MJ (2015) The Phyre2 web portal for protein modeling, prediction and analysis. *Nat Protoc* 10: 845-858.
- [68] Molecular Operating Environment (MOE) 2011.10. Chemical Computing Group (2011) Montreal, Quebec, Canada.
- [69] Brooks BR, Brooks CL 3rd, Mackerell AD Jr, Nilsson L, Petrella RJ et al. (2009) CHARMM: the biomolecular simulation program. *J Comput Chem* 30: 1545-1614.
- [70] Labute P (2008) The generalized Born/volume integral implicit solvent model: estimation of the free energy of hydration using London dispersion instead of atomic surface area. *J Comput Chem* 29: 1693-1698.
- [71] Krivák R, Hoksza D (2015) Improving protein-ligand binding site prediction accuracy by classification of inner pocket points using local features. *J Cheminform* 7: 12.
- [72] Kitchen DB, Decornez H, Furr JR, Bajorath J (2004) Docking and scoring in virtual screening for drug discovery: methods and applications. *Nat Rev Drug Discov* 3: 935-949.
- [73] Wojciechowski M, Lesyng B (2004) Generalized Born model: Analysis, refinement, and applications to proteins. *J Phys Chem B* 108: 18368-18376.
- [74] Labute P (2010) LowModeMD--implicit low-mode velocity filtering applied to conformational search of macrocycles and protein loops. *J Chem Inf Model* 50: 792-800.
- [75] Karczewski KJ, Francioli LC, Tiao G, Cummings BB, Alföldi J et al. (2020) The mutational constraint spectrum quantified from variation in 141,456 humans. *Nature* 581: 434-443 Erratum in: (2021) *Nature* 590: E53.
- [76] Lomize MA, Pogozheva ID, Joo H, Mosberg HI, Lomize AL (2012) OPM database and PPM web server: resources for positioning of proteins in membranes. *Nucleic Acids Res* 40: D370-D376.
- [77] Jo S, Lim JB, Klauda JB, Im W (2009) CHARMM-GUI Membrane Builder for mixed bilayers and its application to yeast membranes. *Biophys J* 97: 50-58.
- [78] Trowitzsch S, Tampé R (2020) Multifunctional chaperone and quality control complexes in adaptive immunity. *Annu Rev Biophys* 49: 135-161.
- [79] Loschwitz J, Olubiyi OO, Hub JS, Strodel B, Poojari CS (2020) Computer simulations of protein-membrane systems. *Prog Mol Biol Transl Sci* 170: 273-403.
- [80] Woolf TB, Roux B (1996) Structure, energetics, and dynamics of lipid-protein interactions: A molecular dynamics study of the gramicidin A channel in a DMPC bilayer. *Proteins* 24: 92-114.
- [81] Phillips JC, Braun R, Wang W, Gumbart J, Tajkhorshid E et al. (2005) Scalable molecular dynamics with NAMD. *J Comput Chem* 26: 1781-1802.
- [82] Klauda JB, Venable RM, Freites JA, O'Connor JW, Tobias DJ et al. (2010) Update of the CHARMM all-atom additive force field for lipids: validation on six lipid types. *J Phys Chem B* 114: 7830-7843.
- [83] Venable RM, Brown FLH, Pastor RW (2015) Mechanical properties of lipid bilayers from molecular dynamics simulation. *Chem Phys Lipids* 192: 60-74.

- [84] Guvenen O, Manojosyula SS, Kaman ER, Hatcher E, Vanommeslaeghe K, et al. (2011) CHARMM additive all-atom force field for carbohydrate derivatives and its utility in polysaccharide and carbohydrate-protein modeling. *J Chem Theory Comput* 7: 3162-3180.
- [85] Jorgensen WL, Chandrasekhar J, Madura JD, Impey RW, Klein ML (1983) Comparison of simple potential functions for simulating liquid water. *J Chem Phys* 79: 926-935.
- [86] Darden T, York D, Pedersen L (1993) Particle mesh Ewald- an  $N \cdot \log(N)$  method for Ewald sums in large systems. *J Chem Phys* 98: 10089-10092.
- [87] Pastor RW, Brooks BR, Szabo A (1988) An analysis of the accuracy of langevin and molecular dynamics algorithms. *Mol Phys* 65: 1409-1419.
- [88] Feller SE, Zhang YH, Pastor RW, Brooks BR (1995) Constant pressure molecular dynamics simulation: the Langevin piston method. *J Chem Phys* 103: 4613-4621.
- [89] Ryckaert JP, Ciccotti G, Berendsen HJC (1977) Numerical integration of cartesian equations of motion of a system with constraints: molecular dynamics of n-alkanes. *J Comput Phys* 23: 327-341.
- [90] Humphrey W, Dalke A, Schulten K (1996) VMD: visual molecular dynamics. *J Mol Graph* 14: 33-38.
- [91] Rock KL, Goldberg AL (1999) Degradation of cell proteins and the generation of MHC class I-presented peptides. *Annu Rev Immunol* 17: 739-779.
- [92] Stryhn A, Pedersen LO, Holm A, Buus S (2000) Longer peptide can be accommodated in the MHC class I binding site by a protrusion mechanism. *Eur J Immunol* 30: 3089-3099.
- [93] Guo HC, Jardetzky TS, Garrett TP, Lane WS, Strominger JL et al. (1992) Different length peptides bind to HLA-Aw68 similarly at their ends but bulge out in the middle. *Nature* 360: 364-366.
- [94] Urban RG, Chiczy RM, Lane WS, Strominger JL, Rehm A et al. (1994) A subset of HLA-B27 molecules contains peptides much longer than nonamers. *Proc Natl Acad Sci U S A* 91: 1534-1538.
- [95] Rock KL, Reits E, Neefjes J (2016) Present yourself! By MHC class I and MHC class II molecules. *Trends Immunol* 37: 724-737.
- [96] Koopmann JO, Post M, Neefjes JJ, Hämmerling GJ, Momburg F (1996) Translocation of long peptides by transporters associated with antigen processing (TAP). *Eur J Immunol* 26: 1720-1728.
- [97] Kisselev AF, Akopian TN, Woo KM, Goldberg AL (1999) The size of peptides generated from proteins by mammalian 26 and 20S proteasomes. *J Biol Chem* 274: 3363-3371.
- [98] Nogales A, DeDiego ML (2019) Host single nucleotide polymorphisms modulating influenza A virus disease in humans. *Pathogens* 8: 168.
- [99] Bordignon E, Seeger MA, Galazzo L, Meier G (2020) From in vitro towards in situ: structure-based investigation of ABC exporters by electron paramagnetic resonance spectroscopy. *FEBS letters* 594: 3839-3856.
- [100] Hofmann S, Janulien D, Mehdi-pour AR, Thomas C, Stefan, E et al. (2019) Conformation space of a heterodimeric ABC exporter under turnover conditions. *Nature* 571: 580-583.
- [101] Stefan E, Hofmann S, Tampé R (2020) A single power stroke by ATP binding drives substrate translocation in a heterodimeric ABC transporter. *eLife* 9: e55943.
- [102] Nöll A, Thomas C, Herbring V, Zollmann T, Barth K et al. (2017) Crystal structure and mechanistic basis of a functional homolog of the antigen transporter TAP. *Proc Natl Acad Sci U S A* 114: E438-E447.
- [103] Armandola EA, Momburg F, Nijenhuis M, Bulbuc N, Früh K et al. (1996) A point mutation in the human transporter associated with antigen processing (TAP2) alters the peptide transport specificity. *Eur J Immunol* 26: 1748-1755.
- [104] Denton AE, Wesselingh R, Gras S, Guillonneau C, Olson MR et al. (2011) Affinity thresholds for naive CD8+ CTL activation by peptides and engineered influenza A viruses. *J Immunol* 187: 5733-5744.
- [105] Sethi DK, Schubert DA, Anders AK, Heroux A, Bonsor, DA et al. (2011) A highly tilted binding mode by a self-reactive T cell receptor results in altered engagement of peptide and MHC. *J Exp Med* 208: 91-102.
- [106] Borbulevych OY, Santhanagopalan SM, Hossain M, Baker BM (2011) TCRs used in cancer gene therapy cross-react with MART-1/Melan-A tumor antigens via distinct mechanisms. *J Immunol* 187: 2453-2463.

**Monikaben Padariya:** Methodology, Conceptualization, Investigation, Writing- Original draft preparation and visualization, Data curation, Writing- Reviewing and Editing, **Sachin Kote:** Methodology, Data curation, Writing- Reviewing and Editing, **Marcos Mayordomo:** Methodology, Data curation, Writing- Reviewing and Editing, **Irena Dapic:** Writing- Reviewing and Editing, **Javier Alfaro:** Writing- Reviewing and Editing, **Ted Hupp:** Investigation, Visualization, Writing- Reviewing and Editing, **Robin Fahraeus:** Conceptualization, Investigation, Writing- Reviewing and Editing, **Umesh Kalathiya:** Methodology, Conceptualization, Investigation, Writing- Original draft preparation and visualization, Formal analysis, Supervision, Writing- Reviewing and Editing.

# Structural determinants of peptide-dependent TAP1-TAP2 transit passage altered-targeted by viral proteins and altered by cancer-associated mutations-variants

Monikaben Padariya<sup>1,†,\*</sup>, Sachin Kote<sup>1</sup>, Marcos Mayordomo<sup>1</sup>, Irena Dapic<sup>1</sup>, Javier Alfaro<sup>1,2</sup>, Ted Hupp<sup>1,2</sup>, Robin Fahraeus<sup>1,3,4,5,\*</sup>, Umesh Kalathiya<sup>1,†,\*</sup>

1 International Centre for Cancer Vaccine Science, University of Gdansk, ul. Kładki 24, 80-822 Gdansk, Poland

2 Institute of Genetics and ~~Molecular Medicine~~Cancer, University of Edinburgh, Edinburgh, Scotland EH4 2XR, United Kingdom

3 Inserm UMRS1131, Institut de Génétique Moléculaire, Université Paris 7, Hôpital St. Louis, F-75010 Paris, France

4 Department of Medical Biosciences, Building 6M, Umeå University, 901 85 Umeå, Sweden

5 RECAMO, Masaryk Memorial Cancer Institute, Zlutykopec 7, 65653 Brno, Czech Republic.

†These authors contributed equally to this work.

\*Correspondence: monikaben.padariya@ug.edu.pl (M.P.), robin.fahraeus@inserm.fr (R.F.), umesh.kalathiya@ug.edu.pl (U.K.)

## Abstract

The TAP1-TAP2 ~~complex~~~~heterodimer~~ transports antigenic peptide substrates into the endoplasmic reticulum (ER).; ~~In the ER, where~~ the peptides are further processed and loaded on the major histocompatibility class (MHC) I molecules by the peptide loading complex (PLC). The TAP ~~complex transporters are~~ linked ~~to with~~ the PLC; ~~and is~~ a target for cancers and viral immune evasion. But ~~how the mechanisms whereby the~~ cancer-derived mutations ~~in TAP1-TAP2~~ or viral factors ~~targeting the PLC~~, interfere ~~with~~ peptide transport ~~are only emerging~~ is ~~not clear~~. This study ~~based on the studied peptides~~ describes that transit ~~of peptides~~ through TAP ~~transport passage~~ can take place via two ~~(4 or 8 helices)~~ different channels ~~(4 or 8 helices)~~ depending on peptide length ~~and sequence~~. Molecular dynamics ~~data~~ and ~~the TAP~~ binding ~~affinity predictions of~~ peptide-transporters ~~demonstrated analyses suggest that~~ that smaller peptides (8-10 mers; e.g. AAGIGILTV, SIINFEKL) can transport quickly through the transport ~~channel-tunnel~~ compared to longer peptides (15-mer; e.g. ENPVVHFFKNIVTPR). In line with a regulated and selective peptide transport by TAPs, the immunopeptidome ~~upon following~~ IFN- $\gamma$  treatment ~~in melanoma A375 cells provokes induced~~ the shorter length (9-mer) peptide ~~production-presentation over MHC-I (3941 peptides presented on MHC-I)~~ that exhibit a ~~relatively~~ weak TAP-binding affinity ~~with TAP~~. A conserved distance between N and C terminus residues of the studied peptides in the ~~transport tunnel were reported~~. Furthermore, by adversely interacting with the TAP transport passage, or affecting TAP<sub>NBD</sub> ~~domains~~ tilt movement, viral proteins ~~and cancer-derived mutations in TAP1-TAP2, may~~ induce allosteric effects ~~in TAP that blocking the conformation of the tunnel-channel in (a closed towards ER lumen position)~~. A ~~similar effect is achieved when introducing cancer-derived mutations targeting allosteric regions of TAP~~. Interestingly, some cancer-associated mutations (e.g. TAP1<sub>R372Q</sub> and TAP2<sub>R373H</sub>) can specifically interfere with selective transport channels (~~essentially i.e.~~ for longer-peptides). These results provide a model for how viruses and cancer-associated mutations ~~targeting~~ TAP interfaces ~~and can~~ affect MHC class I antigen presentation; and how the IFN- $\gamma$  pathway alters MHC-I antigen presentation via the kinetics of peptide transport.

**Keywords:** peptide; transporters; MHC-I; cancer mutations; viral factors; molecular dynamics; kinetics; TAP1; TAP2; in silico peptide screening; immunopeptidome; IFN- $\gamma$

## 1. Introduction

Cytotoxic T lymphocytes response to ~~infected or transformed cells~~~~the pathogenic cells or infection~~ depends on the presentation of peptide antigens on major histocompatibility complex class I (MHC-I) molecules. The majority of MHC-class-I presented peptides are generated in the cytosol by the proteasome ~~and~~. ~~These peptides are then~~ transported into the endoplasmic reticulum (ER)

lumen by the ~~TAP peptide transport complex~~ for further processing by the ERAP aminopeptidases, before loaded onto MHC-I molecules by the dynamic multi-component assembly peptide-loading complex (PLC) (Figure 1) [21-43]. PLC (Figure 1) includes; TAP1 and TAP2 (transporter 1 and 2) ~~heterodimer~~ complex, MHC-I,  $\beta$ 2microglobulin ( $\beta$ 2m), the chaperones tapasin, calreticulin, and ERp57 (ER protein 57) [21-43]. The ~~TAP transporters constitute structural and functionally key constituents components~~ of the ~~antigen presentation pathway~~ PLC are the ~~TAP transporters~~, since they link the cytosolic pool of peptides ~~with the PLC~~ and the ER-resident MHC-I molecules (Figure 1) [21].

The TAP ~~proteins transporters~~ belong to the superfamily of ATP-binding cassette (ABC) transporters. Some of these transporters are associated with severe human diseases like cystic fibrosis [54, 65], and they play major roles in multidrug resistance of pathogenic bacteria, reduced efficacy of antitumor drugs, cholesterol metabolism, cell homeostasis, and immune response [76]. ~~Therefore, Understanding~~ the functional mechanisms of ABC transporters is ~~thus of importance~~ for therapeutic development. ~~The~~ TAP1 (ABCB2) and TAP2 (ABCB3) ~~are heterodimeric~~ transporters, each have an N-terminal transmembrane domain (TMD) and a C-terminal nucleotide-binding domain (NBD) [87]. In the core part of the TMDs, the outer TM helices bind the other PLC component tapasin, the inner helices are responsible for peptide binding and form the channel, which mediates the peptide translocation [98, 109]. Peptide binding to TAP is ATP-independent [110, 121], whereas peptide transport from the cytosol to ~~the~~ ER requires ATP binding and hydrolysis [1312]. The TAP<sub>NBDs</sub> carry out the ATP hydrolysis, to energize the conformational changes of the TMDs required for peptide translocation [21, 1312].

Substantial effort has been made to understand ~~the in detail how~~ peptides ~~that~~ are translocated by the TAP1-TAP2 transporters. Several biochemical studies have identified the nucleotide binding structural motifs, roughly mapped the peptide binding region, and ~~also~~ provided the secondary structures responsible for the crosstalk between ATP hydrolysis in the TAP<sub>NBDs</sub> and conformational changes of the TM helices [21, 1413]. However, the picture is still incomplete, as it has not been conclusively integrated into a robust trajectory of how the TAP dynamics and ~~how~~ the substrates move to carry out a transport cycle. The precise conformational changes that occur as a result of substrate or nucleotide binding to TAP1/TAP2 are also not characterized [21]. The TAP transporters show a common fold with all structurally characterized ABC transporters [76, 1514]. Recent expansion of several new high-resolution ~~transporter structures of these transporters in different conformations tempted produced~~ many structural models of ~~the TAP transporters bases on structures of relatives, and also developed many transport models based on a general ABC transporter~~ [21, 76, 1413, 1615-1918]. Thus, the structural understanding of the TAP1-TAP2 complex is largely based on such extrapolations. However, it has ~~also~~ been ~~also~~ suggested that the transporters most likely do not undergo the same structural cycles and no common mechanism has been proposed [21, 1514]. For this reason, the novel insights of TAP structures will be of importance.

Impaired TAP function results in reduced surface expression of MHC-I, as the empty MHC-I molecules are unable to present antigens to the immune system and is a common target for viral as well as cancer immune evasion [1615, 2019-2423]. Approximately, 15-20% of all human cancers worldwide are linked to viruses and this percentage could grow in the future [2524]. MHC-I surface expression abnormalities have been identified in virus-associated cancers and non-cancerous cells, and thus, delineate a significant mechanism of virus infected cells to evade proper immune response. In most cases, this downregulation has been related to impaired TAP expression, which could be ~~as~~ a result of structural alterations or dysregulation [2625-2928]. ~~Moreover, TAP plays a crucial role in viral peptide loading onto MHC-I, which is reflected by the s~~ several ways viruses have evolved ~~factors that to~~ block the function of TAP [3029]. ~~including. Particularly, viral proteins that target the TAP function belong to~~ herpesviruses such as Epstein-Barr virus, human cytomegalovirus, and herpes simplex virus type 1 ~~that establisheause~~ lifelong persistence in the host [3130]. Association of these viruses with certain types of cancer or human malignancies has been demonstrated and knowledge about their target~~sing~~, as well as functioning mechanisms can be

useful in the development of future antiviral treatment strategies [4231]. In concert with this, we investigated the TAP1 and TAP2 transporters at the atomic level with a particular focus on ~~the consequences of several cancer mutations on peptide binding as well as transportation and the dynamics of different virus encoded inhibitors targeting the TAP plasticity~~. how viruses inhibit TAP-mediated peptide translocation at a molecular level. The dynamics of the following TAP attacking viral immune evasion proteins were studied: BNLF2a from Epstein-Barr virus [4132], CPXV012 from cowpox virus [4233], ICP47 from herpes simplex virus type 1 [4334, 4435], US6 from human cytomegalovirus [4536], and UL49.5 encoded by varicellovirus [4637].

Journal Pre-proofs

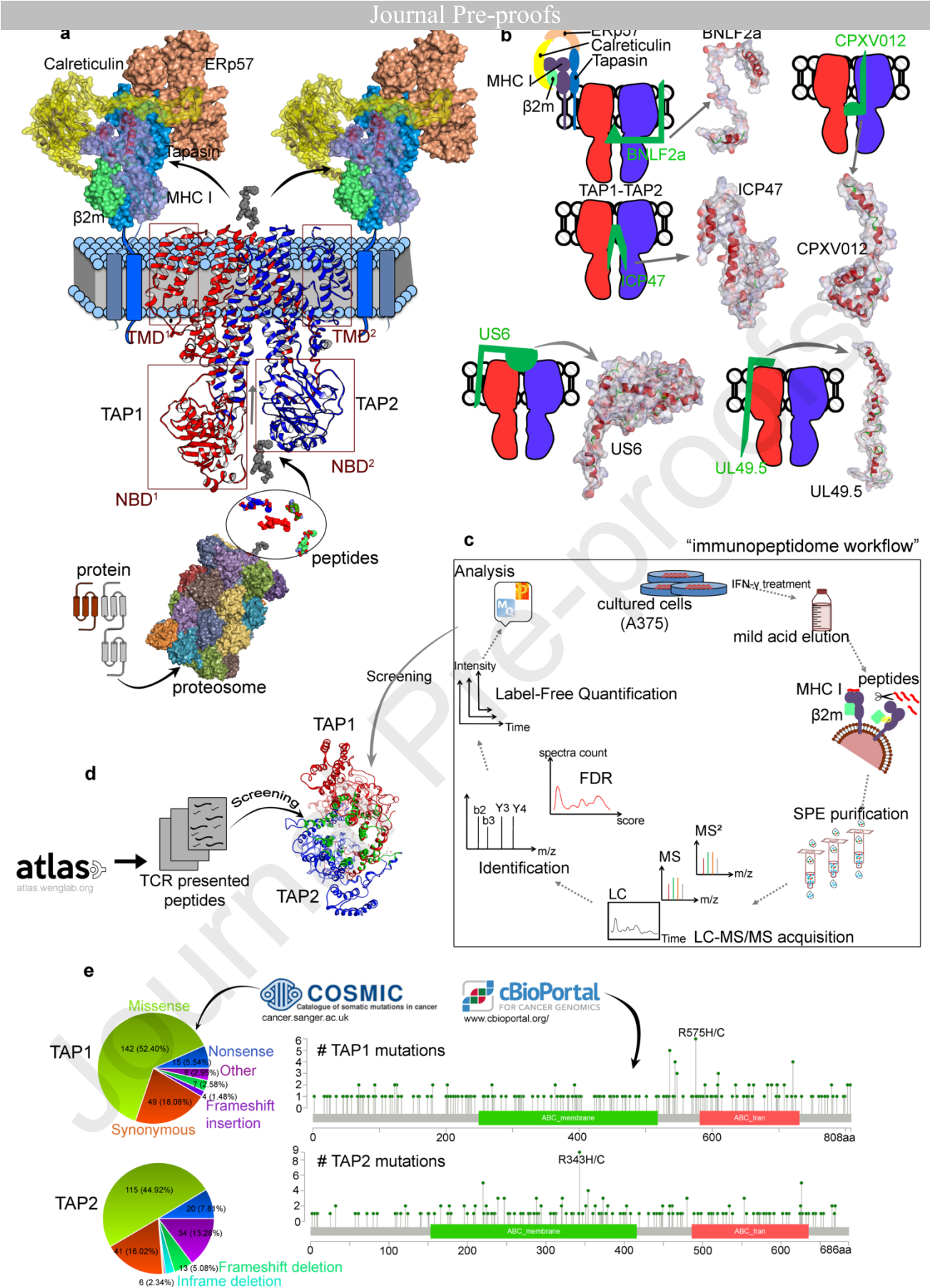


**Figure 1.** The TAP1 and TAP2 transporters molecular and structural aspects in the peptide-loading complex. **(a)** The modeled tertiary structures of TAP1-TAP2 heterodimeric transporters, including the N-terminal transmembrane domains (TMD) that were found missing in the cryo-EM structure

crystal structure (pdb id.PDB: 5u1d) [1918, 2423]. Antigenic peptide presentation by MHC-I begins with the degradation of cytosolic proteins into peptides by the proteasome, which are then transported across the ER membrane by the TAP transporters. Followingly, the peptides can be loaded over the surface of the MHC-I molecules residing in the peptide-loading complex (PLC), accommodated with several other components;  $\beta$ 2m, ERp57, tapasin, and calreticulin [21-34]. **(b)** Viral immune evasion proteins interacting with the TAP transporters. ICP47 binds to TAP from the cytosol and inhibits the peptide binding, US6 blocks ATP binding to TAP by interfering from the ER lumen, UL49.5 blocks TAP dependent peptide transport and also catalyses the degradation of the PLC. BNL2a binds to the core TAP structure and arrest it in a transport-incompetent conformation, CPXV012 inhibits TAP dependent peptide translocation, and thus, interfere with the MHC-I-peptide assembly in the ER [3338]. Cryo-EM structure of human TAP with ICP47 (pdb id.PDB: 5u1d) [1918, 2423] was used as a template to model other TAP binding viral proteins BNL2a, CPXV012, UL49.5, and US6. Three dimensional (3D) structures of viral protein are shown in ribbon representation with molecular surfaces. **(c)** The outline of the immunopeptidome workflow, representing the sample preparation to peptide identification protocol. **(d)** Datasets of TAP transported peptides retrieved from the ATLAS (Altered TCR Ligand Affinities and Structures) database (<http://atlas.wenglab.org/>). The peptides present in the crystal structure of TCR(T cells receptor)-peptide-MHC complexes were collected. In the 3D-structure of TAP, the defined active site for peptide screening is highlighted as green ribbons, red spheres represent hydrophilic and white sphere hydrophobic likeliness of the active site. **(e)** Cancer-associated mutations retrieved from the COSMIC (Catalogue of Somatic Mutations in Cancer; [cancer.sanger.ac.uk](http://cancer.sanger.ac.uk)) and cBioPortal (<https://www.cbioportal.org/>) databases for the TAP transporters. The pie chart from COSMIC represents different types of mutation with a number of samples labeled, as well as the percentage (%) of mutation covered. The scattered plot from cBioPortal, represents cancer mutations for TAP1 and TAP2 proteins along with its frequency.

To form a catalog of peptides likely to be transported by the TAP1-TAP2 complex, a systematic immunopeptidome workflow was applied as shown in Figure 1c. Peptide loaded on the MHC molecules on melanoma A375-cells were identified by acid elution followed by mass spectrometry (MS) analysis. Furthermore, The virus infected cells form one key model with which to are the preferred way to analyze the response of the immune system, however, some viruses escape immune surveillance by altering and inhibiting the MHC-I presentation pipeline. An alternative way to simulate the parts of the cellular immune response that occurs during viral infection can be to treat cells with interferons (IFNs), without infecting them [8439, 8540]. Interferons are important cytokines, produced in response to viral infection, alert the immune system, and enhance cellular response to the infection (increase the presentation of MHC molecules) [8641]. Thus, analyzing the effect of IFNs on the MHC-I immunopeptidome in cultured human cells can provide a model for examining the effects of viral infection on the MHC peptidome [8540]. The type I (IFN- $\alpha$  and IFN- $\beta$ ) and type II (IFN- $\gamma$ ) IFNs are key cytokines in the antiviral response. IFN- $\beta$  is secreted from most cells in response to viral infection involving dendritic cells and many other cell types in the body [8540, 8842]. At the later stages of immune response, IFN- $\gamma$  is secreted from T-cells and other immune cells [8540]. The interferons strongly affect cellular metabolism and gene expression, including MHC-I as well as MHC-II molecules and also upregulate antigen processing and presentation components such as; ER aminopeptidase 1/2 and the TAP transporters [98, 40, 42, 8043, 85, 88, 9144-, 94, 10446]. Moreover, when cells are treated with IFN- $\gamma$ , the regular proteasomes are replaced by the immunoproteasomes [10446]. This replacement has been associated with an enhanced immune response and the peptides produced by immunoproteasomes mainly contain hydrophobic or basic C termini, which are preferred substrates for the TAP transporters and also appear to be more efficient at binding to MHC-I [98, 40, 8043, 85]. Consequently, immunoproteasomes are believed to enhance the MHC-I antigenic peptide generation and presentation [10147]. Additionally, the enhancement of MHC presentation by IFN

treatment may add neoepitopes to the presented peptidome that can induce even stronger immune responses [8540].

Initially to form a catalog of peptides loaded on the MHC molecules expressed on the cell surface melanoma A375 cell surface, a systematic immunopeptidome workflow was applied, followed by mass spectrometry (MS) as shown in (Figure 1c)., since these immunogenic peptides are very likely to be transported by the TAP1-TAP2 complex (Figure 1c). The listed peptides were identified by elution of MHC loaded peptides directly from melanoma A375 cells followed by mass spectrometry (MS) analysis. We were also interested to know if the transport of peptides through the TAP is affected by IFN- $\gamma$  treatment. IFN- $\gamma$  is known to induce the immunoproteasome with a different protease composition and to alter the length and cleavage sites of peptides and we wanted to see if this could affect peptide interaction with the TAP and presentation on MHC molecules. The melanoma A375 cells were treated with IFN- $\gamma$ , and different peptides were identified with and without IFN- $\gamma$  treatment using mass spectrometry techniques. Detected peptides were further studied *in silico* screened with the model of TAP1-TAP2 complex model, to understand/investigate the peptide transport process from the cytosol towards to the ER lumen via the TAP transporters. Additionally, to extend our analysis, a set of peptides from the ATLAS (Altered TCR Ligand Affinities and Structures) database (<http://atlas.wenglab.org>) were compiled, which are known to be presented on TCR as well as the structures of TCR-peptide-MHC complexes is/are known [3448]. Interactions of these peptides with the TAP1-TAP2 complex were analyzed, along with tracing protein-peptide binding affinities.

The cancer-associated mutations and viral proteins both may share a common way trend towards TAP transporters, which is suppression/attenuation of their activity. Defective TAP transporters in few tumor tissues have been identified by down-regulation of TAP mRNA or mutations. It has been proposed that by inducing a TAP suppression/attenuation mechanism the tumor cells escape immune response [4615], and similarly, by down-regulating TAP1 levels, along with reducing MHC-I cell surface expression, the HPV (human papillomavirus) virus evades immune recognition [12049, 12150]. Several studies have linked the TAP transporter polymorphisms and the risk for the high-grade cervical intraepithelial neoplasia (CIN), cervical cancer, and pulmonary tuberculosis [121150]. Einstein et al. suggest that the TAP1 I333V and TAP1 D637G mutations reduce a high-grade CIN [12049, 12150]. The review by Rupert et al. highlighted defects in the TAP1 or TAP2 transporters can be the cause of bare lymphocyte syndrome (BLS) I, and during the viral infection the patients with BLS lacked increased susceptibility [12451]. Ozbas-Gerceker et al. applying the PCR-RFLP (restriction fragment length polymorphism) method investigated/determined that polymorphism in TAP1<sub>-333</sub> and TAP2<sub>-565</sub> can be associated with multiple myeloma-MM and chronic lymphoid leukemia-CLL, respectively [12552]. Moreover, the TAP2<sub>-665</sub> GG genotype could be a risk factor for different hematological malignancies types [12552]. The study of immunohistochemical expression of TAP1 and TAP2 in breast cancer patients suggested that their overexpression could be the cause of an aggressive breast tumor [12653]. In order

Therefore, to analyse the effects of virus encoded proteins and somatic mutations on the TAP1 and TAP2 transporters, a large number of mutational hotspots for TAP1 and TAP2 genes were retrieved from the Catalogue of Somatic Mutations in Cancer (COSMIC, <https://cancer.sanger.ac.uk/cosmic>) [3554], and cBio Cancer Genomics Portal (cBioPortal, <http://cbioportal.org>) databases [3655]. Effects of point mutations on the TAP1-TAP2 plasticity were determined by stability and binding affinity changes with respect to each other as well as with other binding partners. In addition, the TAP1 and TAP2 genes were further investigated considering the single nucleotide polymorphism (SNPs), as well as the number of mutations that have been distributed within the human population. The regions in the TAP1-TAP2 transporters exposed to bind to different viral proteins and were analysed in terms of the frequency of mutations or SNPs in those regions. Recently, a proteasome-dependent, but TAP-independent pathway has been described, showing that the well-known SIINFEKL peptide (the classical peptide epitope from ovalbumin presented by the MHC-I) can be imported into purified phagosomes in an ATP-



dependent but TAP-independent manner [409, 3750-3958]. Considering this fact, SIINFEKL peptide was also included to study its dynamics included with the TAP transporters as model for 8-mer peptides, as well as and to make a comparative analysis with other selected-studied peptides. To analyse the molecular consequences of cancer driving mutation and peptide binding with TAP1-TAP2 complex, Followingly, the functionally important mutations and a set of peptides were further assessed by molecular dynamics simulations (MDS) [4059], to analyse the molecular consequences of cancer driving mutation and peptide binding in TAP1-TAP2 transporters. In addition, to analyze how viruses inhibit TAP-mediated peptide translocation at molecular level, we studied dynamics of TAP attacking viral immune evasion proteins: BNLF2a from Epstein-Barr virus [41], CPXV012 from cowpox virus [42], ICP47 from herpes simplex virus type 1 [43, 44], US6 from human cytomegalovirus [45], and UL49.5 encoded by varicellovirus [46].

## 2. Materials and Methods

### 2.1. Experimental design and the sample preparation

#### 2.1.1. Cell culture with the treatment of IFN- $\gamma$ , as well as peptide isolation by mild acid elution

The melanoma A375 cells were previously described received as a gift from the Prof. Ted Hupp laboratory [4760], and these A375 p53-wild-type status cells were grown in DMEM (Dulbecco's Modified Eagle's Medium) medium (invitrogen) supplemented with 10% heat-inactivated fetal bovine serum, 1% penicillin/streptomycin (invitrogen), and incubated at 37°C with 5% CO<sub>2</sub>. The parental A375 cells were grown over 10 cm diameter plates, and for the treatment cells were exposed to 100 IU/ml IFN- $\gamma$  for 24h. In addition, following the protocol described in [4861], the mild acid elution (MAE) was performed with citrate phosphate pH 3.3 buffer. Biological replicates of 50 × 10<sup>6</sup> cells from both conditions (with and without IFN- $\gamma$  treatment) were used. Major histocompatibility complex (MHC) associated peptides were released by MAE, using 1.5 mL of citrate phosphate buffer at pH 3.3 for the 50 × 10<sup>6</sup> cell samples. Cell suspensions were then pelleted, and the resultant supernatants were considered as MHC-I peptides samples for further purifications. Followingly, the peptide sample extracts were desalted using Oasis HLB cartridges (30 mgs; water). Finally, the bound material was eluted with 1 mL H<sub>2</sub>O/80% methanol (MeOH)/0.2% formic acid (FA) v/v, and diluted to H<sub>2</sub>O/40% MeOH/0.2% FA v/v. Peptides were loaded on ultrafiltration devices (Microcon-10kDa centrifugal filters, Millipore) to isolate peptides < 10,000 Da, and remove higher molecular weight proteins. The resulting flow through content peptides was dried using vacuum centrifugation, which were then stored at -80°C until MS analysis.

#### 2.1.2. Mass spectrometry and the peptide sequencing

Vacuum dried MHC presented peptides were reconstituted in 30  $\mu$ L of loading buffer composed of 0.08% trifluoroacetic acid (TFA)/2.5% acetonitrile (ACN) (v/v), which Further, these peptides were analyzed by LC-MS/MS (Liquid chromatography-mass spectrometry cells) using an Ultimate 3000 nanoLC system coupled online to an Orbitrap Exploris 480 mass spectrometer (both from Thermo Fisher Scientific). The peptide samples (6  $\mu$ L) initially were loaded onto  $\mu$ -precolumn (C18 PepMap 100, 5  $\mu$ m, 100 Å) 300  $\mu$ m.i.d. x 5 mm length cartridge trap column (P/N 160454, Thermo FisherScientific) for 10 min at a 5 $\mu$ L/min flow rate. Peptides were separated on a C18 reversed-phase analytical column (C18 PepMap 100 RSLCnano column) 75  $\mu$ m, i.d. x 150 mm length, 2  $\mu$ m, 100 Å (P/N 164534, Thermo FisherScientific). LC solvents were composed of 0.1% FA in water(v/v) (solvent A) and 0.1% FA in water with 80% ACN (v/v/v) (solvent B). Peptides were eluted over a nonlinear gradient of 2.5-35% and 35-60% of B for 80 min and 15 min, respectively, at a flow rate of 300 nL/min controlled by the Ultimate 3000 nanoLC system. Finally, the column was washed with 95% B for 10 min. Samples were analyzed in data-dependent acquisition (DDA) mode with the following settings: survey scan (MS1) range was set to 300 to 1650 m/z with a resolving power of 120000 (at 200m/z) and an AGC target value of 300% with a maximum injection time of 100 ms. Data was acquired with the data-dependent "top20" method,

isolating the 20 most intense ions and fragment them by higher-energy collisional dissociation (HCD) with applied normalized collision energy 30%. MS/MS resolution was 60000 (at 200 m/z), AGC target value of 100% with a maximum injection time of 100 ms. For the MHC-class-I [presented](#) peptides, in case of unassigned precursor ion charge states, or charge states of four and above, no fragmentation can be performed. Dynamic exclusion of fragmented m/z values from the further selection set for the 20s, and inject 6  $\mu$ L of the first sample again (for technical duplicate). Followingly, the system was washed with two standard wash runs, ~~—~~ before loading any next biological sample.

### 2.1.3. Peptide identification and label-free quantification

The database quests were implemented adopting the MaxQuant package (version 1.6.12.0) [[4962](#), [5063](#)], to search the peak list against the human UniProt ([www.uniprot.org](http://www.uniprot.org)) database (downloaded on 12.08.2020 consisting of 75,093 entries) using the built-in Andromeda search engine [[5164](#)]. Mass tolerances for precursor and product ions were set to 20 ppm and 0.02 Da, respectively. Searches were performed without enzyme specificity and variable modifications for deamidation (N, Q) and oxidation (M). Possible sequence matches were restricted to ~~7- to~~ 25 amino acids (aa), the mass of a maximum peptide of 4600 Da. The initial allowed mass deviation of the precursor ion to 10 ppm, and the maximum fragment mass deviation was set to 10 ppm. Further, the statistical analysis was performed with Perseus software (version 1.6.10.45). The FDR (false discovery rate) level was 5%, and protein abundance calculated using normalized spectral protein intensity (LFQ intensity; label-free quantification) on MaxQuant software, as previously described [[5265](#)]. LFQ intensity values were set as Log2 transformed, and peptide groups quantified in all runs were considered for further analysis.

## 2.2. [PeptideModel](#) structure ~~preparation optimization~~, and [their](#) binding affinities with [the](#) TAP1-TAP2 transporters

### 2.2.1. [TAP transporters](#), [peptides](#), and [the](#) viral factors model generations

Adopting the “Hidden Markov method” implemented in the Phyre2 server (<http://www.sbg.bio.ic.ac.uk/phyre2>) sequence alignments with the known protein structures were generated, and based on the principles of homology modeling [[5366](#), [5467](#)], the derived alignments were used to generate full protein tertiary structures. The intensive mode of Phyre2 successfully inserted the lacking segments in the TAP1, TAP2, and ICP47 structures ([pdb id.PDB: 5u1d](#)) [[4918](#), [2423](#)], as well as generated the complete modeled tertiary structures of BNLF2a, CPXV012, UL49.5, and US6 viral factors. Based on the ~~confidence~~, percentage identity and alignment coverage the following templates were selected to model the proteins structures: TAP1 ([pdb id.PDB: 5u1d-chain A and 5yke-chain B](#)), TAP2 ([pdb id.PDB: 5u1d-chain B and 5ykf-chain-H](#)), ICP47 ([pdb id.PDB: 5u1d](#)), BNLF2a ([pdb id.PDB: 5zaz](#)), CPXV012 ([pdb id.PDB: 2lq0](#)), UL49.5 ([pdb ids.PDB: 6qan and 6qbj](#)), and US6 ([pdb id.PDB: 1otc](#)). The resulting modeled structures were subjected to energy minimization in Molecular Operating Environment (MOE; Chemical Computing Group Inc., Montreal, QC, Canada) [[5568](#)] applying the CHARMM27 forcefield [[5669](#)]. Furthermore, the tertiary structures for the 3957 peptides ~~sequence identified in from~~ immunopeptidome analysis ~~for the A375 melanoma cells~~ (with and without IFN- $\gamma$  treatment), ~~as well as~~ peptides from ATLAS (Altered TCR Ligand Affinities and Structures) database [[3448](#)], and SIINFEKL peptide [[3756](#)], were constructed and energy minimized using the homology modeling algorithms incorporated in the MOE (Chemical Computing Group Inc., Montreal, QC, Canada) package. ~~R~~The relaxed modeled structures of [the](#) peptides, [TAP transporters](#), and viral proteins were subsequently used in the protein-protein or protein-peptide docking pipelines.

### 2.2.2. Protein-protein docking, in silico point mutation, and virtual screening of peptides [with the TAP transporters](#)

The rigid body docking protocol from the MOE (Chemical Computing Group Inc., Montreal, QC, Canada) [[5568](#)] was used to achieve the complexes of TAP1-TAP2 with each viral

protein inhibitor (ICP47, BNLF2a, CPXV012, UL49.5, and US6). [The CHARMM27 forcefield \[5669\]](#) was used for energy minimization, ~~and~~ 500 conformations per protein-protein docking were generated and ranked ~~or~~ /scored using the Generalized Born/Volume Integral (GB/VI, kcal/mol) [\[5770\]](#) binding energies. Following, the refinement step based on molecular mechanics was carried out to analyse the best 100 poses of individual viral protein with the TAP1-TAP2 complex.

Peptides identified in [the](#) immunopeptidome analysis ~~for~~ [from](#) the melanoma A375 cells (with and without IFN- $\gamma$  treatment), and other 57 antigenic peptides (56 from ATLAS ~~(Altered TCR Ligand Affinities and Structures)~~ database [\[3448\]](#) and SIINFEKL [\[3756\]](#)) were screened against the TAP1-TAP2 complex using the MOE package (Chemical Computing Group Inc., Montreal, QC, Canada). The binding site [in the TAP transporters](#) ~~for~~ each peptide was identified through the “MOE site-finder” module, which computes the putative binding sites in a protein structure using a geometric approach with additional physico-chemical information such as; polarity or charge [\[5568, 5871-597260\]](#). The “Alpha Shapes” construction [\[5568, 5972, 60\]](#) geometric method was used to compute the possible residues that can be considered for peptide docking to the pocket formed by the TAP1-TAP2 transporters. Following the determination of potential peptide binding sites in the TAP1-TAP2 complex, [the protein\(TAP\)-peptide docking was performed using the CHARMM27 forcefield \[56\] and the “Triangle Matcher” placement method \(the receptor was defined as rigid and peptide as flexible\) \[55, 59\]. The resulting complexes were evaluated using the GBVI/WSA \(dG or dG, kcal/mol\) binding affinity scoring \[57, 61\], a forcefield based scoring function that calculates the free energy of binding of the peptide from a given position. MOE \(Chemical Computing Group Inc., Montreal, QC, Canada\) package applying the CHARMM27 forcefield \[5669\]. The MOE \(Chemical Computing Group Inc., Montreal, QC, Canada\) docking architecture formulates four different components involving; the generation of ligand-conformation, optional pharmacophore filtering, ligand placement with its scoring in the pocket, and flexible/rigid receptor and ligand refinement with re-scoring. For placement of peptide in the TAP1-TAP2 complex, the “Triangle Matcher” protocol was applied \(the optimized TAP structures were defined as rigid, whereas the peptides were set as flexible allowing their structures a high degree of freedom\) \[5568, 5972\]. Peptides are placed by superposing triplets of peptide atoms and triplets of receptor site points; the poses that clash with the protein were subsequently removed. To treat peptide flexibility in the protein-peptide molecular docking, 1000 conformations of each peptide were produced from their placement in the TAP binding site and the resulting complexes were evaluated using the GBVI/WSA dG \(kcal/mol\) binding affinity scoring \[5770, 6473\], a forcefield based scoring function that calculates the free energy of binding of the peptide from a given position. Particularly, for the dataset containing 3957 immunopeptidome peptides, the best 5 optimized poses as ranked by binding affinity \(GBVI/WSA dG\) with the TAP were stored, and for the 57 peptides retrieved from the available crystal structures, the top 10 poses were saved. Furthermore, these best Ppeptides influencing the binding energies and interactions with TAP proteins were considered for further evaluations.](#)

~~CHotspots of cancer~~ [derived](#) mutations in the TAP1 and TAP2 proteins were subjected to the “Sequence Design” protocol of the protein design module in the MOE (Chemical Computing Group Inc., Montreal, QC, Canada) package. This pipeline computes the frequency with probability of amino acids at the residual mutation sites (mutation expression) [\[5972\]](#). The goal was to obtain the stability ~~or~~ /binding affinity trade-offs, when peptide binds to wild-type and the ~~mutated~~ TAP transporters. In addition to applying this approach, all cancer hotspot residues were mutated ~~by~~ [using other](#) 20 [other](#) amino acids [A, R, N, D, C, Q, E, G, H, I, L, K, M, F, P, S, T, W, Y, and V]. The structural model for each single mutation was generated, the energy window was set to 10 kcal/mol, RMSD limit was 0.25 Å, and residues farther than 4.5 Å were kept fixed. The “LowMode MD” was used with default parameters to produce a thorough conformational ensemble [\[6274\]](#). [The R](#)esultant TAP mutations significantly affecting the stability and peptide binding affinity, were further selected for [the](#) MD simulations [\[4059\]](#).

### 2.2.3. Single nucleotide polymorphisms in [the](#) TAP1 and TAP2 genes

The Genome Aggregation Database (gnomAD) [6575], an online resource containing genome and exome sequencing variants from diverse projects and investigators, was used in order to detect the distribution of the SNPs (single nucleotide polymorphisms) across the TAP1 and TAP2 genes. Variants of these genes were downloaded in CSV format and processed in R environment (version 3.6.3), using the g3viz package to plot the protein modifications occurring downstream of the genome mutations.

#### 2.2.4. The molecular dynamic simulations; and its system setup

The initial position-orientation of the wild-type or mutant TAP1-TAP2 transporters embedded in the membrane, and in complexed with peptide or the viral protein was defined using the PPM server ([https://opm.phar.umich.edu/ppm\\_server](https://opm.phar.umich.edu/ppm_server)) [6476]. Optimizing the free energy of transfer from water to the membrane environment, the PPM server thoroughly cross-verify dozens of transmembrane and peripheral proteins and peptides [6476]. Resulting positioned complexes were used as an input for the CHARMM-GUI membrane builder (<http://www.charmm-gui.org/?doc=input/membrane.bilayer>) [6577], to prepare the membrane-embedded complexes. The CHARMM-GUI platform provides a series of CHARMM inputs necessary to generate membrane embedded complexes for MD simulations [6577]. The supramolecular PLC is expressed in the endoplasmic reticulum, and the TAP1-TAP2 resides in the ER membrane to transport the peptide across the membrane [6678]. Thus, to better understand the protein dynamics in the membrane environment, TAP complexes were embedded in a membrane containing 660 palmitoyloleoyl phosphatidylcholine (POPC) lipids and 66 cholesterol molecules [6779], accommodating the larger separation of TAP<sub>NBDs</sub>. The membrane composition was evenly distributed throughout both leaflets of the bilayer. Other parameters applied were; rectangle box type, tetragonal crystal type, and a water thickness of 22.5 Å on the top as well as on bottom of the system. A heterogeneous lipid bilayer was generated using the replacement method [6577, 6880], and the distance-based algorithm was used as an ion-placing method. The following resulting 24 twenty-four TAP-membrane complexes were further investigated using the MD simulation technique; in apo-form (TAP1-TAP2 and pep18-alone), with viral protein (TAP1-ICP47-TAP2, TAP1-BNLF2a-TAP2, TAP1-CPXV012-TAP2, TAP1-UL49.5-TAP2, and TAP1-US6-TAP2), with peptides (TAP1-SIINFEKL-TAP2, TAP1-pep18-TAP2, TAP1-pep20-TAP2), with mutations (TAP1<sub>E446K/W</sub>-TAP2, TAP1<sub>V437F/I</sub>-TAP2, TAP1<sub>R372Q</sub>-TAP2, TAP1-TAP2<sub>D370N/W</sub>, TAP1-TAP2<sub>G208F/S</sub>, and TAP1-TAP2<sub>R373H</sub>), and mutation+peptide (TAP1<sub>R372Q</sub>-pep18-TAP2, TAP1<sub>R372Q</sub>-SIINFEKL-TAP2, TAP1-pep18-TAP2<sub>R373H</sub>, and TAP1-SIINFEKL-TAP2<sub>R373H</sub>) were further investigated using the MD simulation technique.

The MD simulations were performed using the NAMD package [6981] with CHARMM36 forcefield [7082-7284], and the TIP3P [7385] water model. The particle-mesh Ewald method [7486] was used to treat long-range electrostatics with a grid spacing of 1 Å, and a cut-off of 12 Å was used for van der Waals interactions. The force based switching was used with a switching distance of 10 Å. Periodic boundary conditions (PBC) were applied with constant pressure and temperature (NPT) ensemble to avoid finite size effects. Langevin dynamics [7587] was used to maintain constant temperature with a damping coefficient of 1 ps<sup>-1</sup>. The Nose-Hoover Langevin piston method [7688] was applied to control the constant pressure with a decay period of 50 fs with a damping timescale of 25 fs. SHAKE algorithm [7789] with a time step of 2 fs was used to constrain all the non-polar bonds involving hydrogen atoms. Equilibration of the system was performed for 10 ns at 303.15 K and the equilibrated systems were subsequently used to perform MD production runs for 100 ns at 303.15 K. The visual molecular dynamics (VMD) [7890], MOE (Chemical Computing Group Inc., Montreal, QC, Canada), and BIOVIA Discovery Studio visualizer (Dassault Systèmes, BIOVIA Corp., San Diego, CA, USA) packages were used to analyse the molecular dynamics trajectories.

### 3. Results and discussions

A systematic immunopeptidome workflow was implemented, and a set of peptides presented over the MHC-I molecules in the melanoma A375 cells were isolated (Figure 1c). ~~Based on the The~~ sequences ~~or datasets~~ of the MHC-I-bound peptides, ~~were determined, and~~ their tertiary structures were generated using the homology modeling techniques; in order to analyse the pattern of binding as well as peptide translocation through TAP transporters. Furthermore, the binding and dynamics of viruses ~~with TAP complex as well as the and~~ cancer mutations targeting the TAP transporter ~~process function~~ were analyzed, ~~thereby altering the MHC-I antigen presentation.~~

### 3.1. Human melanoma cells immunopeptidome ~~datasets~~, and ~~screening of~~ peptides ~~screened~~ against the TAP transporters

The melanoma A375 cells were grown *in vitro* under typical cell culture conditions, and the cells characterized with and without ~~Interferon- $\gamma$~~  (IFN- $\gamma$ ) treatment ~~in order to define~~ ~~terminated that~~ the IFN- $\gamma$  induced changes on the MHC antigen processing and presentation ~~machinery pathway~~ (Figure 1c). The distribution and length of the identified peptides from the both conditions (~~with and without IFN- $\gamma$  treatment~~; Figure 2a and Table S1-S3), suggest that there were more peptides identified in the IFN- $\gamma$  treated cells (3081 peptides, Table S1) compared to that of the ~~non-treated~~ (~~termed as wild-type in this study~~) ~~wild-type~~ cells (1968 peptides, Table S2). About 1104 peptides were common in IFN- $\gamma$  treated and non treated samples, whereas 1974 peptides were found only IFN- $\gamma$  treated cells and 863 peptides only in the wild-type (non-treated) (Figure 2b-2f). ~~Exclusively, in the IFN- $\gamma$  treated samples, a few self-peptides from the TAP1 (AALPAAALW, LLYESPERY, RSLQENIAY, RTALPRIF, SAMPTVRSF, and TEVDEAGSQL) and TAP2 (YLHSQVVSV) were identified (Figure 2g).~~

Interestingly, the immunopeptidome data highlights that the majority of MHC-I associated peptides have a length distribution of 9 ~~and or~~ 10 mers (Figure 2d), and a few peptides ~~with around 15-mer in length~~ (Figure 2d). ~~In addition, exclusively for the IFN- $\gamma$  treated samples, few peptides also from TAP1 (AALPAAALW, LLYESPERY, RSLQENIAY, RTALPRIF, SAMPTVRSF, and TEVDEAGSQL) and TAP2 (YLHSQVVSV) were identified (Figure 2g).~~ Particularly, the MHC-I antigen processing involves proteasome-mediated protein degradation as well as TAP-mediated peptide transport, and these ~~both~~ processes can generate and handle ~~such longer peptides longer~~ than the canonical 8-10 aa (amino acids) long [10591, 10692]. Stryhn et al. [10692] examined the size dependence of peptide binding to MHC-I as well as stimulating T-cells, in proteolytically controlled assay systems by systematically extended the N- and/or C-terminals of optimally sized peptides. Their findings support the consensus view that MHC-I binding and T-cell recognition tends to focus on short well-defined peptides; ~~h~~However in some cases, longer peptides can also bind to MHC-I and such extensions may be accommodated by protrusion out of the MHC-I and can potentially be recognized by T-cells [10692]. ~~In some cases~~ ~~the MHC-I and T-cell~~ ~~in some cases~~ can detect the identity of the extension (that it could be part of the specificity of the T-cell immune response) and such extensions may play a physiological role [10692]. The crystal structures of peptide bound MHC-I molecules argue in the favor of peptide-size restrictions and suggest that when the anchors are appropriately positioned, slight variations in size can be accommodated through zigzagging or bulging in the middle [10692, 10893]. However, structures involving a protruding C+1 extension has been determined in which, the C-terminal residue was found to extend up and out of the F-pocket and the corresponding side chains of MHC-I was found to be re-oriented to accommodate the peptide extension [10692]. This explains the flexibility of the otherwise apparently closed binding cleft of the MHC-I allowing for binding of different peptide sizes as long as the binding energy is sufficient [10692]. Moreover, it has been shown that naturally bound peptides eluted off the MHC-I spans a size range from 6-33 residues, although the majority (~ 80%) were of the canonical 8-11 aa [10692, 11294, 95]. The proteasome generates peptides varying in size from 4-24 aa, and it has been estimated that ~30% of the peptides are 8 aa or longer. The TAP transporter can translocate peptides up to 40 residues long, though 8-13 residues long peptides are transported most efficiently [10692, 11496].

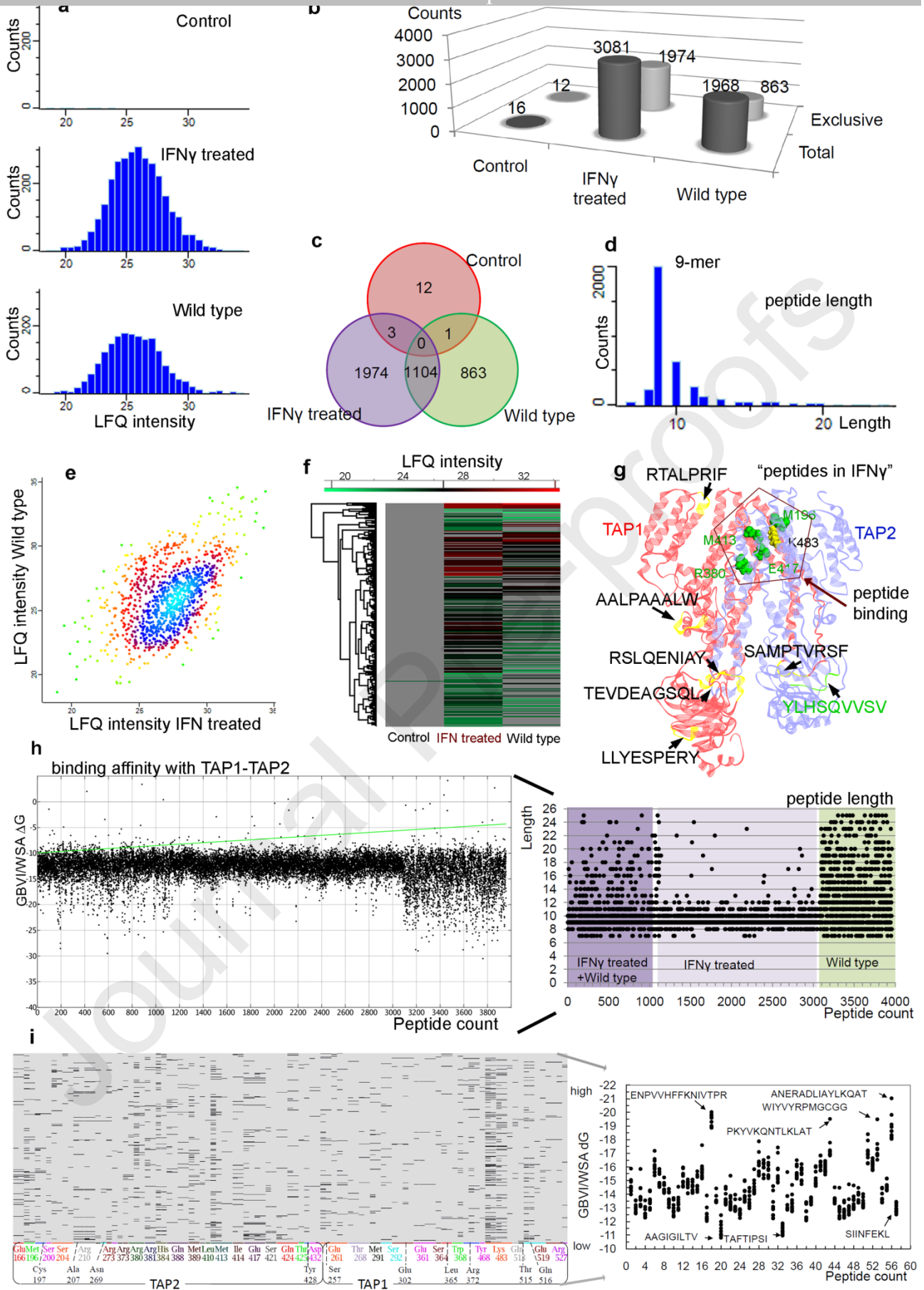


**Figure 2.** Comparative immunopeptidome analysis. **(a)** Logarithmized  $\log_2(x)$  data, after reverse filtering the rows using categorical columns, for the MHC-I peptide presentation from the control,

IFN- $\gamma$  treated, and ~~non-treated wild-type~~ (~~non-treated~~ termed as wild-type in this study) samples. **(b)** Peptide counts ~~identified~~ per sample, as well as the exclusive MHC-I peptides for a particular sample. **(c)** Venn diagram representing the common and unique peptides in all three/two respective samples. **(d)** Length distribution of the MHC-I peptide ~~that were~~ identified in all three samples (control, IFN- $\gamma$  treated, and ~~untreated~~/wild-type). **(e)** and **(f)** Scatter plot and heat map describing the LFQ intensities between wild-type vs IFN- $\gamma$  treated samples. **(g)** TAP1 and TAP2 peptides identified (presented over MHC-I molecule) only in the IFN- $\gamma$  treated samples, labelled in black (marked yellow) are from TAP1 and in green are from TAP2. **(h)** Identical 3957 peptides from three samples (control, IFN- $\gamma$  treated, and ~~non-treated wild-type~~) were screened against the TAP1 and TAP2 ~~transporters~~. Right panel represents the peptide length (differentiated according to the samples), and the left panel represents particular peptide binding affinity with TAPs (five different conformations per peptide). In panel **g**; residues K483 (TAP1) and M196, R380, M413, and E417 (TAP2) were found ~~commonly~~ interacting with the 3957 peptides (from control, IFN- $\gamma$  treated, and ~~non-treated wild-type~~), docked with TAP1 and TAP2 are highlighted (yellow from TAP1 and green from TAP2). **(i)** Barcodes represent (left panel) fingerprint analysis of peptides (from the ATLAS database [3448]) forming interactions with TAP1 and TAP2 proteins (Table S4), and the selected peptide fingerprints as a matrix (one row per entry, one column per fingerprint bit) in which a set bit is drawn as a black rectangle. X-axis shows the residue numbers that correspond to each group of fingerprint bits, and is coded with an arbitrary sequence of colors. The scattered plot (right panel) represents the binding affinity of each peptide against TAP transporters. Peptides with the highest and lowest binding affinity are highlighted, and few were selected for MD simulations in order to examine their kinetics. The plot (right panel) presents a binding affinity of 10 conformations for each peptide against the TAP1-TAP2 transporters.

*In silico* virtual screening of peptide datasets was performed against the TAP1-TAP2 transporters ~~and~~; the resultant TAP-peptide complexes were ranked by the docking score (GBVI/WSA dG, kcal/mol; Figure 2h and 2i). The MHC-I peptide having the length of 8, 9, or 10 mers shows ~~the a~~ binding affinity between -10 to -15 kcal/mol (GBVI/WSA dG, ~~kcal/mol~~; Figure 2h) with the TAP1-TAP2 transporter. ~~Followingly, P~~peptides having ~~a~~ length of 14-26 amino acids formed binding affinities ~~with the TAP transporters~~ in ~~thea~~ range of -20 to -25 kcal/mol (GBVI/WSA dG, ~~kcal/mol~~; Figure 2h) ~~with the TAP transporters~~. Overall, the peptides identified from the IFN- $\gamma$  treated samples ~~exhibited were found to have~~ less ~~binding affinity~~ with the TAP proteins, compared to the peptide from ~~the untreated wild-type samples~~ cells. ~~Besides~~In addition, these binding affinity difference of peptides from IFN- $\gamma$  treated and ~~untreated wild-type~~ samples ~~exhibited~~; a correlation with the length ~~of peptide was noticed~~, i.e. - ~~and~~ peptides from IFN- $\gamma$  treated ~~have~~s short length (peptides 1100-3100 in Figure 2h and Table S5), whereas peptides from ~~untreated wild-type~~ are comparatively longer (peptides 3100-3957 in Figure 2h and Table S5). ~~Based on the peptides binding affinities with TAP transporters and the higher number of 9-10 mers identified in the immunopeptidome peptides identified~~ (Figure 2d and 2h), it could be proposed ~~These data suggest that~~ peptides ~~having weak that are less binding affinity~~ with the TAP1-TAP2 transporters could ~~exhibit have a~~ faster ~~be transported~~ from the cytosol to ~~the ER, and theorize that the ER could be occupied with a greater number of shorter length peptides~~. Moreover, it has ~~previously been reported that TAP transporters can translocate 8-13 residue s long peptides most efficiently~~ [10692, 96, 11397, 114]. The IFN- $\gamma$  treated ~~cells~~ ~~had~~s a higher number of peptides identified ~~compared to than~~ the ~~untreated wild-type~~, suggesting ~~that upon~~ inducing immunity, ~~and has with~~ a majority of shorter length peptides ~~that have a lower less TAP1-TAP2 binding affinity with the TAP1-TAP2~~ (Figure 2d and 2h). In addition, more residues (M196, R380, M413, and E417) from TAP2 were involved in interacting with the peptide, and fewer peptides were detected from TAP2 itself, whereas the reversed was observed for the TAP1 (only residue K483 binds to the peptide; Figure 2g). These ~~peptide interacting on TAP residues found interacting with peptides from TAP transporters~~, were ~~also~~ previously ~~reported noted~~ in different works [1615].

Alongside the immunopeptidome dataset from the melanoma cells, ~~to~~ turner investigate and validate the findings, ~~a~~ peptide datasets from the ATLAS database [3448] ~~were~~ retrieved alongside the immunopeptidome dataset from the melanoma cells. For these peptides the structures of each TCR-peptide-MHC complex is known, and were screened against the TAP1-TAP2 transporter model (Figure 2i, S1, S2, and Table S4). ~~Findings suggest a correlating behavior (Figure 2h and 2i) between the peptides~~ Analysis of ~~the~~ from immunopeptidome data and peptides from ATLAS database [3448] (Figure 2h and 2i) ~~correlate~~s with each other, in terms of ~~binding affinity versus peptide length data (Figure S311a and S311b).~~ Most ~~higher number of the~~ peptides with 8 or 9 ~~mers exhibited lower~~ have shown less binding affinity compared to the longer peptides (Figure S311c and S311d). TAP1 and TAP2 residues forming the interactions with the studied set of peptides were identified, ~~which highlights an overlap between that the majority of interacting residues were found common for immunopeptidome peptides and peptides from ATLAS database that were screened against transporters (Figure S311a and S311b).~~ and ~~Additionally,~~ the binding conformations of ~~individual~~ a few peptides showing highest and least affinity to TAP were ~~evaluated~~: pep56 (ANERADLIAYLKQAT) -21.03 kcal/mol, pep18 (ENPVVHFFKNIVTPR) -20.02 kcal/mol, pep53 (WIYVYRPMGCGG) -19.49 kcal/mol, pep43 (PKYVKQNTLKLAT) -19.52 kcal/mol, pep57 (SIINFEKL) -13.44 kcal/mol, pep20 (AAGIGILTV) -12.46 kcal/mol, and pep33 (TAFTIPSI) -11.87 kcal/mol. Among which the ~~molecular dynamics of the~~ pep18, pep20, and SIINFEKL (8-mer model) peptides ~~with the TAP1-TAP2 transporters~~ were ~~further analysed~~ selected for further MD analysis in complex with the TAP1-TAP2 transporters, in order to ~~make comparative analysis of their kinetic behavior~~ (Figure 2i and S24).

### 3.2. Scaling effects of viral proteins and somatic mutations on the TAP transporters

The modeled viral protein structures were screened against the predicted active sites, and the data suggests that all selected viral protein inhibitors targeted the peptide transport pockets of TAP proteins ~~by exhibiting through~~ different possible interactions. The binding free energy reports (GBVI/WSA dG; kcal/mol) and binding mode of viral proteins ~~s~~ to TAP structure are shown in Figure 3a. Among different viral proteins ~~s~~ screened against the TAP1-TAP2 complex, the ICP47 protein formed the highest affinity (-108.18 kcal/mol), and in the second position is the BNLf2a protein with binding affinity of -90.08 kcal/mol, whereas the proteins CPXV012, US6, and UL49.5 obtained almost similar affinity (-81.71 kcal/mol, -85.27 kcal/mol, and -85.28 kcal/mol, respectively). ~~The~~ ~~B~~ binding mode of viral protein inhibitors to TAP correlates with the proposed models [3338]; ~~and shows that~~ four out of five viral proteins targeted the ~~helical~~ regions (Figure 3a) of TAP1 ~~structure~~ and showed a similar pattern of blocking the peptide translocation cavity of ~~the~~ TAP transporter. ~~Whereas,~~ ~~†~~ The US6 protein binds to both ~~TAP~~ transporters (~~TAP1 and TAP2~~) at the loop regions toward ~~the~~ ER lumen, with almost similar affinity ~~points to its precise mechanism of inhibition~~ (Figure 3a).

~~The~~ ~~s~~ Single nucleotide polymorphisms (~~SNPs~~) are ~~considered as~~ one of the most common forms of genetic variation ~~or nucleotide modifications~~, and a large number of human genes associated with viral infections comprise SNPs [7998]. ~~This kind of SNPs analysis in the human genome has a growing emphasis, since they have been linked to multiple human diseases. For both~~ Therefore, TAP1 and TAP2 ~~genes~~ transporters, the SNPs were identified ~~and to assess the polymorphisms, and importantly the residues from;~~ the TAP transporters TAP residues involved in binding with the ~~within 8 Å of the~~ viral proteins (~~within 8 Å~~; BNLf2a, CPXV012, ICP47, US6, and UL49.5) were traced (Figure 3b and Table S6-S7) ~~were highlighted to assess the polymorphisms (Figure 3b and Table S6-S7).~~ Overall, both TAP1 and TAP2 transporters behave differently when ~~correlating SNPs to that of the TAP interacting residues with viral proteins. Particularly~~ Exclusively for ~~the~~ TAP1 ~~protein~~, the frequency of SNPs was found lower in the regions binding to viral proteins. (Figure 3b). ~~From †~~ These data suggest it could be proposed ~~A possible explanation of this event in TAP1 could be that the viruses~~ may aim for ~~the~~ most conservative ~~TAP1~~ regions ~~as an adaptive mechanism, which could assist to overcome the problem of protein-protein interaction that might result from amino acid changes due to SNPs~~ (Figure 3b and Table S6-S7). ~~On the~~



~~conary, by contrast~~ ~~form~~ TAP2, the frequency of SNPs was found higher in the regions binding with viral proteins (Figure 3b). ~~In addition,~~ ~~All~~ like the SNPs in the TAP transporters (Figure 3b), a similar trend was observed in the analysis of cancer-associated mutations ~~for in both~~ TAP proteins transporters (Figure 1 and 3b), i.e., for TAP1 protein regions with less cancer variants were targeted by viruses, whereas in TAP2 highly mutated regions were involved in binding with viral protein (Figure 1e and 3b).-

Journal Pre-proofs

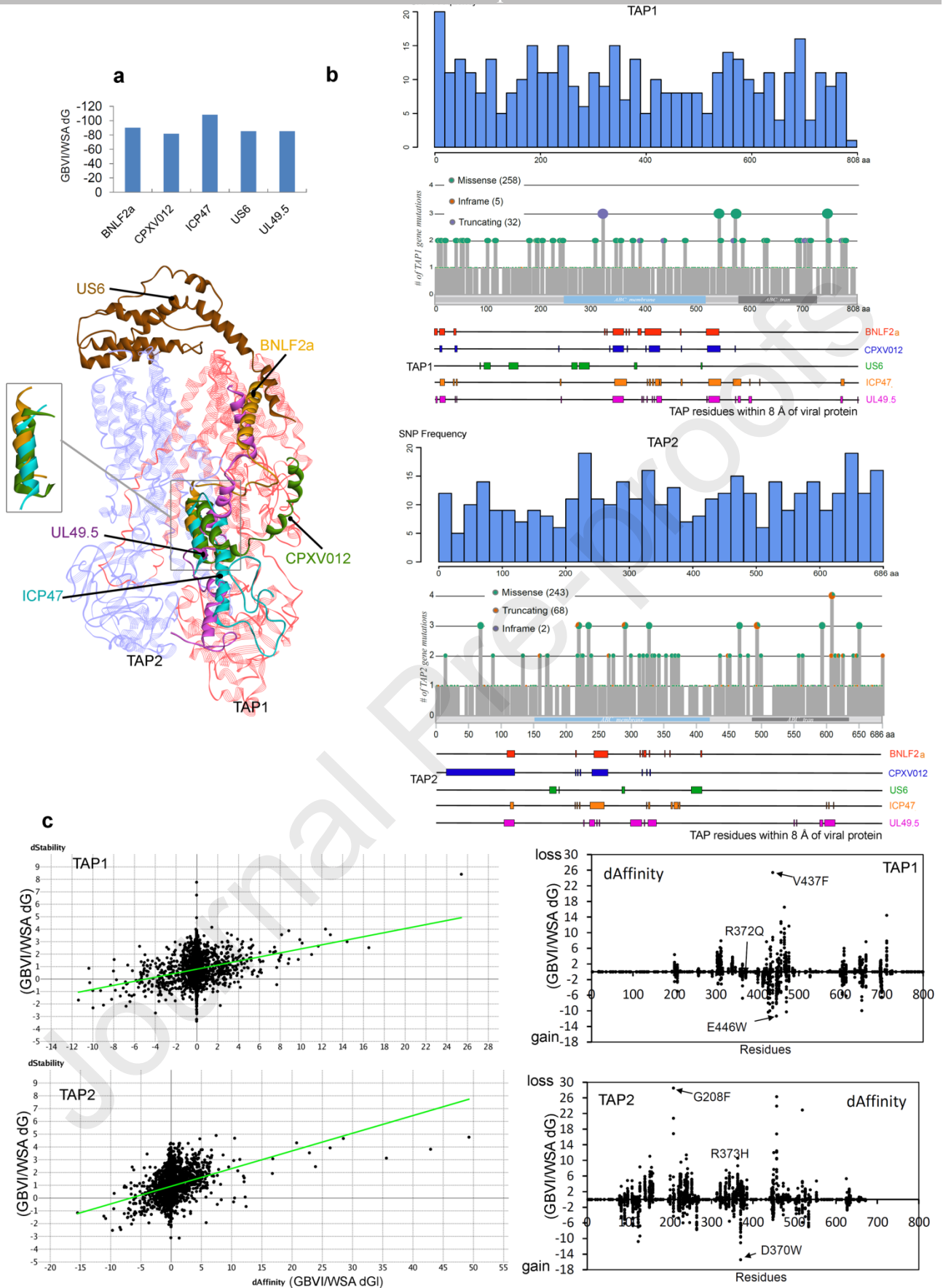


**Figure 3.** *Virtual In silico* screening of viral proteins, peptides, and cancer-associated mutations on the TAP1-TAP2 transporters. **(a)** Viral proteins (BNL<sub>f</sub>2a, CPXV012, ICP47, US6, and UL49.5) docked with the TAP transporters, and the binding conformations for each studied viral components

resembles almost a complementary state ~~as shown in~~ (Figure 1b), as well as proposed in different studies [33, 1918, 2423, 3338]. In addition, 4 out of 5 viral proteins assembled a similar conformational pattern to block the peptide transportation cavity in TAP proteins. **(b)** Lollipop plots for the TAP1 and TAP2 gene mutations, colours in the figure represent different types of polymorphism. In the top panel of each lollipop plot, a bar plot represents the cumulative frequency of mutations for each 20 amino acids. On the bottom panel, the regions of interaction from the TAP1 and TAP2 proteins with the viral proteins are represented in different colours (identified in virtual screening; Figure 3a). **(c)** Mutational landscape of TAP1 and TAP2 proteins, datasets of cancer variants from COSMIC (cancer.sanger.ac.uk) and cBioPortal (www.cbioportal.org) were screened with the TAP transporters tracing their change in ~~stability~~ (GBVI/WSA dG, kcal/mol) and ~~affinity~~ (GBVI/WSA dG, kcal/mol) upon mutation (applying residue scan methodology in MOE [5568]). In addition to the cancer-associated mutations from COSMIC (cancer.sanger.ac.uk) and cBioPortal (www.cbioportal.org), each amino acid was mutated with other 20 amino acids [A, R, N, D, C, Q, E, G, H, I, L, K, M, F, P, S, T, W, Y, and V] to ~~search for mutations that identify the~~ change ~~in~~ binding affinity (GBVI/WSA dG, kcal/mol). ~~The~~ Left panel describes a comparison of change in structural stability with change in binding (TAP1-TAP2) affinity upon introducing each amino acid variant. The right panel scatter plot describes the effects of mutant ~~(from TAP1 or TAP2)~~ residues ~~(from TAP1 or TAP2)~~ on the protein-protein binding affinity (GBVI/WSA dG, kcal/mol).

Mutations in a protein may affect its structural stability, disrupt protein ~~interactions,~~ ~~interactions with other partner biomolecules~~ and render proteins non-functional, and potentially promote tumor progression [5972]. Therefore, along with the cancer-associated variants from the TAP transporter retrieved from the COSMIC (cancer.sanger.ac.uk) and cBioPortal (www.cbioportal.org), ~~and~~ screened for change in structural stability and ~~in~~ binding (TAP1-TAP2) affinity, these hotspots regions or amino acids were also ~~screened by~~ mutated ~~by with the~~ other 20 amino acids (Figure 3c). The findings suggest that ~~upon~~ point mutations ~~in~~ either ~~in~~ TAP1 or TAP2 ~~is~~ sufficient to alter the protein-protein ~~binding interactions,~~ which can significantly affect the peptide binding or the peptide transport process (Figure 3c). ~~Screening (fingerprint) analysis indicate that The~~ TAP1 or TAP2 ~~amino acids binding with peptides in screening (fingerprint) analysis peptide interacting interface phase~~ (Figure 2i), ~~were are~~ also found mutated in different cancer types. Such residue variants are; R372Q, S364R, S364I, Q516K, E519K, and R527K from TAP1 protein, and E166G, E166K, M196V, R210L, R373H, and S200F from TAP2 (Figure 3c). Considering the peptide binding region [4615] and protein-protein interface, cancer mutations and their binding affinity ~~analysis,~~ TAP1<sub>R372Q</sub> and TAP2<sub>R373H</sub> were further studied by MD simulations. In addition, the cancer ~~hotspot regions as well as their derived~~ mutants ~~that have obtained~~ inducing highest (best) and lowest ~~binding~~ affinity were selected for MD ~~simulation analysis:~~ TAP1<sub>V437I</sub> (-7.92 kcal/mol), TAP1<sub>V437F</sub> (25.43 kcal/mol), TAP1<sub>E446K</sub> (-5.99 kcal/mol), TAP1<sub>E446W</sub> (-11.35 kcal/mol), TAP2<sub>D370N</sub> (-1.23 kcal/mol), TAP2<sub>D370W</sub> (-15.43 kcal/mol), TAP2<sub>G208S</sub> (1.62 kcal/mol), and TAP2<sub>G208F</sub> (28.53 kcal/mol) (Figure 3c).

### 3.3. Viral components with similar modulatory actions towards the TAP transporters

~~Virus or the v~~ Viral proteins (for example; BNL2a, CPXV012, ICP47, US6, and UL49.5) can significantly manipulate the peptide transport process by binding directly with the TAP1 or TAP2 transporters ~~from the PLC complex.~~ Therefore, to understand the molecular recognition of the TAP1-Virus-TAP2 ~~is an ultimate need,~~ and ~~in this work particular the~~ different viral proteins (BNLF2a, CPXV012, ICP47, US6, and UL49.5) we ~~simulated their interactions re-investigated by~~ ~~simulating~~ with the TAP transporters (Figure 4a, represents TAP1-ICP47-TAP2 complex). Evaluating ~~the~~ stability for simulated systems solving the RMSD (root-mean-square deviation; ~~of~~ ~~all non-hydrogen atoms~~) equation, suggests that the majority of the viral protein predominantly destabilizes TAP1 (Figure 4b), ~~compared to that of the TAP2 protein alone. whereas contrary behavior was observed towards TAP2.~~ Particularly, ~~for TAP1~~ such a visible difference was detected

for the viral proteins; UL49.5 and BNLF2a (Figure 4b), whereas for TAP2 the UL49.5 induced the highest fluctuation and BNLF2a the least (Figure 4b). The apo-form of TAP1 showed a persistent RMSD plot (~8 Å) during the 100 ns of MD simulations, whereas the TAP2 showed a slightly increasing flexibility over time that stabilized between ~70-100 ns (Figure 4b). Among the studied viral proteins self-RMSD findings suggest that, the UL49.5 exhibited the highest fluctuations and BNLF2a was the most stable of the viral proteins (Figure 4b).

Moreover, solving the RMSF (root mean square fluctuation) equation over C $\alpha$  atoms of each amino acid revealed a similar nature for both TAP proteins-transporters was noticed, i.e., a majority of residues in the apo-system were shown comparatively more stability compared as compared that to the viral-bound binding systems, except for some residues in TAP2 (for example 390-410 aa; Figure 4c). Such behavior of TAP2 residues from RMSF correlates with the RMSD data which showed a slightly increasing flexibility of TAP2 over time (Figure 4b). The dynamics of the TAP1/2-viral protein complex dynamics suggest that Upon binding of the viral proteins, an allosteric effect inducing increased amino acid fluctuations in several regions of both TAP1 and TAP2 genes-transporters were analyzed-indicated (Figure 4c). Interestingly, the peptides from TAP1 peptides (97RTALPRIF104, 206AALPAAALW214, 432SAMPTVRSF440, 653RSLQENIAY661, 694TEVDEAGSQL703, and 744LLYESPERY752) and TAP2 peptide (541YLHSQVVS549) presented on MHC-I that were identified in the immunopeptidome data upon IFN- $\gamma$  treated melanoma cells (Figure 2a), originates from the highly fluctuating regions directly interacting with upon viral factors binding or the allosterically affecteds of by viral binding (Figure 4c).

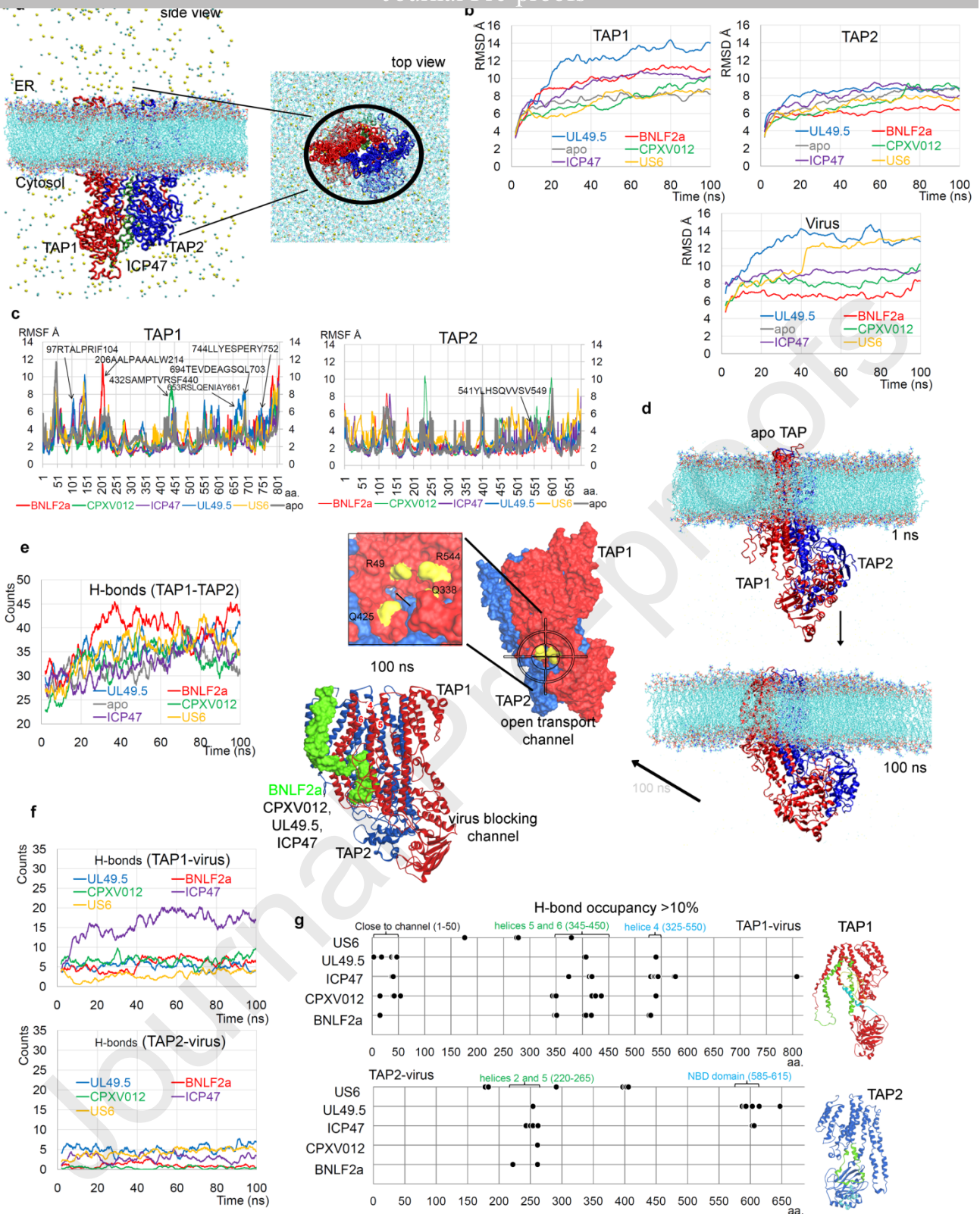


**Figure 4.** The binding interfaces of different viral proteins (BNLF2a, CPXV012, ICP47, US6, and UL49.5); with the TAP1 and TAP2 transporters. **(a)** One molecular dynamic cell in periodic boundary conditions (for example, the TAP1-ICP47-TAP2 complex), which includes proteins, water, and ions. **(b) and (c)** RMSDs and RMSFs of the TAP transporters from the MD simulations, respectively and the bottom panel describes the RMSDs of viral factors. **(c)** RMSFs of individual amino acids from both TAP transporters. **(d)** Structural dynamics of the TAP1-TAP2 transporters representing the tilt movement of the TAP1/2<sub>NBD</sub> domains forming an entry gate or transport channel open toward the cytosol. In addition, the majority of the studied viral proteins in this work

were found interacting with the passage or open transport channel which could block the peptide from invading the transport channel. TAP1 helices (helix\_4; 501-544 aa, helix\_5; 338-376 aa, helix\_6; 384-425 aa) forming an open cytosolic passage and binding with the viral proteins are labeled. (e) The intermolecular hydrogen bond interactions formed between the TAP1 and TAP2 proteins during the MD simulation time course and with occupancy  $\geq 10\%$ , in the presence and absence of different viral proteins. (f) Hydrogen bond interactions between the viral protein and the TAP transporters. (g) Residues from TAP1 or TAP2 involved in binding the viral proteins with occupancy  $\geq 10\%$ , and the right panel represents the position of these regions over the protein structure.

The structural dynamics of the TAP1-TAP2 complex in the presence and absence of a viral proteins, revealed that, in all simulated systems the TAP<sub>NBD</sub> domains formed a tilt movement toward the cytosol membrane cytosol-faced (as shown in Figure 4d and Videos S1, S2). Upon such displacement of the TAP<sub>NBD</sub> domains, a passage or the peptide in the transport channel formed by TAP1 (helix\_4; 501-544, helix\_5; 338-376, helix\_6; 384-425) and TAP2 (helix\_5; 249-289, helix\_6; 294-344), which is opened towards the cytosol (Figure 4d). From these data it may be proposed that the opening or closing of this cytosolic passage opening or closing confirmation by the TAP transporters (TAP<sub>NBD</sub> domains) can also be associated with ATP hydrolysis, and, thus, resulting in the peptides being directly presented to the PLC complex. This cytosolic "open-state" transport channel by of the TAP proteins, that may intake peptides from cytosol-towards-ER and was targeted by 4 (BNLF2a, CPXV012, ICP47, and UL49.5) out of 5 studied viral proteins blocking the transport channel (Figure 4d and S43).

The presence of the different Systems with Viral proteins have increased in the complex induces the protein-protein intermolecular interactions between TAP transporters-TAP2 interactions compared to that of the apo-system form (Figure 4e and Table S8). and In addition, the glutamic acid-arginine residues pairs were dominant in TAPs protein-protein interactions (Figure 45e and Table S8). A slight difference is observed concerning the viral proteins when interacting with TAP1 or TAP2, i.e., Investigating the binding between the viral protein and TAP transporters, revealed that the viral proteins; BNLF2a, CPXV012, and ICP47 viral components formed a higher number of interactions with TAP1, whereas UL49.5 and US6 shared relatively equal interactions with both transporters TAP proteins (Figure 5f4f). Correlating these intermolecular transporter-viral interactionsse data (Figure 4e4f) together with the SNPs data and cancer mutations in TAP1-TAP2 (Figure 1 and 3) complex, suggest that for in the case of TAP1 protein regions with lower SNPs frequency and as well as a few cancer variants was found making higher interactions with viral factors. On the contrary whereas the viral protein factors binds to highly mutated TAP2 regions which is highly mutated. Amino acids involved in the intermolecular H-bond interactions between TAP-viral proteins were identified, and long lasting interactions  $\geq 150$  ns between TAP-viral proteins were identified and are presented in Table S9. Particularly, a higher number of residues from the TAP1 protein, residues that were involved in the interactions with viral components, compared to the TAP2 gene (Table S9). In TAP1 amino acids from belongs to the helices 4, 5, and 6 (residues range 345-450 aa and 325-550 aa), as well as from residue range 1-50 aa which is located close to the transport channel were found to interact with viral factors binding-virus (Figure 4g and Table S9). Additionally, the TAP2 residues in range 220-265 aa (from helices 2 and 5) and 585-615 aa (TAP<sub>NBD</sub> domain) from TAP2 were involved in binding with the viral proteins (Figure 4g and Table S9). Several amino acids from TAP1 or TAP2 were found in common when interacting with BNLF2a/CPXV012/ICP47/UL49.5 viral factors. Exceptionally, the US6 protein have a unique interacting residues froms with the transporters that were not identified in other studied TAP-virus complexes (Figure S43b). For the TAP1 protein, residue E540 was found interacting with three different viral proteins (UL49.5, ICP47, and CPXV012), and residues D15/R347/E350 and R40/E418/E536 were found common binding with BNLF2a/CPXV012 and ICP47/ CPXV012, respectively. From the TAP2 transporter, residues S254 and K603 were involved in binding with the ICP47 and UL49.5 viral factors (Figure S43b).

### 3.4. Distinctive behavior by TAP transporters to drive short vs long peptide antigens towards the ER lumen

The TAP transporters are well known for actively transporting the antigens or peptides that are presented on the MHC-I molecule or the cell surface to T-cell receptors. Therefore, to understand the kinetics or of movements of the peptides through TAP transport tunnel, the MD simulations were performed for three different peptides that vary in lengths; pep18 (15 aa), pep20 (9 aa), and SIINFEKL (8 aa). The deviation and fluctuation plots (Figure S54) explains that all systems have reached their stability, and in particular, TAP1 showed more flexibility in complex with longer peptide; pep18 peptide (Figure S45a). Individual amino acid fluctuations for the TAP proteins suggest that the presence of shorter peptides (pep20 and SIINFEKL) induced stability in the transporter, compared to that with the pep18 peptide pep18 (15-mer; Figure S54b). Moreover, for the self-peptides of TAP1 and TAP2 identified in the immunopeptidome data (Figure 2) from the TAP1 and TAP2 proteins and that were highly flexible region in viral bound systems (Figure 4b), the majority of these regions lacked such fluctuations differences in the peptide-bound systems (Figure S54a).

Visualizing the structural movements of the cavity or passage formed by the TAP transporters open towards the ER lumen, suggests that to transport the peptides from the cytosol to ER the TAP transporters can have two separate cytosol-to-ER peptide passages different ways of ER opening (Figure 5a and 5b). Figure 5b, represents four helices from each TAP protein that can be involved in the placing or pushing the of the peptides toward the ER lumen, and to measure the opening or closing of the transportation cavity the area based on the C $\alpha$  (C-alpha) atoms from the respective helices were identified; area 1 (TAP1; S496 and S501, TAP2p; D185) and area 2 (TAP1; ASP278, TAP2; S393 and S408) (Figure 5b, 6, and 7). Particularly, for the SIINFEKL (8-mer) that is smaller in length compared to the pep18 (15-mer), only the passage formed by two helices from each TAP1 and TAP2 was found open. Passage 1 or area 1 is in the closed conformation, whereas area 2 is in the open state that could allow the SIINFEKL peptide to be transported. In the presence of pep20 (9-mer), a moderate opening as well as closing state of the transport passage was observed, i.e., during the first 25 ns only area 2 formed an open-state conformation, whereas at the end of MD simulation (~85-100 ns), the only area 1 formed an open-state (Figure 5a and 5b). However, the pep20 system comparatively had less differences between both areas as compared that of the SIINFEKL system; this could be a consequence of a different sequence composition of peptides that can have different interactions with TAP transporters. For the system with pep18 peptide, both passages or areas formed by 8 helices (4 from each TAP1 and TAP2) are in the open state. These differences in conformations by TAP correlates well with the areas computed as shown in Figure 5a, i.e., area 1 for systems with SIINFEKL peptide reaches upto 250 Å<sup>2</sup> and area 2 is mainly limited to 90 Å<sup>2</sup>. On the contrary, with pep18, both area 1 and area 2 are found in the open state, which ranges from ~110-300 Å<sup>2</sup> (Figure 5a). Overall, based on the areas computed on TAP transporter towards ER-opening, a difference in the transport of longer vs shorter peptides was identified; however, the sequence composition of the peptide can also affect the rate of such conformation by the transporters (Figure 5a and 5b).

Additionally, there are efforts made in the literature to understand the mode of substrate translocation and transports by different ABC exporters, and the most common proposed/suggested is the IF-to-OF (inward- to outward-facing) conformational transition/switch [11599-118102]. Particularly, the IF-to-OF switch has been confirmed by the cryo-electron microscopy (cryo-EM) [116100] for the heterodimeric TmrAB (Thermus thermophilus multidrug resistance proteins A and B); a TAP structural homolog which also can restore antigen processing in human TAP-deficient cells [116100, 118102]. In the TmrAB transporters during the inward-facing (IF state; TmrAB allows binding of nucleotides and peptide, which has a closed state at the top) conformations of the NBD domain can obtain a wide distance and in the outward-facing (OF state; abolished peptide binding and nucleotide exchange, which opens in the top) the conformation the NBD domains is represented in a close contact. Hence, to analyze such conformational switch movements by the

NBD domains (TAP1<sub>NBD</sub> 550-808 aa and TAP2<sub>NBD</sub> 450-686 aa) from the TAP1 and TAP2 heterodimer, we measured the distance centre of mass between NBD domains from both TAP transporters in the presence or absence of the peptide. The dynamic behavior of the apo-systems; wild-type (Figure 4d) and mutated (Figure 4c), have shown a closed conformation towards the ER lumen (IF conformation; NBD has wide distance), whereas in the presence of peptide the transport channel is found in the open state towards the ER lumen (OF conformation; NBD has close contact; Figure S610). The distance between NBD domains in the wild-type apo-wild-type system remained higher (~42.31 Å) throughout the MD simulations (Figure S610), whereas in the presence of peptide the distance dropped to 34.03 Å from 42.31 Å. These findings correlate with the area computed for the transport channel (Figure 5a), that when the channel opens towards the ER lumen, the NBD domain forms a closed conformation (Figure S610), as observed in the IF-to-OF conformational switch for other ABC transporters [11599-118102].



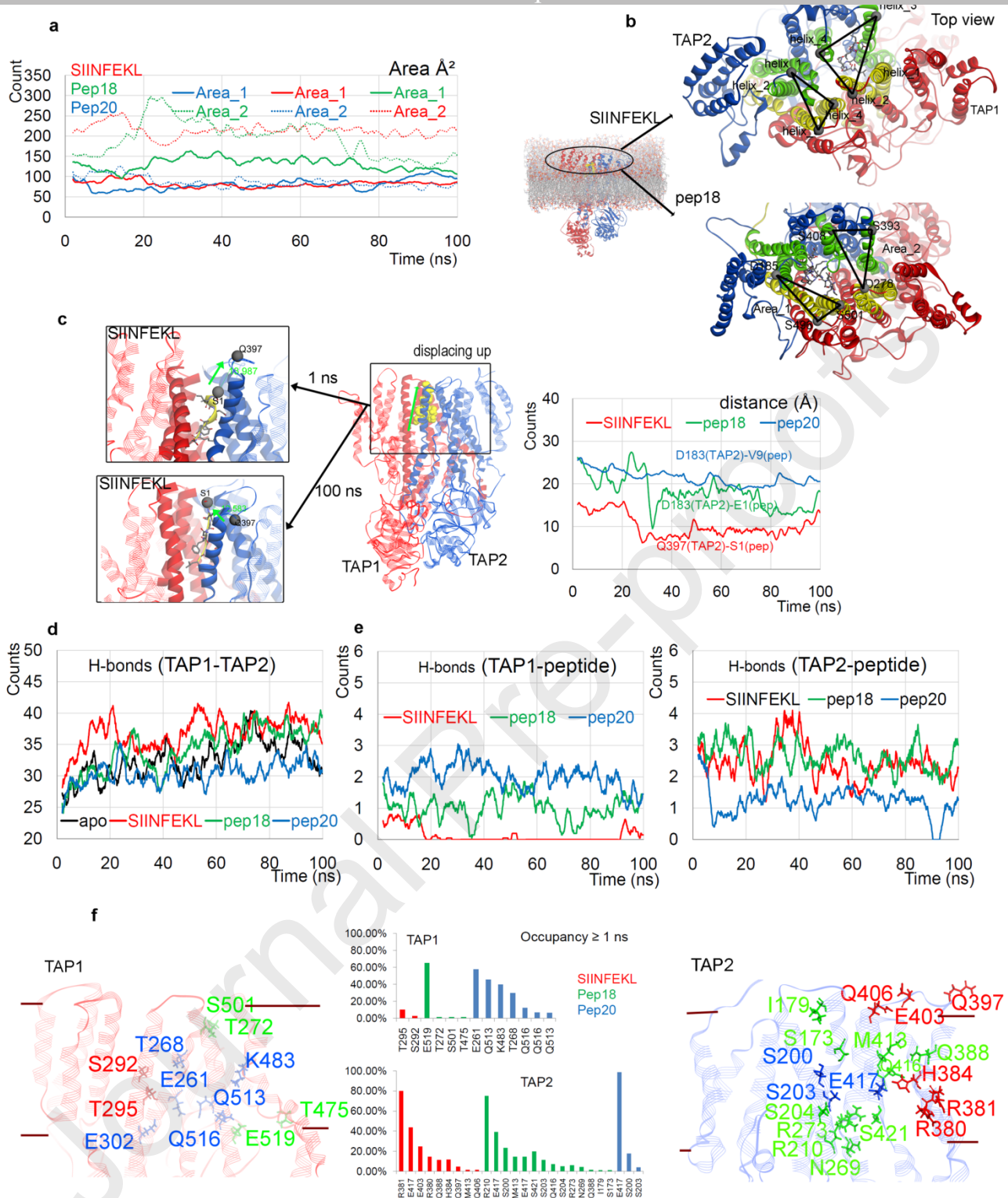


**Figure 5.** The binding interface with dynamics of the pep18, pep20, and SIINFEKL peptides with the TAP transporters. **(a)** and **(b)** Area computed considering the four helices each from TAP1 or TAP2 involved in forming the passage for the transportation of the peptide, as represented in **b**. C-alpha (CA or C $\alpha$ ) atoms coordinates of each residues were traced over time evaluation of the molecular dynamics; area 1 = TAP1 (SER496 and SER501) and TAP2 (ASP185) and area 2 = TAP1 (ASP278) and TAP2 (SER393 and SER408). Helices residues range; TAP1 = 256-275 aa (helix\_1), 281-329 aa (helix\_2), 451-495 aa (helix\_3), 501-544 aa (helix\_4), and TAP2 = 145-181 aa (helix\_1), 189-226 aa (helix\_2), 356-395 aa (helix\_3), and 405-440 aa (helix\_4). **(c)** The displacement of the peptides from the centre of the transportation cavity towards the ER lumen (upward movements). In addition, to measure the movements of peptides in the capacity transport

tunnel, distance between the TAP2 (from top, toward ER lumen) and peptide C $\alpha$  atoms were computed for the selected amino acids; Q397(TAP2)-S1(SIINFEKL), D183(TAP2)-E1(pep18), and D183(TAP2)-V9(pep20). (d) and (e) Intermolecular hydrogen bond interactions between the TAP1 and TAP2 (protein-protein), and TAP1/TAP2-peptide, respectively. (f) TAP residues involved in forming hydrogen bond interactions with peptides-pep18, pep20, and SIINFEKL peptides with an occupancy of  $\geq 1\%$ .

To understand the kinetics of the peptide inside the TAP transportation-cavity, the distance between the TAP residue from the top or surface open towards the ER lumen and the residue from the peptide heading towards-upwards in the cavity was traced (Figure 5c). The distance between Q397(TAP2)-S1(SIINFEKL) dropped from 15 Å to 5 Å (Video S3), suggesting the-a peptide upward displacement mechanism. A sSimilar trend in the drop of distance between TAP amino acids from top and from the peptide residue was observed for pep18 and pep20 peptides-(Figure 5c and Video S4). Comparing the drop down of distances s with each peptide, it was observed that a shorter peptide (SIINFEKL) has initiated movements s relatively earlier compared to the longer peptide (pep18; Figure 5c). Considering the conformational dynamics and visualizing such distance movement by the peptide in the channel, it is suggested that the actual movement is coming from the peptides could reflect coming only from the TAP2 residues by, and therefore, we visualized the structures as presented on the left panel of Figure 5c, and confirmed it is the actual movement coming from the peptide-(figure 5c).

Hydrogen bonds between the-TAP1-TAP2 proteins-in the presence of the peptide (Figure 5d), suggest that a higher number of interactions between these proteins was observoccurred when there is an increase in the movement, i.e. (opening of the cavity as shown in Figure 5a and 5b). Particularly, the system with the SIINFEKL and pep18 peptides has-obtained more number-of protein-protein interactions compared to that of the apo-form and the-pep20 system (Figure 5d). In addition, higher numbers of arginine-glutamic acid residue pairs were observed forming the TAP1-TAP2 interaction interface (Table S10). Furthermore, the interactions between the peptides and TAP1/or-TAP2, suggests that SIINFEKL and pep18 obtained very-few interactions with TAP1 and but higher-more interactions with TAP2, whereas the opposite behavior was observed for pep20 peptide-(Figure 5e). These findings suggest-demonstrate that when the TAP1-TAP2 cavity is in its open conformation towards the ER lumen and the SIINFEKL peptide reaches the top of the TAP transport channel (as shown in Figure 5c) ready to be placed in the ER lumen, where peptide it mostly during this time peptides mainly mostly have interactions with the TAP2 protein-(Figure 5e). In addition, it can also be proposed that the-TAP1 protein is mostly-can be responsible for pulling the peptide from the cytosol and positioning it in the TAP cavity, which further is transported toward the ER lumen. From the TAP1 protein-ffFor each peptide systems (pep18/pep20/SIINFEKL) different amino acids from TAP1 were involved in binding with peptides, and a similar behavior was observed for TAP2 proteins-but with some exceptions (Figure 5f and Table S11). The S203, Q388, and M413 amino acids from the TAP2 proteins were found to be involved in common in at least two peptide systems (Figure 5f and Table S11), and this data correlates with previous findings [14]. The review by Elisa et al. [98] described thea 3D homology model of the human TAP complex based on TmrAB along with essential residues necessary for the antigen processing by TAP [98, 119103]. Comparing such residues with our peptides screened against the TAP transporters and molecular dynamics data (occupancy > 1 ns), suggest several common residues traced by Elisa et al. [98, 119103]. Particularly, the TAP1 E519 and TAP2 R380 residues forming high occupancy interactions 65.03 % and 14.59 % (Table S11) with the peptides, respectively, were found similar with the TAP homology model provided by Elisa et al. [9]. Additionally, TAP1 residues T475, K483, S501, Q513, Q516, and E519 (Table S11) withform high occupancy interactions with the studied peptides residinges into the peptide binding regions P435-M480 and Q513-R547 determined by mutation studies [98, 119103]. Similarly, the TAP2 residues R380, R381, H384, Q388, M413, Q416, E417, and S421 (Table S11) showing stable high occupancy interactions with the studied peptides, and belongs to the peptide binding region R354-

M389 and I414-M433 determined by mutagenesis [98, 8043, 119103]. Moreover, here we would like to highlight that during our screening of peptides to the TAP complex, the peptide binding cleft was selected for screening (Figure 2g and S2), and therefore, higher number of residues that were identified from MD simulation data associate to the peptide binding regions [98, 8043, 119103].

The electron paramagnetic resonance (EPR) studies have shown a conserved distance of  $\sim 2.5$  nm or  $\sim 25$  Å between the N and C terminus of the peptides bound with TAP proteins [98, 8043]. Hence, to trace such behavior of peptides varying in length studied by MD simulations, we measured the distance based on the C $\alpha$  atoms (Figure S79a) of N and C terminus residues of the peptides; pep57 (SIINFEKL), pep18 (ENPVVHFFKNIVTPR), and pep20 (AAGIGILTV). All three studied peptides have ~~a reached~~ a similar N and C terminus distance at a particular time step, ~~similar to as that of the~~ EPR studies [98, 8043]. Particularly, the 15-mer (pep18) peptide has ~~thea~~ maximum distance of 37.38 Å, the 9-mer peptide (pep20) has the highest distance of 21.57 Å, and the 8-mer peptide (SIINFEKL) has 21.92 Å distance (Figure S79a). Furthermore, during the 100 ns MD simulation the average distance for the SIINFEKL peptide termini was 19 Å, ~~for the~~ pep18 was 32 Å, and ~~for the~~ pep20 was 14 Å. Comparing these N and C terminus distances with the movements of the peptide towards the ER lumen in the TAP binding cavity during simulations (Figure 5c), it was observed that ~~the~~ pep20 has ~~shown~~ comparatively slower movements as that of other two peptides (SIINFEKL and pep18), and higher number of interactions with TAP1 ~~as that of the compared to TAP2 transporter~~ (Figure 5c). These observations may suggest that the conformation of the peptides can influence the distance and the movement / kinetics of the peptides within the transporter cavity, and from the structural aspects these conformations may vary based on the peptide sequences. The crystal structure of the SIINFEKL peptide with MHC-I is available (pdb id.: 3p9l [81104]), as well as for the peptides pep18 (pdb id.: 3pl6 [82105]) and pep20 (pdb id.: 3qdj [83106]) ~~are complexed available~~ with the MHC-I and TCR receptors (Figure S79b). Therefore, we computed the distance between N and C terminus of peptides when presented to MHC-I molecules, which correlates with the highest distance observed for each peptide during MD simulations (Figure S79a).

### 3.5. Cancer-associated variants affecting protein-protein interface, as well as ~~the~~ peptide transportation

~~Single The single~~ cancer-associated point ~~caner~~ mutations can significantly affect the heterodimer formation of the TAP transporters as well as the peptide transport process, and thus, to elucidate ~~such this~~ mechanism, ~~the~~ MD simulations were performed for the selected mutations ~~in TAP~~ showing high versus low binding ~~affinity from the initial screen~~ (Figure 3c). The cancer-associated variants at positions 446/437 and 208/370 (located at the protein-protein interface; Figure 6a right panel) in the TAP1 and TAP2 proteins, respectively, produce a distinctive binding affinity between TAP1-TAP2 complexes (TAP1<sub>E446K</sub>, -5.99 kcal/mol; TAP1<sub>E446W</sub>, -11.35 kcal/mol; TAP1<sub>V437F</sub>, 25.43 kcal/mol; TAP1<sub>V437I</sub>, -7.92 kcal/mol; TAP2<sub>D370N</sub>, -1.23 kcal/mol; TAP2<sub>D370W</sub>, -15.43 kcal/mol; TAP2<sub>G208F</sub>, 28.53 kcal/mol, and TAP2<sub>G208S</sub>, 1.62 kcal/mol; Figure 3c). In addition, the mutant TAP1<sub>R372Q</sub> and TAP2<sub>R373H</sub> were also considered for MD ~~simulations~~S, because of its placement at the region where the peptide binds (Figure 6a right panel). ~~These mutations~~ were studied in the presence ~~or~~ absence of two different ~~size of~~ peptides (pep18 and SIINFEKL). ~~Particularly, cancer-associated variants TAP1<sub>R372Q</sub> (found in cervical squamous cell carcinoma, colon adenocarcinoma, glioblastoma multiforme, and cervical squamous cell carcinoma), TAP2<sub>R373H</sub> (prostate adenocarcinoma and glioblastoma multiforme), and TAP2<sub>D370N</sub> (found in skin cancer, non-melanoma) are positioned in the peptide binding region (Figure S812). Additionally, in this position the cancer variant TAP1<sub>I333V</sub> (found in B-Lymphoblastic Leukemia/Lymphoma and Acute myelomonocytic leukemia (cBioPortal, <http://cbioportal.org>)), is well studied in terms of its involvement in cancer [12049, 12150]. Since these cancer-associated mutations (Figure 6a and S95a) maybe involved in the TAP suppression mechanism and reducing MHC-I cell surface, a set of ~~Overall~~, 14 mutated TAP1-TAP2 systems were constructed for MD simulations ~~in the presence or absence of peptide~~ considering the cancer mutants, and variants with the peptides (Figure 6 and 7).~~

Except the ~~anete~~ TAP1<sub>V437I</sub> all other variants (TAP1<sub>E446K</sub>, TAP1<sub>E446W</sub>, TAP1<sub>V437F</sub>, and TAP1<sub>R372Q</sub>) have induced flexibility in the TAP1 transporter (Figure 6a, S95, and S106), ~~and~~ ~~Upon~~ mutation in TAP1, ~~protein~~ the complexed TAP2 protein showed a stable behaviour in all mutated constructs (Figure 6a and S95a). On the contrary, the majority of cancer-associated mutations in TAP2 (TAP2<sub>D370N</sub>, TAP2<sub>D370W</sub>, TAP2<sub>G208S</sub>, and TAP2<sub>R373H</sub>) have induced stability in the TAP2 protein; excluding the TAP2<sub>G208F</sub> (Figure 6a, S95a, and S106b). In addition, the TAP1 protein only showed higher flexibility when complexed TAP2<sub>G208F</sub> has shown higher flexibility (Figure 6a and S95a). These findings suggest that cancer-associated variants affect both TAP transporters ~~in-with~~ significantly different manner-effects (Figure 6a). Furthermore, RMSDs of individual mutated residues at the protein-protein interface suggest that similar as found in initial screen (Figure 3c) both variants TAP1<sub>E446K/W</sub> and TAP1<sub>V437F/I</sub> have contrary behavior, and complementarity was observed for TAP2<sub>D370N/W</sub> and TAP2<sub>G208F/S</sub> (Figure S95b). Interestingly, the variants located at the peptide binding pocket of the TAP1-TAP2 complex have diverse conformations; the TAP1<sub>R372Q</sub> variant was found highly stable, whereas the TAP2<sub>R373H</sub> showed a paradoxical data (Figure S95b).

Increasing flexibility in TAP1 in the mutated form (in the absence of peptide), induced a higher number of intermolecular protein-protein intermolecular (hydrogen bonds; H-bonds) interactions compared to that of the wild-type system, except for the TAP1<sub>V437F</sub> variant (Figure 6b and Table S12). Though, adversely for the TAP2 protein, upon inserting cancer-associated mutation which induces stability (Figure 6a), there werehave been higher protein-protein interactions found for mutant apo-systems (Figure 6b and Table S12). These findings suggest that the cancer-associated mutations either induce stability or flexibility in the TAP1 or TAP2 proteins (in the absence of peptide) and can, unfavorably affect the TAP1-TAP2 complex, by forming a higher number of protein-protein interactions. The conformation dynamics of the TAP transporters in the TAP1<sub>E446K/W</sub> (446 aa is also positioned at the region presented to MHC I; Figure 2g) systems suggest that, upon mutation, TAP<sub>NBD</sub> domains lack the tilt movement, which results in the distortion in the opening of pore towards the cytosol, and the closed ER lumen conformation (Figure 6c; left panel). TAP1<sub>V437F</sub> and TAP1<sub>V437I</sub> systems formed a closed ER lumen pore, whereas only TAP1<sub>V437F</sub> showed tilt movement of the TAP<sub>NBD</sub> domain lacking the complete opening of the cytosolic pore.

The TAP2 mutations at position 370 belongs to the region where it can hinder the movement of the helices (as shown in Figure 5b) and also affects the pore opening towards the cytosol; TAP2<sub>D370W</sub> showed a distorted but open cytosolic pore with moderate tilt movement of the TAP<sub>NBD</sub>, whereas the TAP2<sub>D370N</sub> lacked such conformation. Analysis of the structural behavior as well as the RMSDs suggest that TAP2<sub>D370W</sub> induces rigidity resulting in the opened cytosolic pore, though, with moderate tilt TAP<sub>NBD</sub> movement (Figure 6c; right panel). For both TAP2<sub>G208F</sub> and TAP2<sub>G208S</sub> systems the tilt TAP<sub>NBD</sub> movement is observed as well as the open cytosolic pore, however, it is closed toward the ER lumen (Figure 6c). The mutations at the peptide binding region (TAP1<sub>R372Q</sub> and TAP2<sub>R373H</sub>) have the tilt movement with the open cytosolic passage, but TAP2<sub>R373H</sub> lacks the ER lumen opening. Overall, mutations in TAP1 completely block both ER and cytosolic pores of the TAP transporter that may hinder the intake and evacuation of the peptides from cytosol-to-ER, whereas mutation in the TAP2 protein mainly blocks only the ER lumen pore (Figure 6c).

Protein-protein long-lasting interactions with an occupancy  $\geq 50\%$  (from 100 ns) were identified in the studied mutated systems (Figure S113). Comparing TAP1-TAP2 intermolecular binding residues from mutated systems with the wild-type, suggests that TAP1 residues E302, D357, and R639 wereare frequently involved in TAP2 binding for the mutated systems, but not in wild-type system (Figure S113). Except for the TAP1<sub>E446K</sub> mutated systems, TAP1 residues D306, E334, E443, and E446 were interacting with TAP2 in wild-type as well as in the mutated systems. Particularly, in the wild-type situation, the TAP1 E446 residue was involved in the binding with TAP2, which whenupon E446K mutation hindered the such an interaction. In addition, the mutated TAP1<sub>E446K</sub> and wild-type system lack anycommon protein-protein interactions in common (Figure S113). From TAP2 protein the R373 residue fromof TAP2-amino-acid was traced in the majority of the mutated systems (Figure 6 and S113) as well as wild-type binding with TAP1,

excluding the TAP2<sub>R373H</sub> mutated system. Additionally, the TAP2 residues R255, E348, E349, Y366, Y366, and R381 binding with TAP1 were frequently traced in mutated systems (Figure S113).

Journal Pre-proofs

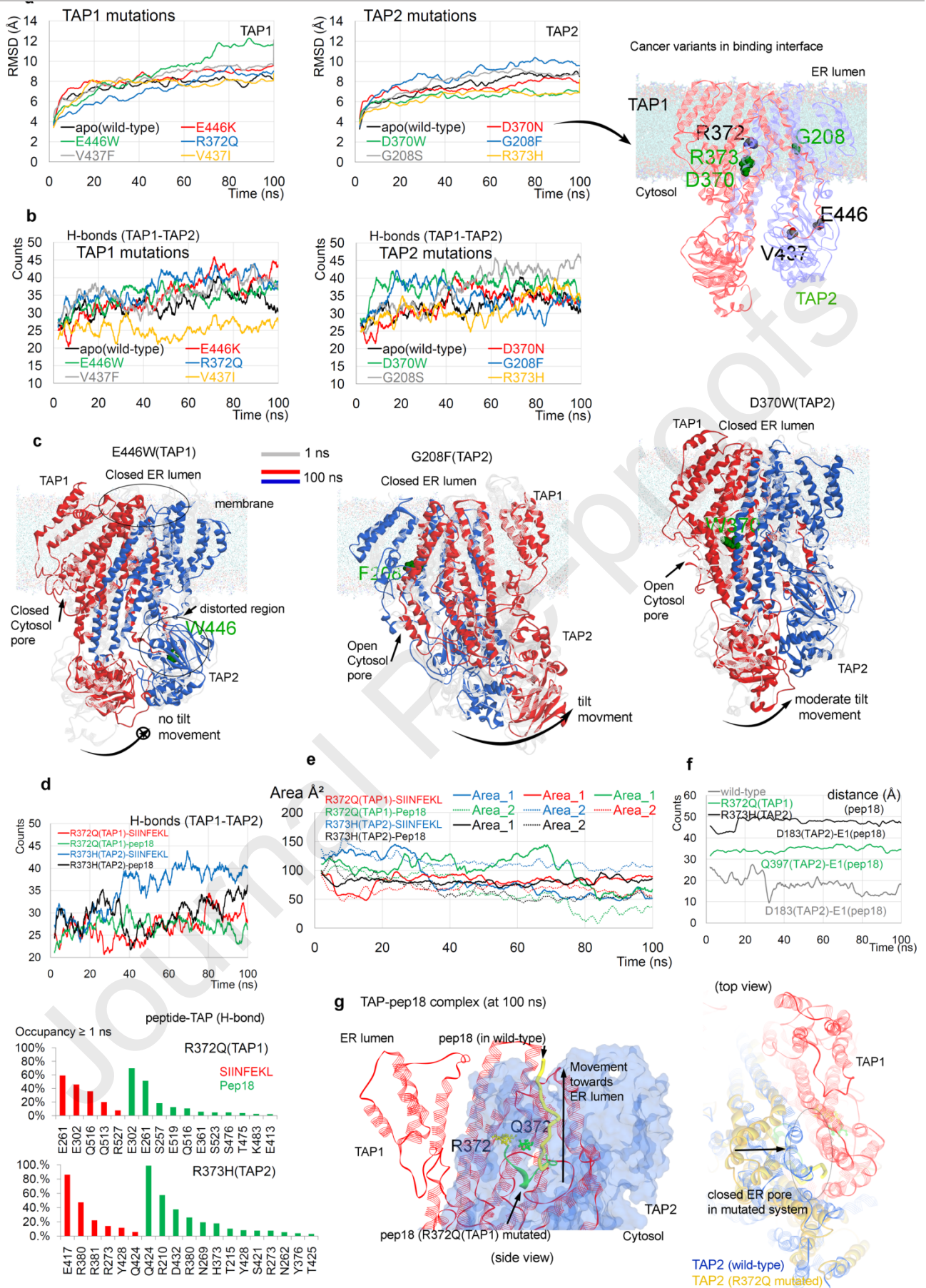


**Figure 6.** Mutations affecting the protein-protein interfaces of the TAP transporters, as well as the transport of the peptides. **(a)** RMSDs of the TAP transporters in the presence of the cancer-

associated mutations, and the right panel of the protein structure represents positions of cancer-associated mutations on the protein-protein interface. **(b)** Intermolecular protein-protein hydrogen bonds between TAP transporters in presence of the cancer-associated variants. **(c)** Conformation dynamics of the TAP proteins from different mutated systems, representing distinct ways-of conformational states upon point mutations. The protein structures were retrieved from the beginning and end of the MD simulations. **(d)** Intermolecular hydrogen bond interactions between TAP transporters, and the bottom panel represents binding residues of TAP with SIINFEKL or pep18 peptides in the presence of mutations. **(e)** Area computed for four helices forming the passage for the transportation of the peptide, as represented in Figure 5b. **(f)** Distance between the peptide residue and the TAP2 (from top) residues facing from the ER lumen-facing. **(g)** Conformation dynamics with comparison of the mutated and wild-type system, showingrepresent that the mutated variants induces rigidity and hinders the transportation of the peptide from ccytosol to the ER lumen. Protein coordinates were extracted from the end of the MD simulations.

The direct consequences of cancer-associated variants over the peptide transport process by TAP heterodimer were evaluated; by performing MD simulation of peptide in the presence of mutated TAP1-TAP2 complex. Both TAP1<sub>R372Q</sub> and TAP2<sub>R373H</sub> cancer-associated mutations are located in the peptide binding interface-region and were involved in the interactions with peptides, hence were selected for MD simulations with two different peptides; pep18 and SIINFEKL (Figure 2i). During the initial screen (Figure 2i), the-pep18 peptide pep18-produced a good-strong binding affinity (-20.02 kcal/mol) with the TAP1-TAP2 complex and-but the SIINFEKL peptide (-13.44 kcal/mol) had comparatively weak affinity. The mutated TAP1 was found highly flexible compared to the mutated TAP2, and pep18 as well the variant residue TAP1<sub>R372Q</sub> itself were found destabilized (Figure S127). Among The-mutatedion systems with peptide, the TAP1-SIINFEKL-TAP2<sub>R373H</sub> complex had a higher number of protein-protein interactions, and the TAP1<sub>R372Q</sub>-pep18-TAP2 complex is the lowest to form such binding (Figure 6d and Table S13). Comparing these protein-protein interactions from peptide bound mutated systems (TAP1<sub>R372Q</sub> and TAP2<sub>R373H</sub>; Figure 6d) with mutated apo-systems (Figure 6b), the data suggest that peptide bound system has comparatively less TAP1-TAP2 intermolecular interactions.

Peptide-protein interactions suggest that both pep18 and SIINFEKL peptides formed a higher number of hydrogen bond interactions with the TAP2 protein, compared to that of the TAP1 (Figure S127c and Table S14). Particularly, the-pep18 peptide pep18-formed more-a-higher-number of interactions with TAP1 protein in the TAP1<sub>R372Q</sub>-pep18-TAP2 complex-system (Figure S712c). For the TAP1<sub>R372Q</sub> systemmutated-protein, the SIINFEKL peptide formed H-bond with more number of residues having an occupancy  $\geq 1$  ns. The pep18 peptide pep18-and TAP1(E519) residue formed high occupancy interactions in the wild-type system (Figure 5f), whereas lower occupancy binding with TAP1 is observed in the TAP1<sub>R372Q</sub> system (Figure 6d). In addition, for the TAP2<sub>R373H</sub> proteinsystem, the SIINFEKL peptide had residues E417, R380, and R381 in common with the wild type and mutated systems (Figure 5f and 6d), similarly the pep18 peptide formed interactions with R210, S421, R273, and N269 residues.

The area from the top of the TAP transport tunnelers (towards the ER lumen; residues as described in Figure 5b) for all four mutated systems with peptides (Figure 6e), suggest a closed ER lumen conformation in the mutated complexes. For both peptides pep18 and SIINFEKL, the mutation in the TAP1<sub>R372Q</sub> and TAP2<sub>R373H</sub> blocks the movement of the peptide to upwards from cytosol-to-ER (Figure 6f, 6g, S138, and Videos S4, S5), particularly the TAP2<sub>R373H</sub> residue was found interacting with the-pep18 peptide pep18-(Table S14). Distances between the peptide residue and the TAP residuesamino-acid from the top (ER lumen; Figure 6f) demonstrates that, in the mutated TAP1<sub>R372Q</sub> and TAP2<sub>R373H</sub> systems, the-pep18 peptide has a higher distance value. Analysing the structural conformations of peptides in the presence of the mutation and wild type systems, the cancer-associated mutation induces rigidity in the TAP1-TAP2 complex, and hence, lacks an 'open' conformation towards the ER lumen. For an example (Figure 6g, 7, S138, and Video S5), the movement of pep18 in the wild type as well as mutant system is shown, the peptide

can snit upwards to the ER for the wild-type system, whereas for mutant the cavity pore is closed towards the ER lumen. For the opening of the cavity pore towards the ER in the wild-type system, a higher degree of conformations is-were observed in the TAP2 protein (Figure 6g; left panel). Moreover, one shall also consider that mutations often may have selection over each peptide, i.e., different cancers or the same cancer might have different mutations. Therefore, the mutational effect that blocks the movement of the peptide to upwards from cytosol-to-ER (Figure 6g and S138) maybe seen in TAP1<sub>R372Q</sub> (found in cervical squamous cell carcinoma, colon adenocarcinoma, glioblastoma multiforme, and cervical squamous cell carcinoma) and TAP2<sub>R373H</sub> (found in prostate adenocarcinoma and glioblastoma multiforme).

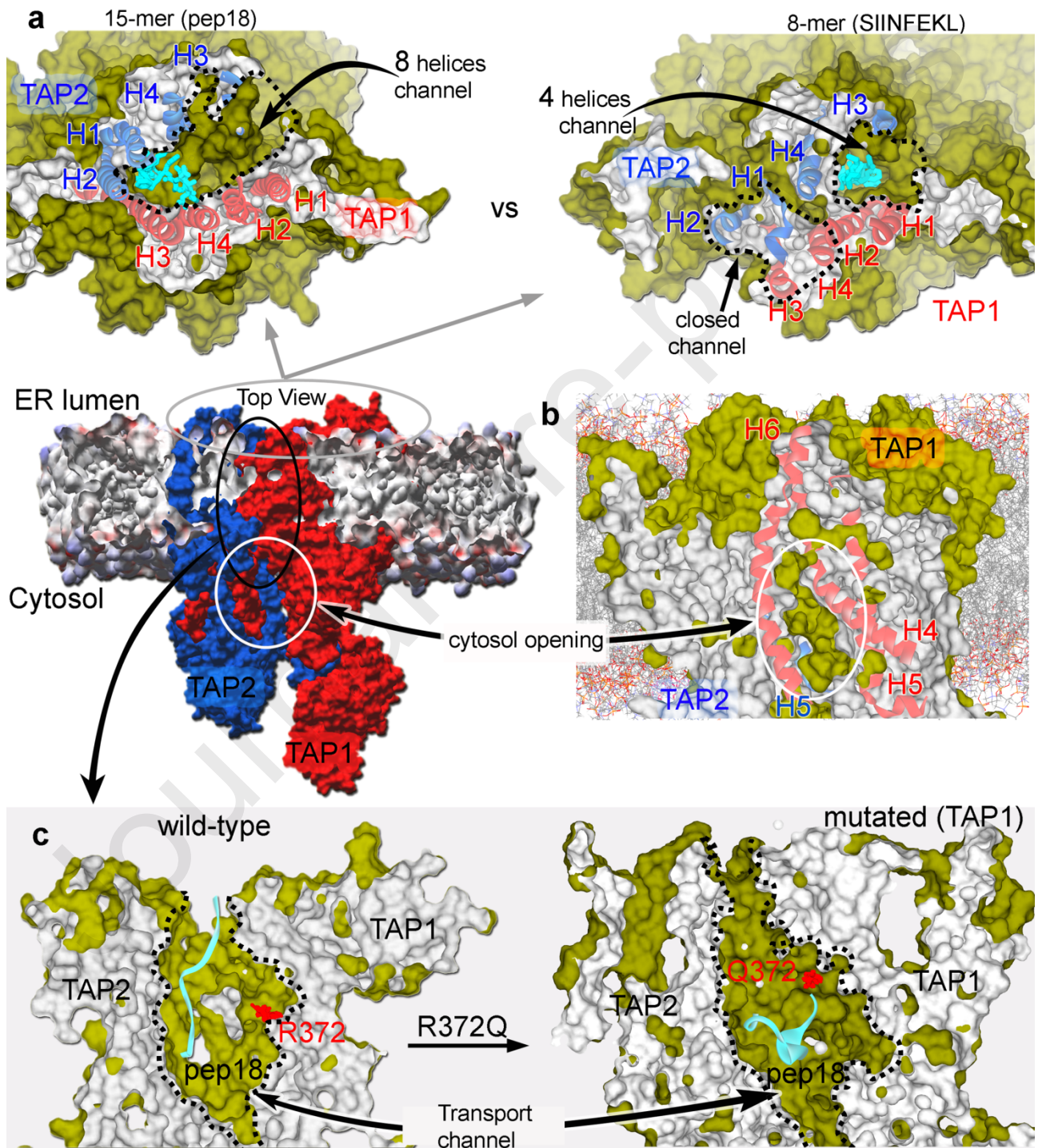


**Figure 7.** Structural rearrangements of TAP1-TAP2 transporters examined in the presence of peptide or cancer-associated variants. The protein structures retrieved from the end of MD simulations are represented as surface and slab view, and therefore, the internal regions are in silver



color and the surface regions are in dark green. **(a)** TAP transporters adopted different conformations to transport peptides from cytosol-to-ER, based on the peptide length (for example; 15-mer, ENPVVHFFKNIVTPR, pep18; and 8-mer, SIINFEKL). For a 15-mer peptide, TAP has a 8-helices (four helices from each TAP) transport channel, whereas for an 8-mer peptide, it has a 4-helices (two helices from each TAP) transport channel. Helices are numbered according to Figure 5b. **(b)** Cytosolic facing passage in an ‘open state’ observed during MDS, formed by helix\_4 (501-544 aa), helix\_5 (332-376 aa), helix\_6 (384-425 aa) from TAP1 and helix\_5 (250-288 aa) from TAP2. Alone, helix\_4 from TAP1 is involved in the-ER opening as well as the-cytosolic opening. **(c)** Mutation in the TAP transport channel (shown in green) can block the peptide in the cavity, for example, TAP1<sub>R372Q</sub> hinders the-peptide movement towards ER. *Color Scheme*; TAP1 in red, TAP2 in blue, and peptide in cyan.

#### 4. Conclusions

Our work highlights the structural and functional insights into the molecular architecture of the peptide transport-transit by the TAP1 and TAP2 transporters, and how cancer-derived mutations (from COSMIC and cBioPortal) and as well as different viral factors (BNLF2a, CPXV012, ICP47, US6, and UL49.5) targeting TAP proteins may suppresses the MHC class I pathway were highlighted in this work. This results in immune escape by the cancer and/or virus-carrying cell. In order to investigate the kinetics of the peptide transport process, different immunopeptidome datasets (MHC-I bound peptides presented by melanoma A375 cells) were generated in the presence/absence of interferon- $\gamma$  (IFN- $\gamma$ ) treated samples to obtain peptides lists-datasets for the TAP models, along with considering as well as few a set of peptides known to be presented on the TCR (from ATLAS database) were also considered. Higher numbers of peptides were identified in the IFN- $\gamma$  treated melanoma cells (3081 peptides) compared to that of the wild-type untreated cells (1968 peptides), suggesting an induced anti-cancer immunity pathway is being activated, and These IFN- $\gamma$  treated cells generated with peptides with length of 8 to, 9, or 10 mers showing that showed the binding affinity between -10 to -15 kcal/mol (GBVI/WSA dG) with the modeled TAP1-TAP2 transporters model. The Majority of shorter length peptides from IFN- $\gamma$  treated cells have less binding affinity with the TAP transporters. In addition, Exclusively infor the IFN- $\gamma$  treated samples cells the following, few peptides were identified from the TAP transporters itself; from TAP1 (AALPAAALW, LLYESPERY, RSLQENIAY, RTALPRIF, SAMPTVRSF, and TEVDEAGSQL) and TAP2 (YLHSQVVSU) were identified suggesting the degradation of the TAP transporters itself. The IFN- $\gamma$  treated sample having a higher number of peptides identified suggests induced immunity, and has a majority of shorter length peptides that have a less binding affinity with the TAP1-TAP2 transporters. In addition, more residues from TAP2 were involved in interacting with the peptides, and fewer peptides were detected from TAP2 itself, whereas the opposite was observed for the TAP1. Overall, considering the binding affinities of the peptide it could be proposed that smaller peptides (8, 9, or 10 mer) may transport comparatively quickly through the transport channel.

Viral proteins predominantly destabilizes the TAP1 protein, compared to that of whereas contrary behavior was observed towards the TAP2 protein, particularly, for the UL49.5 and BNLF2a. Among the studied viral proteins, the UL49.5 protein exhibited the highest fluctuations and BNLF2a was the most stable protein. Interestingly, the peptides identified in the immunopeptidome data upon IFN- $\gamma$  treated melanoma cells, originates from the highly fluctuating regions of the TAP transporters upon viral binding (or the allosteric effects). The structural dynamics of the TAP1-TAP2 complex in the presence and absence of a viral protein in the complex, revealed that in all simulated systems the TAP<sub>NBD</sub> domains formed a tilt movement toward the membrane cytosolic faced, which generates a passage or the peptide transport channel open towards the cytosol. This cytosolic passage was targeted by 4 (BNLF2a, CPXV012, ICP47, and UL49.5) out of 5 studied viral proteins, blocking the transport passage. The BNLF2a, CPXV012, and ICP47 viral proteins formed a higher number of interactions with TAP1, whereas

UL49.5 and US6 shared relatively equal interactions with both TAP proteins. In addition, the TAP1 regions with lower SNPs frequency and cancer variants were found making higher interactions with viral factors ([proposing an adaptive mechanism, overcoming the protein-protein interactions that might result from amino acid changes](#)), whereas the viral protein binds to the TAP2 region which is highly mutated. [Exceptionally, the US6 protein has unique interactions with the transporters, whereas, other BNLf2a/CPXV012/ICP47/UL49.5 viral factors have several amino acids in common when binding with TAP proteins.](#)

Individual amino acid fluctuations for the TAP proteins suggest that presence of shorter peptides (pep20 and SIINFEKL) induced stability in the transporter, compared to ~~that with the~~ longer peptide (pep18). ~~The TAP (itself)~~ peptides or regions from the immunopeptidome showing higher flexibility in viral systems, lacked such behavior in the peptide-bound systems. The structural movements of the cavity formed by the TAP transporters open towards the ER lumen, which ~~can may~~ be proposed to transport the peptides from cytosol-to-ER in two different ways [via an opening of the tunnel/channel or passage](#) (4 or 8 helices involvement). Particularly, for the SIINFEKL (8-mer), which is smaller in length compared to that of the pep18 (15-mer), only the one passage formed by two helices from each TAP1 and TAP2 was found open, whereas for pep18 both passages, or areas, formed by 8 helices (4 from each TAP1 and TAP2) were in the open state. [However, such difference in the opening of the passage towards the ER lumen may also vary based on the peptide sequences, along with peptide length.](#) The distance measured for each peptide from the top of ~~the~~ TAP models towards ~~the~~ ER lumen suggests that a shorter peptide (SIINFEKL) has ~~an~~ initiated movement relatively earlier compared to the longer peptide (pep18). At a point when the TAP1-TAP2 cavity is in its open conformation [towards the ER](#), and the peptide [reaches the top of the transport tunnel is ready to be placed in the ER lumen](#), ~~peptides it~~ mainly interacts with the TAP2 protein. The S203, Q388, and M413 amino acids from the TAP2 proteins were found common in at least two peptide systems. [Similar as that observed in the EPR studies, a conserved distance of about 25 Å between the N and C terminus of the peptides bound with TAP proteins was observed in our analysis; the 15-mer \(pep18\) has a distance of 37.38 Å, the 9-mer \(pep20\) has 21.57 Å distance, and 8-mer \(SIINFEKL\) has 21.92 Å distance.](#)

The TAP1 or TAP2 amino acids binding with peptides in fingerprint analysis, were also found mutated in different cancer types, which suggest that ~~upon~~ point mutation either from TAP1 or TAP2 is sufficient to alter the protein-protein binding [which may that can significantly](#) affect the peptide transport process. Interestingly, the variants located at the peptide binding pocket of the TAP1-TAP2 complex have diverse conformations; ~~the~~ TAP1<sub>R372Q</sub> variant was found highly stable [compared to that of](#), ~~whereas~~ the TAP2<sub>R373H</sub> ~~showed a paradoxical data~~. The mutations in TAP1 ~~may~~ completely block both ER and cytosolic passage of ~~the~~ TAP transporter which ~~may~~ hinders the intake and evacuation of the peptides from cytosol-to-ER ([blocks the IF-to-OF conformation](#)), whereas mutation in the TAP2 protein ~~mainly mostly can~~ blocks the ER pore only. The mutated system TAP1-SIINFEKL-TAP2<sub>R373H</sub> had a higher number of protein-protein interactions, and the TAP1<sub>R372Q</sub>-pep18-TAP2 complex is one of the lowest to form such binding. ~~For Considering~~ both ~~peptides~~ pep18 and SIINFEKL ~~peptides~~, the mutation in the TAP1<sub>R372Q</sub> and TAP2<sub>R373H</sub> blocks the movement of the peptide upwards [in the transport channel from cytosol to ER](#). For the opening of the [transport](#) cavity pore towards the ER lumen in the wild-type system, a higher degree of conformations is observed in the TAP2 protein, whereas the structural conformations of peptides in the presence of the mutation systems suggest that the cancer mutation induces rigidity in the TAP1-TAP2 complex, and ~~hence therefore~~, lacks the 'open' conformation towards the ER lumen.

[Overall, considering the binding affinities of the peptide with transporters it could be proposed that smaller peptides \(8, 9, or 10 mers\) may transport comparatively quickly through the transport channel. Furthermore, by adversely interacting with the TAP transport passage, or affecting the TAP<sub>NBD</sub> tilt movement, viral proteins and cancer-derived mutations may induce allosteric effects or rigidity in the TAP complex blocking the IF-to-OF conformation of the tunnel. The areas from the TAP transporter towards ER-opening and the distance centre of mass between TAP<sub>NBD</sub> domains, highlights a difference in the transport of longer vs shorter peptides.; However,](#)

the sequence composition of peptide can affect the rate of such conformations by the transporters. These findings ~~from our study~~, would propose a model for how different viral factors and cancer-derived mutations ~~that may~~ alter the peptide transport process by directly targeting the TAP proteins, and how the IFN- $\gamma$  induced signaling pathway alters ~~such~~ TAP-peptide loading and, ultimately, MHC-I antigen presentation.

## Fundings

The APC was funded by the International Centre for Cancer Vaccine Science, University of Gdansk (Fundacja na rzecz Nauki Polskiej: MAB/3/2017). U.K. is supported by the grant: 2020/36/C/NZ2/00108, from The National Science Centre (Narodowe Centrum Nauki, Krakow, Poland). Partly funded by European Regional Development Fund (ENOC, CZ.02.1.01/0.0/0.0/16\_019/0000868), MH CZ – DRO (MMCI, 00209805), CancerforskningsfondenNorr, Cancerfonden (160598).

## Acknowledgments

The International Centre for Cancer Vaccine Science project is carried out within the International Research Agendas programme of the Foundation for Polish Science co-financed by the European Union under the European Regional Development Fund. Authors would also like to thank the PL-Grid Infrastructure, Poland for providing their hardware and software resources.

## Conflicts of Interest

The authors declare no conflict of interest.

## References

- [1] Robertson M. Antigen presentation. *Curr Biol*. 1998;8(23):R829-R831. doi:10.1016/s0960-9822(07)00523-4.
- [21] Praest P, Liaci AM, Förster F, Wiertz EJHJ (2019) New insights into the structure of the MHC class I peptide-loading complex and mechanisms of TAP inhibition by viral immune evasion proteins. *Mol Immunol* 113: 103-114.
- [32] Sadasivan B, Lehner PJ, Ortmann B, Spies T, Cresswell P (1996) Roles for calreticulin and a novel glycoprotein, tapasin, in the interaction of MHC class I molecules with TAP. *Immunity* 5: 103-114.
- [43] Park B, Lee S, Kim E, Cho K, Riddell SR et al. (2006) Redox regulation facilitates optimal peptide selection by MHC class I during antigen processing. *Cell* 127: 369-382.
- [54] Stefková J, Poledne R, Hubáček JA (2004) ATP-binding cassette (ABC) transporters in human metabolism and diseases. *Physiol Res* 53: 235-243.
- [65] Perria CL, Rajamanickam V, Lapinski PE, Raghavan M (2006) Catalytic site modifications of TAP1 and TAP2 and their functional consequences. *J Biol Chem* 281: 39839-39851.
- [76] Parcej D, Tampé R (2010) ABC proteins in antigen translocation and viral inhibition. *Nat Chem Biol* 6: 572-580  
Erratum in: (2010) *Nat Chem Biol* 6: 782.
- [87] Dean M, Annilo T (2005) Evolution of the ATP-binding cassette (ABC) transporter superfamily in vertebrates. *Annu Rev Genomics Hum Genet* 6: 123-142.
- [98] Lehnert E, Tampé R (2017) Structure and dynamics of antigenic peptides in complex with TAP. *Front Immunol* 8: 10.
- [109] Marijt KA, van Hall T (2020) To TAP or not to TAP: alternative peptides for immunotherapy of cancer. *Curr Opin Immunol* 64: 15-19.
- [110] van Endert PM, Tampé R, Meyer TH, Tisch R, Bach JF et al. (1994) A sequential model for peptide binding and transport by the transporters associated with antigen processing. *Immunity* 1: 491-500.
- [111] Uebel S, Meyer TH, Kraas W, Kienle S, Jung G et al. (1995) Requirements for peptide binding to the human transporter associated with antigen processing revealed by peptide scans and complex peptide libraries. *J Biol Chem* 270: 18512-18516.
- [112] Neeffjes JJ, Momburg F, Hämmerling GJ (1993) Selective and ATP-dependent translocation of peptides by the MHC-encoded transporter. *Science* 261: 769-771  
Erratum in: (1994) *Science* 264: 16.
- [113] Seyffer F, Tampé R (2015) ABC transporters in adaptive immunity. *Biochim Biophys Acta* 1850: 449-460.
- [114] Locher KP (2016) Mechanistic diversity in ATP-binding cassette (ABC) transporters. *Nat Struct Mol Biol* 23: 487-493.
- [115] Eggenesperger S, Tampé R (2015) The transporter associated with antigen processing: a key player in adaptive immunity. *Biol Chem* 396: 1059-1072.
- [116] Abele R, Tampé R (2011) The TAP translocation machinery in adaptive immunity and viral escape mechanisms. *Essays Biochem* 50: 249-264.

- [4817] Mayemoler FC, Tampé R (2015) Antigen translocation machineries in adaptive immunity and viral immune evasion. *J Mol Biol* 427: 1102-1118.
- [4918] Oldham ML, Hite RK, Steffen AM, Damko E, Li Z et al. (2016) A mechanism of viral immune evasion revealed by cryo-EM analysis of the TAP transporter. *Nature* 529: 537-540.
- [2019] Lankat-Buttgereit B, Tampé R (2002) The transporter associated with antigen processing: function and implications in human diseases. *Physiol Rev* 82: 187-204.
- [2420] Ljunggren HG, Stam NJ, Ohlén C, Neefjes JJ, Höglund P et al. (1990) Empty MHC class I molecules come out in the cold. *Nature* 346: 476-480.
- [2221] Praest P, Luteijn RD, Brak-Boer IGJ, Lanfermeijer J, Hoelen H et al. (2018) The influence of TAP1 and TAP2 gene polymorphisms on TAP function and its inhibition by viral immune evasion proteins. *Mol Immunol* 101: 55-64.
- [2322] Yewdell JW, Bennink JR (1999) Mechanisms of viral interference with MHC class I antigen processing and presentation. *Annu Rev Cell Dev Biol* 15: 579-606.
- [2423] Oldham ML, Grigorieff N, Chen J (2016) Structure of the transporter associated with antigen processing trapped by herpes simplex virus. *Elife* 5: e21829.
- [2524] McLaughlin-Drubin ME, Munger K (2008) Viruses associated with human cancer. *Biochim Biophys Acta* 1782: 127-150.
- [2625] Ritz U, Seliger B (2001) The transporter associated with antigen processing (TAP): structural integrity, expression, function, and its clinical relevance. *Mol Med* 7: 149-158.
- [2726] Hicklin DJ, Marincola FM, Ferrone S. (1999) HLA class I antigen downregulation in human cancers: T-cell immunotherapy revives an old story. *Mol Med Today* 5: 178-186.
- [2827] Marincola FM, Jaffee EM, Hicklin DJ, Ferrone S (2000) Escape of human solid tumors from T-cell recognition: molecular mechanisms and functional significance. *Adv Immunol* 74: 181-273.
- [2928] Seliger B, Maeurer MJ, Ferrone S (1997) TAP off--tumors on. *Immunol Today* 18: 292-299.
- [3029] Verweij MC, Horst D, Griffin BD, Luteijn RD, Davison AJ et al. (2015) Viral inhibition of the transporter associated with antigen processing (TAP): a striking example of functional convergent evolution. *PLoS Pathog* 11: e1004743.
- [3130] Vossen MT, Westerhout EM, Söderberg-Nauclér C, Wiertz EJ (2002) Viral immune evasion: a masterpiece of evolution. *Immunogenetics* 54: 527-542.
- [3231] Tashiro H, Brenner MK (2017) Immunotherapy against cancer-related viruses. *Cell Res* 27: 59-73.
- [4132] Hislop AD, Rensing ME, van Leeuwen D, Pudney VA, Horst D et al. (2007) A CD8+ T cell immune evasion protein specific to Epstein-Barr virus and its close relatives in Old World primates. *J Exp Med* 204: 1863-1873.
- [4233] Alzhanova D, Edwards DM, Hammarlund E, Scholz IG, Horst D et al. (2009) Cowpox virus inhibits the transporter associated with antigen processing to evade T cell recognition. *Cell Host Microbe* 6: 433-445.
- [4334] Hill A, Jugovic P, York I, Russ G, Bennink J et al. (1995) Herpes simplex virus turns off the TAP to evade host immunity. *Nature* 375: 411-415.
- [4435] Früh K, Ahn K, Djaballah H, Sempé P, van Endert PM et al. (1995) A viral inhibitor of peptide transporters for antigen presentation. *Nature* 375: 415-418.
- [4536] Hewitt EW, Gupta SS, Lehner PJ (2001) The human cytomegalovirus gene product US6 inhibits ATP binding by TAP. *EMBO J* 20: 387-396.
- [4637] Koppers-Lalic D, Reits EA, Rensing ME, Lipinska AD, Abele R et al. (2005) Varicelloviruses avoid T cell recognition by UL49.5-mediated inactivation of the transporter associated with antigen processing. *Proc Natl Acad Sci U S A* 102: 5144-5149.
- [3338] Loch S, Tampé R (2005) Viral evasion of the MHC class I antigen-processing machinery. *Pflügers Arch* 451: 409-417.
- [8439] Schuren AB, Costa AI, Wiertz EJ (2016) Recent advances in viral evasion of the MHC class I processing pathway. *Curr Opin Immunol* 40: 43-50.
- [8540] Komov L, Melamed Kadosh D, Barnea E, Admon A (2021) The effect of interferons on presentation of defective ribosomal products as HLA peptides. *Mol Cell Proteomics* 20: 100105.
- [8641] García-Sastre A (2017) Ten strategies of interferon evasion by viruses. *Cell Host Microbe* 22: 176-184.
- [8842] Padariya M, Sznarkowska A, Kote S, Gómez-Herranz M, Mikac S et al. (2021) Functional interfaces, biological pathways, and regulations of interferon-related DNA damage resistance signature (IRDS) genes. *Biomolecules* 11, 622.
- [8043] Herget M, Baldauf C, Schölz C, Parcej D, Wiesmüller KH et al. (2011) Conformation of peptides bound to the transporter associated with antigen processing (TAP). *Proc Natl Acad Sci U S A* 108: 1349-1354.
- [9144] Saric T, Chang SC, Hattori A, York IA, Markant S et al. (2002) An IFN-gamma-induced aminopeptidase in the ER, ERAP1, trims precursors to MHC class I presented peptides. *Nat Immunol* 3: 1169-1176.
- [9445] Zhou F (2009) Molecular mechanisms of IFN- $\gamma$  to up-regulate MHC class I antigen processing and presentation. *Int Rev Immunol* 28: 239-260.
- [10446] Strehl B, Seifert U, Kruger E, Heink S, Kuckelkorn U et al. (2005) Interferongamma, the functional plasticity of the ubiquitin-proteasome system, and MHC class I antigen processing. *Immunol Rev* 207: 19-30.

- [4047] Arenano-Garcia ME, Misuno K, Han SD, Hu S (2014) Interferon- $\gamma$  induces immunoproteasomes and the presentation of MHC I-associated peptides on human salivary gland cells. *PLoS One* 9: e102878.
- [3448] Borrmann T, Cimons J, Cosiano M, Purcaro M, Pierce BG et al. (2017) ATLAS: A database linking binding affinities with structures for wild-type and mutant TCR-pMHC complexes. *Proteins* 85: 908-916.
- [12049] Natter C, Polterauer S, Rahhal-Schupp J, Cacsire Castillo-Tong D, Pils S et al. (2013) Association of TAP gene polymorphisms and risk of cervical intraepithelial neoplasia. *Dis markers* 35: 79-84.
- [12150] Einstein MH, Leanza S, Chiu LG, Schlecht NF, Goldberg GL et al. (2009) Genetic variants in TAP are associated with high-grade cervical neoplasia. *Clin Cancer Res* 15: 1019-1023.
- [12451] Abele R, Tampé, R (2004) The ABCs of immunology: structure and function of TAP, the transporter associated with antigen processing. *Physiology (Bethesda)* 19: 216-224.
- [12552] Ozbas-Gereker F, Bozman N, Gezici S, Pehlivan M, Yilmaz M et al. (2013) Association of TAP1 and TAP2 gene polymorphisms with hematological malignancies. *Asian Pac J Cancer Prev* 14: 5213-5217.
- [12653] Henle AM, Nassar A, Puglisi-Knutson D, Youssef B, Knutson, KL (2017) Downregulation of TAP1 and TAP2 in early stage breast cancer. *PloS one* 12: e0187323.
- [3554] Forbes SA, Beare D, Boutselakis H, Bamford S, Bindal N et al. (2017) COSMIC: somatic cancer genetics at high-resolution. *Nucleic Acids Res* 45: D777-D783.
- [3655] Cerami E, Gao J, Dogrusoz U, Gross BE, Sumer SO et al. (2012) The cBio cancer genomics portal: an open platform for exploring multidimensional cancer genomics data. *Cancer Discov* 2: 401-404 Erratum in: (2012) *Cancer Discov* 2: 960.
- [3756] Grotzke JE, Sengupta D, Lu Q, Cresswell P (2017) The ongoing saga of the mechanism(s) of MHC class I-restricted cross-presentation. *Curr Opin Immunol* 46: 89-96.
- [3857] Merzougui N, Kratzer R, Saveanu L, van Endert P (2011) A proteasome-dependent, TAP-independent pathway for cross-presentation of phagocytosed antigen. *EMBO Rep* 12: 1257-1264.
- [3958] Lawand M, Abramova A, Manceau V, Springer S, van Endert P (2016) TAP-dependent and -independent peptide import into dendritic cell phagosomes. *J Immunol* 197: 3454-3463.
- [4059] Karplus M, McCammon JA (2002) Molecular dynamics simulations of biomolecules. *Nat Struct Biol* 9: 646-652 Erratum in: (2002) *Nat Struct Biol* 9: 788.
- [4760] Faktor J, Grasso G, Zavadil Kokas F, Kurkowiak M, Mayordomo MY et al. (2020) The effects of p53 gene inactivation on mutant proteome expression in a human melanoma cell model. *Biochim Biophys Acta Gen Subj* 1864: 129722.
- [4861] Lanoix J, Durette C, Courcelles M, Cossette É, Comtois-Marotte S et al. (2018) Comparison of the MHC I immunopeptidome repertoire of B-cell lymphoblasts using two isolation methods. *Proteomics* 18: e1700251.
- [4962] Cox J, Matic I, Hilger M, Nagaraj N, Selbach M et al. (2009) A practical guide to the MaxQuant computational platform for SILAC-based quantitative proteomics. *Nat Protoc* 4: 698-705.
- [5063] Cox J, Hein MY, Luber CA, Paron I, Nagaraj N et al. (2014) Accurate proteome-wide label-free quantification by delayed normalization and maximal peptide ratio extraction, termed MaxLFQ. *Mol Cell Proteomics* 13: 2513-2526.
- [5164] Tyanova S, Temu T, Cox J (2016) The MaxQuant computational platform for mass spectrometry-based shotgun proteomics. *Nat Protoc* 11: 2301-2319.
- [5265] Cox J, Neuhauser N, Michalski A, Scheltema RA, Olsen JV et al. (2011) Andromeda: a peptide search engine integrated into the MaxQuant environment. *J Proteome Res* 10: 1794-1805.
- [5366] Kelley LA, Sternberg MJ (2009) Protein structure prediction on the web: a case study using the Phyre server. *Nat Protoc* 4: 363-371.
- [5467] Kelley LA, Mezulis S, Yates CM, Wass MN, Sternberg MJ (2015) The Phyre2 web portal for protein modeling, prediction and analysis. *Nat Protoc* 10: 845-858.
- [5568] Molecular Operating Environment (MOE) 2011.10. Chemical Computing Group (2011) Montreal, Quebec, Canada.
- [5669] Brooks BR, Brooks CL 3rd, Mackerell AD Jr, Nilsson L, Petrella RJ et al. (2009) CHARMM: the biomolecular simulation program. *J Comput Chem* 30: 1545-1614.
- [5770] Labute P (2008) The generalized Born/volume integral implicit solvent model: estimation of the free energy of hydration using London dispersion instead of atomic surface area. *J Comput Chem* 29: 1693-1698.
- [5871] Krivák R, Hoksza D (2015) Improving protein-ligand binding site prediction accuracy by classification of inner pocket points using local features. *J Cheminform* 7: 12.
- [5972] Kitchen DB, Decornez H, Furr JR, Bajorath J (2004) Docking and scoring in virtual screening for drug discovery: methods and applications. *Nat Rev Drug Discov* 3: 935-949.
- [60] Edelsbrunner, H. The union of balls and its dual shape. *Discrete Comput Geom.* 1995;13(3-4):415-440. doi: 10.1007/bf02574053
- [6173] Wojciechowski M, Lesyng, B (2004) Generalized Born model: Analysis, refinement, and applications to proteins. *J Phys Chem B* 108: 18368-18376.
- [6274] Labute P (2010) LowModeMD--implicit low-mode velocity filtering applied to conformational search of macrocycles and protein loops. *J Chem Inf Model* 50: 792-800.

- [6375] Karczewski KJ, Francioni LC, Hao G, Cummings BB, Abadi J et al. (2020) The mutational constraint spectrum quantified from variation in 141,456 humans. *Nature* 581: 434-443 Erratum in: (2021) *Nature* 590: E53.
- [6476] Lomize MA, Pogozheva ID, Joo H, Mosberg HI, Lomize AL (2012) OPM database and PPM web server: resources for positioning of proteins in membranes. *Nucleic Acids Res* 40: D370-D376.
- [6577] Jo S, Lim JB, Klauda JB, Im W (2009) CHARMM-GUI Membrane Builder for mixed bilayers and its application to yeast membranes. *Biophys J* 97: 50-58.
- [6678] Trowitzsch S, Tampé R (2020) Multifunctional chaperone and quality control complexes in adaptive immunity. *Annu Rev Biophys* 49: 135-161.
- [6779] Loschwitz J, Olubiyi OO, Hub JS, Strodel B, Poojari CS (2020) Computer simulations of protein-membrane systems. *Prog Mol Biol Transl Sci* 170: 273-403.
- [6880] Woolf TB, Roux B (1996) Structure, energetics, and dynamics of lipid-protein interactions: A molecular dynamics study of the gramicidin A channel in a DMPC bilayer. *Proteins* 24: 92-114.
- [6981] Phillips JC, Braun R, Wang W, Gumbart J, Tajkhorshid E et al. (2005) Scalable molecular dynamics with NAMD. *J Comput Chem* 26: 1781-1802.
- [7082] Klauda JB, Venable RM, Freites JA, O'Connor JW, Tobias DJ et al. (2010) Update of the CHARMM all-atom additive force field for lipids: validation on six lipid types. *J Phys Chem B* 114: 7830-7843.
- [7183] Venable RM, Brown FLH, Pastor RW (2015) Mechanical properties of lipid bilayers from molecular dynamics simulation. *Chem Phys Lipids* 192: 60-74.
- [7284] Guvench O, Mallajosyula SS, Raman EP, Hatcher E, Vanommeslaeghe K, et al. (2011) CHARMM additive all-atom force field for carbohydrate derivatives and its utility in polysaccharide and carbohydrate-protein modeling. *J Chem Theory Comput* 7: 3162-3180.
- [7385] Jorgensen WL, Chandrasekhar J, Madura JD, Impey RW, Klein ML (1983) Comparison of simple potential functions for simulating liquid water. *J Chem Phys* 79: 926-935.
- [7486] Darden T, York D, Pedersen L (1993) Particle mesh Ewald- an  $N \cdot \log(N)$  method for Ewald sums in large systems. *J Chem Phys* 98: 10089-10092.
- [7587] Pastor RW, Brooks BR, Szabo A (1988) An analysis of the accuracy of langevin and molecular dynamics algorithms. *Mol Phys* 65: 1409-1419.
- [7688] Feller SE, Zhang YH, Pastor RW, Brooks BR (1995) Constant pressure molecular dynamics simulation: the Langevin piston method. *J Chem Phys* 103: 4613-4621.
- [7789] Ryckaert JP, Ciccotti G, Berendsen HJC (1977) Numerical integration of cartesian equations of motion of a system with constraints: molecular dynamics of n-alkanes. *J Comput Phys* 23: 327-341.
- [7890] Humphrey W, Dalke A, Schulten K (1996) VMD: visual molecular dynamics. *J Mol Graph* 14: 33-38.
- [10591] Rock KL, Goldberg AL (1999) Degradation of cell proteins and the generation of MHC class I-presented peptides. *Annu Rev Immunol* 17: 739-779.
- [10692] Stryhn A, Pedersen LO, Holm A, Buus S (2000) Longer peptide can be accommodated in the MHC class I binding site by a protrusion mechanism. *Eur J Immunol* 30: 3089-3099.
- [10893] Guo HC, Jardetzky TS, Garrett TP, Lane WS, Strominger JL et al. (1992) Different length peptides bind to HLA-Aw68 similarly at their ends but bulge out in the middle. *Nature* 360: 364-366.
- [11294] Urban RG, Chicz RM, Lane WS, Strominger JL, Rehm A et al. (1994) A subset of HLA-B27 molecules contains peptides much longer than nonamers. *Proc Natl Acad Sci U S A* 91: 1534-1538.
- [9595] Rock KL, Reits E, Neefjes J (2016) Present yourself! By MHC class I and MHC class II molecules. *Trends Immunol* 37: 724-737.
- [11496] Koopmann JO, Post M, Neefjes JJ, Hämmerling GJ, Momburg F (1996) Translocation of long peptides by transporters associated with antigen processing (TAP). *Eur J Immunol* 26: 1720-1728.
- [11397] Kisselev AF, Akopian TN, Woo KM, Goldberg AL (1999) The size of peptides generated from proteins by mammalian 26 and 20S proteasomes. *J Biol Chem* 274: 3363-3371.
- [7998] Nogales A, DeDiego ML (2019) Host single nucleotide polymorphisms modulating influenza A virus disease in humans. *Pathogens* 8: 168.
- [11599] Bordignon E, Seeger MA, Galazzo L, Meier G (2020) From in vitro towards in situ: structure-based investigation of ABC exporters by electron paramagnetic resonance spectroscopy. *FEBS letters* 594: 3839-3856.
- [116100] Hofmann S, Janulienė D, Mehdipour AR, Thomas C, Stefan, E et al. (2019) Conformation space of a heterodimeric ABC exporter under turnover conditions. *Nature* 571: 580-583.
- [117101] Stefan E, Hofmann S, Tampé R (2020) A single power stroke by ATP binding drives substrate translocation in a heterodimeric ABC transporter. *eLife* 9: e55943.
- [118102] Nöll A, Thomas C, Herbring V, Zollmann T, Barth K et al. (2017) Crystal structure and mechanistic basis of a functional homolog of the antigen transporter TAP. *Proc Natl Acad Sci U S A* 114: E438-E447.
- [119103] Armandola EA, Momburg F, Nijenhuis M, Bulbuc N, Früh K et al. (1996) A point mutation in the human transporter associated with antigen processing (TAP2) alters the peptide transport specificity. *Eur J Immunol* 26: 1748-1755.
- [81104] Denton AE, Wesselingh R, Gras S, Guillonneau C, Olson MR et al. (2011) Affinity thresholds for naive CD8+ CTL activation by peptides and engineered influenza A viruses. *J Immunol* 187: 5733-5744.

- [82105] Seim DK, Schubert DA, Anders AK, Heroux A, Bonsor, DA et al. (2011) A highly tilted binding mode by a self-reactive T cell receptor results in altered engagement of peptide and MHC. *J Exp Med* 208: 91-102.
- [83106] Borbulevych OY, Santhanagopalan SM, Hossain M, Baker BM (2011) TCRs used in cancer gene therapy cross-react with MART-1/Melan-A tumor antigens via distinct mechanisms. *J Immunol* 187: 2453-2463.

Journal Pre-proofs

